NTNU – Trondheim
Norwegian University of
Science and Technology

Oxidation of silicon powder in humid air

Anne Marthe Nymark

Chemical Engineering and Biotechnology
Submission date: June 2012
Supervisor: Mari-Ann Einarsrud, IMTE
Co-supervisor: Johan P. Svanem, Elkem AS Silicon Materials
Harry Rong, Elkem AS Silicon Materials

Norwegian University of Science and Technology
Department of Materials Science and Engineering

Preface

The work of this master thesis has been carried out at the Department of Material Science and Engineering at the Norwegian University of Science and Technology (NTNU) through the spring 2012, and has been in collaboration with Elkem. The report presents the results done on the study of the development of an oxide layer on the silicon surface and the evolution of hydrogen gas from the aqueous oxidation the silicon powder.

The master thesis has been carried out independently, honest and in accordance with the examination regulations of NTNU.

Trondheim, June 2012

Anne Marthe Nymark

Acknowledgement

First of all I wish to express my sincere gratitude to my supervisor, Prof. Mari-Ann Einarsrud for being very helpful and encouraging, for organising weekly meetings, giving me frequent feedback and discussions of the results. MSc Johan S. Svanem from Elkem deserves a lot credit for great support and many fruitful discussions.

A big thank to Dr. Spyros Diplas from SINTEF for doing the X-ray photoelectron spectroscopy (XPS) analysis of my powders, and valuable interpretation of the XPS data. Thanks to Anne Støre at SINTEF for doing oxygen analysis, Dr. Julien Romann for performing the Raman Spectroscopy, Tina Kristiansen for performing DRIFTS analysis and Anne Forwald at Elkem for doing SEM analysis. Great thanks are also addressed to engineer May Grete Sætran, chief engineer Eli-Beate Jakobsen and engineer Elin Albertsen for essential help and support.

Last but not least, I want to thank Carl Erik Lie Foss for great support during the work with the thesis.

Abstract

Silicon undergoes oxidation at room temperature, causing a formation of an oxide layer on its surface. Gaining knowledge about the oxide layer formed during ageing, is valuable with regards to production of high quality ceramics, like Si_3N_4, especially for the slip casting process.

In this work silicon powders were exposed to humid air at different temperatures for different periods of time. From the XPS analysis, the oxygen and hydroxide content were found to be higher for powders aged at higher humidity compared to powder aged at lower humidity. This was verified by the estimated oxide thickness, which was larger for powder aged at higher humidity. No obvious difference could be observed for short and long ageing time in low humidity atmosphere. Results from Raman spectroscopy showed a more amorphous powder after storage in humid air. A clear shift and broadening of the crystalline silicon peak were observed for powders exposed to air at low and high humidity. The powders aged in humid air were further reacted with water at pH 9.4 and temperature of 60 °C. The onset time for hydrogen evolution was observed to be later for samples exposed longer times to humid air. This indicates that the reactivity of the powder decreases as the oxide layer formed during ageing develops. The amount of hydrogen evolved seemed to be dependent on the hydrogen evolution time rather than the time of exposure to humid air. This was verified by the surface area, which was about the same for all samples, showing only a slightly decrease for increasing exposure time. The oxygen content measured was linearly related to the surface area for the main section of the samples. Higher hydroxide content seemed to catalyse the aqueous oxidation reacting, resulting in an earlier onset time for hydrogen evolution and a higher hydrogen flow. This was stated by a higher surface area and higher oxygen content for these samples. Powder thermally treated, at 300 °C and 900 °C, were also investigated. XPS analysis showed a thicker oxide layer for powder treated at 900 °C. No hydrogen was formed in the aqueous oxidation of powder treated at 300 °C. This was verified by a low surface area.

Regarding the slip casting of silicon powders, a defect free green body can be obtained by reducing the hydrogen formation. Based on the results found, this can be obtained by the formation of a passivation oxide layer on the particle surface, formed during ageing of the powders in humid atmosphere before processing. Higher humidity and longer ageing time seems to affect the development of the oxide layer formed on the surface more than low humidity and short ageing time. To minimise the hydrogen formation, it is crucial to be able to control the hydroxide concentration in the aqueous oxidation accurately.

Samandrag

Silisium blir spontant oksidert i romtemperatur, noko som førar til danning av eit oksidsjikt på partikkeloverflata. Auka kunnskap om oksidsjiktet som blir danna under lagring, er verdifullt med omsyn på produksjon av keramer med høg kvalitet, som Si_3N_4. Dette er spesielt viktig for den vassige slikkerstøypingmetoda.

I dette arbeidet blei silisiumpulver eksponert for fuktig luft ved forskjellige temperaturar og med forskjellig varigheit. XPS analyse av pulveret viste at oksygen- og hydroksidinnhaldet var lågare for pulver eksponert for låg luftråme samanlikna med pulver eksponert for høg luftråme. Ingen tydeleg forskjell kunne observerast for kort og lang eksponeringstid i låg luftråme. Toppen for krystallinsk silisium, i Raman spekteret, var tydeleg breiare og skifta til lågare energi etter eksponering i fuktig luft. Dette var tilfelle for eksponering i både låg og høg luftråme, og tydar på eit amorft materiale. Pulvera som vart lagra i fuktig luft blei vidare reagert med vatn med pH på 9.4 og temperatur på 60 °C. Initieringstida for hydrogendanning blei observert å vere seinare for pulver som vart eksponert lenger i fuktig luft. Dette indikerer at reaktiviteten til pulveret blir mindre som ein konsekvens av at oksidlaget på overflata utviklar seg og blir tjukkare når eksponeringa i fuktig luft aukar. Den totale mengda hydrogen som vart danna verkar å vere meir avhengig av tida hydrogenet får verte utvikla på, enn eksponeringstida i fuktig luft. Dette blei verifisert av det målte overflatearealet, som var omlag det same for alle prøver. Berre ein liten avtakande trend kunne sjåast med aukande eksponeringstid i fuktig luft. Oksygeninnhaldet viste ein lineær samanheng med overflate arealet for dei fleste prøvene. Ein høgare hydroksidkonsentrasjon såg ut til å katalysere den vassige oksideringsreaksjonen. Dette resulterte i tidligare initieringstid for hydrogenutvikling og høgare hydrogenstraum. Eit høgare overflateareal og eit høgare oksygeninnhalde blei målt for desse prøvene, noko som stadfestar teorien om at hydroksidkonsentrasjonen er viktig for hydrogen danninga i oksidasjonsreaksjonen av silisium i vatn. I Pulver termisk behandla i 300 °C og 900 °C blei også studert. XPS analyse påviste eit tjukare oksidlag for pulver behandla i 900 °C. Vassig oksidasjon av pulver behandla i 300 °C gav ingen hydrogen utvikling, noko som blei verifisert av eit lågt overflate areal.

For slikkerstøyping av silisiumpulver, kan ein oppnå ein defektfri grønkropp ved å redusere hydrogen danninga. Basert på dei oppnådde resultata, kan dette gjerast ved at eit passiverande oksidlag vert danna på partikkeloverflata ved lagring i fuktig luft. Luft med høg luftråme og lenger lagring kan verke å ha større betyding for danninga av oksidlaget, samanlikna med lågare luftråme og kortare lagringstid. For å minimalisere hydrogendanning er det også naudsynt å kunne kontrollere hydroksidkonsentrasjonen i den vassige oksidasjonsreaksjonen nøyaktig.

List of Abbreviation

- Silica - Silicon dioxide.
- Silicic acid - General name for a chemical compound of the elements silicon, hydrogen and oxygen, with the general formula $[SiO_x(OH)_{4-2x}]_n$.
- Silicate - A compound containing an anion in which one or more central silicon atoms are surrounded by electronegative ligands.
- Siloxane - Chemical compound composed of units of the form X_2SiO, where X is a hydrogen atom or a hydrocarbon group.
- Silanol - Expression for any OH group attached to silicon.
- Colloid - A substance dispersed evenly throughout another substance.
- Suspension - A heterogeneous fluid containing solid particles that are sufficiently large for sedimentation.
- Slip - Suspension in water of materials used in the production of ceramics.
- PZC - Point of zero charge. The pH that gives a net zero charge on the particle surface.
- Zeta potential - The potential at the shear plane of a particle.
- PSD - Particle size distribution
- RH% - Relative humidity
- XPS - X-ray photoelectron spectroscopy
- BET - Method of measuring the specific surface area of particles.
- LECO - Combustion analysis for determination of elements such as oxygen.
- DRIFTS - Diffuse Reflectance Infra-red Fourier Transform spectroscopy
- TGA - Thermogravimetric analysis

Contents

Chapter 1

Introduction

1.1 Motivation

Silicon is used as a raw material in the production of a wide variety of ceramic products. One example is Si_3N_4, which is a ceramic with a unique set of outstanding properties [1]. Si_3N_4 has a high strength over a wide temperature range, high fracture toughness and good thermal shock resistance. This makes Si_3N_4 suitable for several wear, mechanical and thermal applications. Some important application areas for Si_3N_4 are the production of Si_3N_4-bonded SiC as kiln furniture for the porcelain industry and reusable Si_3N_4 crucibles for the solar cell industry. In Figure 1.1 rotors made of Si_3N_4-bonded SiC is shown. There are many different synthesis routes that can be utilised for the production of Si_3N_4. Nitridation of silicon powder, is a commercially used route [1], where silicon powder is exposed to controlled nitrogen atmosphere at high temperatures, Eqaution 1.1.

$$3\,Si(s) + 2\,N_2(g) \longrightarrow Si_3N_4(s) \tag{1.1}$$

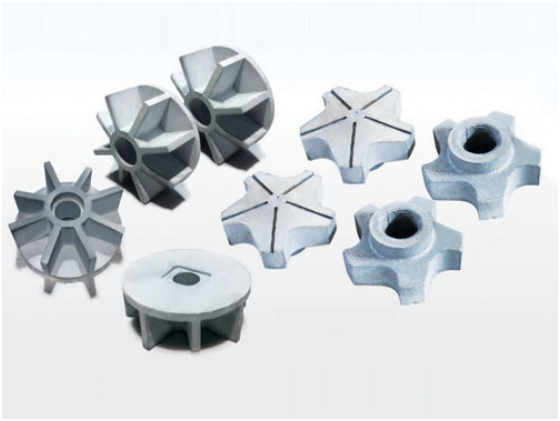

Figure 1.1: Silicon nitride bonded silicon carbide rotors [2].

Production of silicon based ceramics often involves a water based slip casting process. Slip casting is a simple and inexpensive casting method for the production

of materials with high green density. Large green bodies with complex shapes, that can be used for a wide variety of applications, are easily produced. There are many challenges concerning the aqueous slip casting method, and one of them is the hydrogen formation originating from the oxidation of silicon in water [3], according to Equation 1.2. To ensure best possible dispersion of the silicon powder in the slip, the pH is controlled to about 9. Silicon will hydrolyse in basic solutions causing hydrogen formation, as seen in Equation 1.3.

$$\mathrm{Si(s)} + 2\,\mathrm{H_2O(l)} \longrightarrow \mathrm{SiO_2(s)} + 2\,\mathrm{H_2(g)} \tag{1.2}$$

$$\mathrm{Si(s)} + 4\,\mathrm{OH^-} \longrightarrow \mathrm{SiO_4^{4-}(aq)} + 2\,\mathrm{H_2(g)} \tag{1.3}$$

The formation of hydrogen gas is the source of many unwanted effects, like porosity in the final product seen as spherical gas bubbles. This porosity can affect the density of the green body and thus the mechanical properties of the products and therefore make them useless for the intended use.

Silicon will spontaneously oxidise when it is exposed to air at room temperature. The nature of this oxide layer formed is among other factors affecting the reaction between both silicon and nitrogen in the nitridation process and silicon and water in the slip casting process. Gaining knowledge about the oxide layer formed during ageing is therefore valuable in the production of high quality Si_3N_4 and defect free green bodies. An oxide layer on the surface is believed to retard the hydrogen formation because the oxide layer has to be dissolved before the reaction between silicon and water can take place. The formation and growth of the oxide layer are believed to be dependent on the conditions the powder is stored at, like temperature and humidity [4]. The duration of the storing, from milling of the powder until it is processed is also believed to be an important factor concerning the development of the oxide layer. It is therefore important to gain more knowledge and better understanding of the oxidation mechanisms of silicon in humid air compared to dry air and further investigate how this will affect the hydrogen evolution when the silicon powder is reacted with water.

1.2 Aim of work

The primary goal of this study is to investigate how ageing of silicon powder in humid air will influence the oxide layer formed on the particle surface. This will be studied by surface analysis of the humid powders and by measuring the hydrogen formed in reaction with water. A previous study by the author [5] investigated how exposure to humid air at 22 °C influenced the silicon powder. To get a clearer picture of the processes involved, we want to study how exposure to lower humidity affects the powder. Lower humidity data will not only yield a more complete set of data of the processes involved, but will also be closer to the actual industrial storing conditions. Therefore in the present study, in addition to investigating the powder exposed to humid air at 22 °C, powder exposed to humid air 10 °C will

also be investigated. To simulated the ageing process powder is exposed to humid air in tight containers, where the atmosphere is controlled.

After exposing the powder to humid air at different temperatures and durations the powder is reacted with water. A slurry of silicon and water is heated in a purpose-built apparatus and the hydrogen formed in the reaction, Equation 1.2, is measured. From these measurements the onset time for hydrogen formation and the total amount of hydrogen gas evolved in the aqueous oxidation can be found. The aim is to find trends and correlations between these parameters. Information about how exposure to humid air affects the hydrogen formation can be used to control the passivation of the silicon surface. Controlling the passivation of the silicon surface can be useful in relation to further processing, like slip casting. If the hydrogen formation is minimised, or not present, defect products may be avoided.

Different analysis methods are evaluated as potential techniques for studying the oxide layer and potentially identify changes that occur over time. Both the surface area and the oxygen content of the reacted powders is measured. Relating this to the ageing history can give information about how the aqueous oxidation is affected by exposing the unreacted silicon powder to humid air. Scanning electron microscopy (SEM) is used to picture the particle surface in desire to find differences related to ageing and oxygen content. X-ray photoelectron spectroscopy (XPS) is used to analyse the surface of the unreacted silicon powder to give an idea of how the oxide layer change during exposure to humid air, and how thermal oxidation affects the surface. Diffuse Reflectance Infra-red Fourier Transform (DRIFTS) and Raman Spectroscopy are both used to analyse the surface of reacted and unreacted silicon powder to give an idea of how the oxide layer develops.

To summarise, the main focus of this study is to investigate how exposure to humid air affect the oxide development on the silicon surface. The main characterisation methods used are listed below.

- Hydrogen measurements
  - Investigate the reactivity of silicon powder in reaction with water
  - Identify the initiation time for hydrogen evolution and measure the total hydrogen amount formed in the reaction with water
  - Measure surface area and oxygen content of reacted powder
- X-ray photoelectron spectroscopy
- Vibrational spectroscopy

Chapter 2

Theory

2.1 Silicon and the oxidised surface

Silicon is a tetravalent Group IV element. It is a metalloid having properties of both metals and non-metals. Silicon is the second most abundant element on the Earths crust after oxygen making up 27.7% of the crust by mass. It is hardly found in its free elemental form, but occurs widely distributed in the nature as silicon dioxide and silicates [6]. Silicon has high affinity for oxygen and an oxide layer will spontaneously form on the surface when it is exposed to air even at room temperatur [7], according to Equation 2.1.1. The oxophilic nature of silicon makes it reasonable to compare the surface properties of silicon to that of silica (SiO_2) [8].

$$Si(s) + O_2(g) \longrightarrow SiO_2(s) \tag{2.1.1}$$

When silicon reacts with water a spontaneous hydrolysis is expected based on the negative standard reduction potential (E^0=-0.888V) [9, 3], according to Equation 2.1.2.

$$Si(s) + 2\,H_2O(l) \longrightarrow SiO_2(s) + 2\,H_2(g) \tag{2.1.2}$$

The oxide layer produced forms a protective layer that will affect the surface reactivity of silicon. This outer silica layer is relatively stable under acidic or neutral pH conditions [9], but can be destroyed in basic solutions [3], as seen in Equation 2.1.3.

$$SiO_2 + 2\,OH^-(l) \longrightarrow SiO_3^{2-}(s) + H_2O \tag{2.1.3}$$

The surface structure of silica is mainly composed of relatively unreactive siloxane links, -Si-O-Si-, and surface hydroxyl groups, -Si-OH-, called silanols. Silanol-groups is the result of incomplete condensation during the polymerisation process that forms silica, and/or the tendency of the surface oxygen to form two bonds

like the other atoms in the interior of the structure [8]. Figure 2.1 shows the two surface structures of silica.

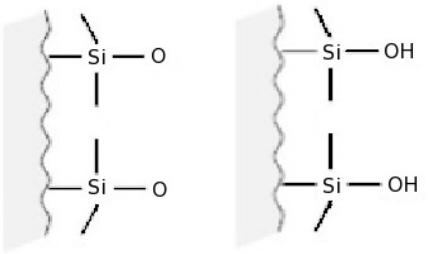

(a) (b)

Figure 2.1: a) Siloxane links at the silica surface, b) silanol groups adsorbed on the silica surface [8].

2.2 Properties of the silica surface

The surface structure of silica is mainly composed of relatively unreactive siloxane, -Si-O-Si-, and silanols, Si-OH, as already mentioned. In addition to the consequence of incomplete condensation during the polymerisations process the silanol-groups can also be the result of the reaction between the siloxane surface and water at ambient temperatures according to Equation 2.2.1. The unsatisfied surface valence of the oxide is saturated by chemisorption of water and consequently leads to formation of hydroxyl groups at the surface.

$$\mathrm{Si{-}O{-}Si} + \mathrm{H_2O} \longrightarrow \mathrm{Si{-}OH} + \mathrm{Si{-}OH} \tag{2.2.1}$$

If silica is exposed to water for longer times, the surface will hydrolyse further, which can result in dissolution of the surface species to form bulk silicic acid and exposing the underlaying silicon to water. The hydrolysis of silica in aquous solution is illustrated in Figure 2.2.2. Hydrolysis followed by dissolution will continue until solid solution equilibrium is reached [8].

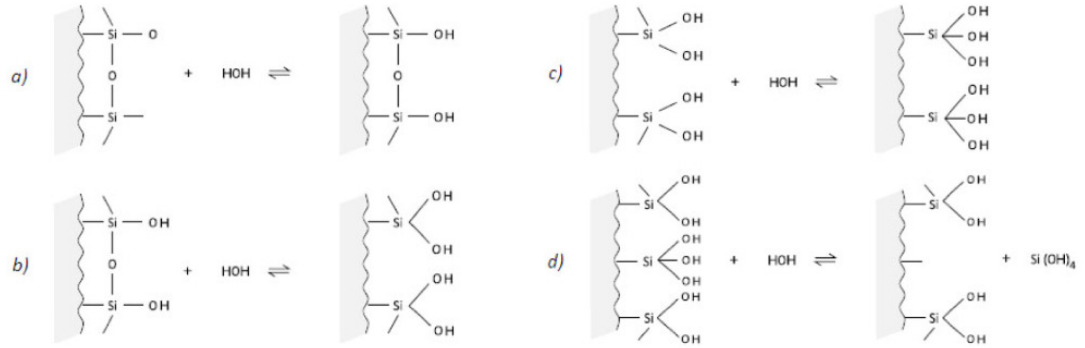

Figure 2.2.2: The hydrolysis process of silica in aqueous solution. a) Hydrolysis of the fresh silica surface in contatc with water giving rise to silanol groups at the surface. b) Further hydrolysis of silica when it is exposed to water for longer intervalls, forming $=Si(OH)_2$ at the surface. c) Formation of more silanol groups. d) Further hydrolysis can result in dissoultion of the surface species to form bulk silicic acid and expose underlaying silicon to the bulk water [8].

The surface properties of silica particles is determined by the degree of hydration of the surface, like the number and type of silanol groups adsorbed. The rate of hydrolysis is a function of the solutions pH, temperature and ionic strength. Pretreatment of silica, such as acid treatment, can result in changes in the surface properties [8].

Since the silicon atoms on the surface are not in a regular geometrical arrangement, the hydroxyl groups attached to the surface are not equidistant from each other [10]. They will therefore not be equivalent in their behavior in both adsorption and chemical reactions. When silica particles are formed in water the number of OH^- groups formed can be affected in several ways [10]. One effect is the particle size, which will play a role in the packing of adsorbed molecules on the particle surface. As can be seen from Figure 2.2.3, the hydroxyl groups are less crowded per unit area on small particles with positive curvature, resulting in fewer hydrogen bonds formed between them. On larger particles on the other hand, the hydroxyl groups are closer together and thus forms more stable hydrogen-bonded pairs.

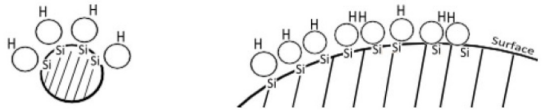

Figure 2.2.3: The particle size affect the number of hydroxyl groups adsorbed on the silica particle in water. a) Hydroxyl groups are less crowded per unit area on small particles. b) On larger particles the hydroxyl groups are closer together, thus forming more stable hydrogen-bonded pairs [10].

2.3 Mechanism of dissolution of silica in water

In order to get a reaction between silicon and water the oxide layer formed on the particle surface of silicon must be dissolved. The rate at which silica is dissolved in water is influenced by many factors, however for dissolution to occur the presence of a catalyst is always required. Dissolution of silica in water is basically a depolymerisation through hydrolysis. Iler [10] defines the "solubility" of silica as the concentration of $Si(OH)_4$ reached when a steady state equilibrium between depolymerisation and polymerisation is set, according to Equation 2.3.1.

$$SiO_2(s) + 2\,H_2O(l) \longrightarrow Si(OH)_4(aq) \tag{2.3.1}$$

The catalyst for the dissolution process is a material that can chemisorb to the silica surface and increase the coordination number of the silicon atoms to more than four. This results in weakening of the oxygen bond to the underlaying silicon atoms. For basic solutions the hydroxyl group (OH^-) is the catalyst [10]. The dissolution process is therefore strongly affected by pH. The dissolution process of silica in basic solution yields monomeric silica, $Si(OH)_4$, as shown in Equation 2.3.2 [11].

$$(\equiv Si{-}O{-}Si \equiv)_{surface} + 4\,OH^- \longrightarrow (\equiv Si{-}O^-)_{surface} + Si(OH)_4 \tag{2.3.2}$$

A proposed mechanism of the dissolution process of silica is shown in Figure 2.3.1. The first step is the adsorption of OH^- ions, resulting in that a silicon atom goes into solution as a silicate ion. For pH below 11 the silicate ion will hydrolyse further to soluble silica ($Si(OH)_4$) and OH^- ions and the process is repeated [10, 11].

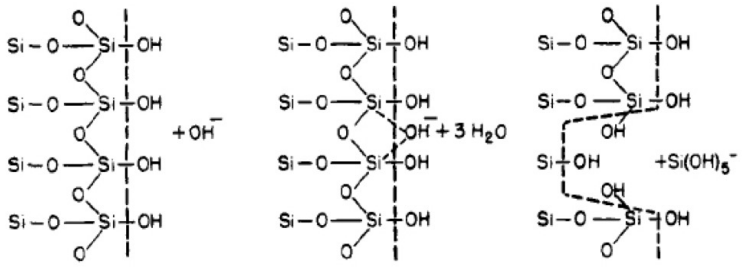

Figure 2.3.1: Proposed mechanism of dissolution of silica in water in the presence of hydroxyl ions. The dotted lines represent the interface between silica on the left and water on the right. OH^- is adsorbed on the surface resulting in a silicon atom going into the solutions as a silicate ion [10].

Dissolution of the silica surface will expose underlaying silicon atoms to the solution. In basic solution silicon will react with OH^- ions and produce hydrogen gas and SiO_4^{4-} ions according to Equation 2.3.3.

$$Si(s) + 4\,OH^- \longrightarrow SiO_4^{4-}(aq) + 2H_2(g) \tag{2.3.3}$$

The total reaction occurring when silicon is mixed with water in basic solution is given in Equation 2.3.4. As can be seen from the reaction, silicic acid and hydrogen forms.

$$\mathrm{Si(s)} + 4\,\mathrm{H_2O(l)} \longrightarrow \mathrm{Si(OH)_4(aq)} + 2\,\mathrm{H_2(g)} \tag{2.3.4}$$

The dissolution of silica in water is influenced by many factors. In Figure 2.3.2 the solubility of amorphous silica is shown as a function of both temperature and pH. As seen from the figure the solubility increases with increasing temperature, pH or both. There is an appararent increase in solubility from pH 7 to 9. The high increase in solubility at this pH is caused by the formation of silicate ions in addition to monomers, which is in equilibrium with the solid phase [10]. The solubility of silica is also affected by the particle size with regards to the radius of curvature, as illustrated in Figure 2.3.3. For particles with small positive radius of curvature the equilibrium solubility is higher compared to particles with negative radius of curvature.

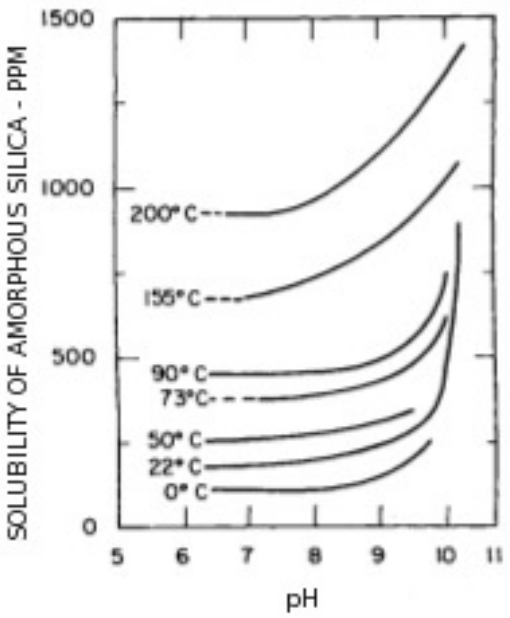

Figure 2.3.2: Solubility of amorphous silica vs. pH at different temperatures [10]. The solubility is increasing with increasing pH and temeprature.

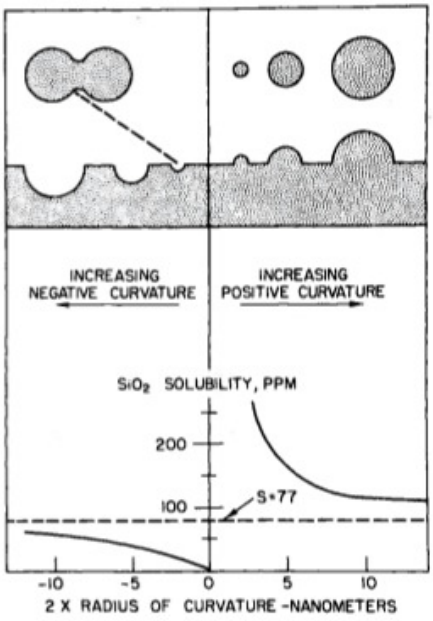

Figure 2.3.3: The lower figure shows the variation of dissolution of silica with radius of curvature of the silica surface. The upper right figure show positive radius of curvature as particles pointing out from the surface. The particles with negative radius of curvature are shown as holes in the silica surface and in the crevice between two particles, upper left figure [10].

2.4 Condensation of silica

Dissolution of silica yields monomeric silca, $Si(OH)_4$, as given in Equation 2.3.4. Monomeric silica can polymerise by condensation to form dimers and higher molecular weight species of silicic acid. Iler [10] describes the polymerisation process of monomeric silica in several steps, a brief summary of the main steps in the process is listed below. The succeeding steps in the process is presented schematically in Figure 2.4.1.

- Polymerisation of monomeric silica by condensation to form dimers and higher molecular weight species of silicic acid
- Growth of particles due to Ostwald Ripening [12]
- Formation of gel networks due to rearrangement and linking of particles

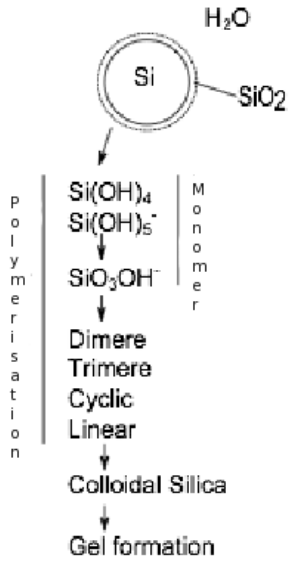

Figure 2.4.1: Dissolution of silica followed by polymerisation of silicic acid and silicates resulting in colloidal silica or eventually silica gel [13].

Monosilic acid is soluble and stable in water at 25 °C for long periods of time as long as the concentration is less than 100 ppm as SiO_2 [10]. When a solution of monomers, $Si(OH)_4$, is formed at a concentration higher than this and in the absence of solid phase where soluble silica may deposit, polymerisation to form dimers and higher weight molecular species of silica can occur. The further growth of condensed silica is controlled by various parameters, like pH, temperature and initial size of colloidal silica. Because the solubility of small particles is higher than for larger particles, the particles grow in average size and decrease in number as small particles dissolve and is deposited on the larger particles, due to Ostwald ripening [12]. The higher solubility of smaller particles is only pronounced when the particle diameter is smaller than about 5 nm. For pH above 7, Ihler [10] states that the rate of dissolution and deposition of silica is high and that the growth of the particles continuous at ordinary temperatures until the particles are about 5-10 nm in diameter, where the growth slow down. At higher temperatures, growth continues to larger sizes. Rearrangement of the particles into branching chains leads to the formation of gel networks. Solution and deposition of silica leads to growth of the necks between the particles resulting in a stronger gel structure [10].

2.5 Oxidation of silicon

As explained earlier an oxide layer will spontaneously form on the silicon surface when it is exposed to air, according to Equation 2.1.1. The oxidation of silicon occurs at the Si/SiO_2 interface. When the oxide layer starts to build up the oxidation species must diffuse through the growing oxide layer and react with silicon at the interface to form SiO_2. At room temperature the diffusion through the oxide layer will be limited, and the growth rate will decrease. As the oxide

layer grows thicker the silicon is consumed. Literature show that both exposure time and humidity of the air are factors affecting this oxidation.

Surface oxidation of silicon wafers has been extensively studied, and because it is believed that a similar oxidation process occur at the particle surface of silicon powder these studies are used as a reference in this study. However, Okada and Iijima [14] reports that oxide growth rate of small particles is less than the growth rate on silicon wafers and decreases with decreasing particle size. They studied almost spherical particles ranging from about 20 to 500 nm in diameter. This must be considered when using wafers as references for the further study of the oxidation of silicon powder.

Most of the silicon wafers studied in the literature are treated with hydrogen fluoride (HF), giving a hydrogen-terminated surface. The silicon powders studied in this project are acid-treated, which makes it reasonable to assume that the same oxidation mechanism occur. The acid treatment will probably affect the surface properties of the silicon powder.

The surface of HF-treated wafers is terminated by Si-H and Si-H_2 bonds. An IR-study of the initial stages of oxidation of hydrogen terminated Si-wafers stored in air, done by Niwano *et al.* [4] show that the intensity of Si-H and Si-H_2 decreased as the exposure time to air increased. This suggest that surface Si-H bonds were attacked by oxidants present. Figure 2.5.1 gives an illustration of the suggested oxidation process.

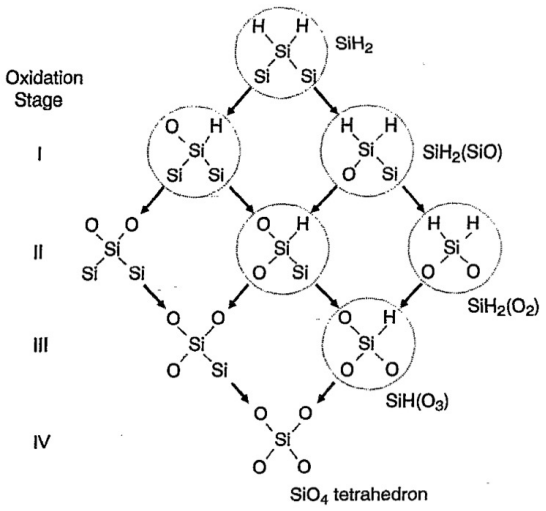

Figure 2.5.1: Schematic illustration of the different oxidation stages occurring on the silicon surface. I) Attack of Si-H bonds or back bond to form $SiH_2(SiO)$, II) Generation of $SiH_2(O_2)$ as two back bonds are converted into Si-O bonds, III) Completion of back bond oxidation and oxidation of surface Si-H bonds, giving $SiH(O_3)$, IV) Replacement of all bonds around the surface Si-atom with Si-O bonds, resulting in the SiO_4 tetrahedron [4].

The configurations which are enclosed by circles exhibit S-H vibration modes. At the first stage (I) of oxidation oxygen attacks Si-H bonds or the back bond of the surface Si-atom. In this stage $SiH_2(SiO)$ is produced when one of the back bonds

is converted into Si-O bonds with the two surface Si-H bonds left unbroken. The breaking of the Si-H bonds leads to a decrease in the concentration of Si-H_2. When the exposure time to air increases, $SiH_2(O_2)$ is generated as the two back bonds are converted in to the Si-O bond, shown in the second stage (II). When the back bond oxidation is completed the remaining Si-H bonds at the surface Si atoms is replaced with Si-O bonds, resulting in generation of $SiH(O_3)$. Stage four (IV) in the figure shows the SiO_4 tetrahedron, which is the result of replacement of all the bonds around the surface Si-atoms with Si-O bonds. Here, the S-H vibration mode disappear. These studies show that the exposure time to air affect the oxidation of the silicon wafer surface. Increasing exposure time leads to a higher degree of oxidation.

2.5.1 Effect of exposure to dry air on the oxide growth

Mortia *et al.* [15] found that the oxide layer hardly grew at all during seven days exposure to air when the H_2O concentration was suppressed to less than 0.1 ppm. XPS analysis of silicon powder before and after storage in a bag contained with silica (dry air) did not show any difference in the thickness of the oxide layer on the particle surface [5]. Aging of silicon powder in dry air is not believed to affect further growth of the oxide layer, and it will therefore not affect the reactivity of silicon in reaction with water, Equation 2.1.2.

2.5.2 Effect of exposure to humid air on the oxide growth

Niwano *et al.* [4] report that the presence of water is crucial to the initiation stages of oxidation of hydrogen terminated Si surfaces aged in air. When the Si-wafers are exposed to humid air a reaction between oxidation species and the hydrogen-terminated surface will occur. The oxygen and water will most likely react in different ways. Samples stored in 10 % humidity compared to 40 % humidity, showed retardation of oxidation of $Si-H_2$ bonds, which strengthens the theory that water molecules is predominantly involved in the oxidation of surface Si-H_2 bonds. According to Mortia *et al.* [15] the oxide thickness on the Si-surface increases with H_2O concentration in air. Thus, by reducing the concentration of moisture in air, the growth rate of the oxide layer can be reduced.

Mortia *et al.* [15] and Niwano *et al.* [4] have extensively studied the surface oxidation of Si-wafers. To understand the mechanism of oxide growth in air the factors controlling the oxidation have been studied. Both n-type, n^+- and p^+- type Si wafers have been investigated, showing different thickness of the native oxide films, indicating that the oxidation is dependent on crystallographic directions. The Si-wafers were exposed to an average humidity of 42%(RH) (0.1214 atm) and the different oxide thickness obtained is illustrated in Figure 2.5.2. The graph indicates an approximately stepwise increase of the oxide thickness for all the wafer types, which can be the result of a layer-by-layer growth of the oxide. For exposure to higher humidity a thicker and more stable oxide layer is expected to form.

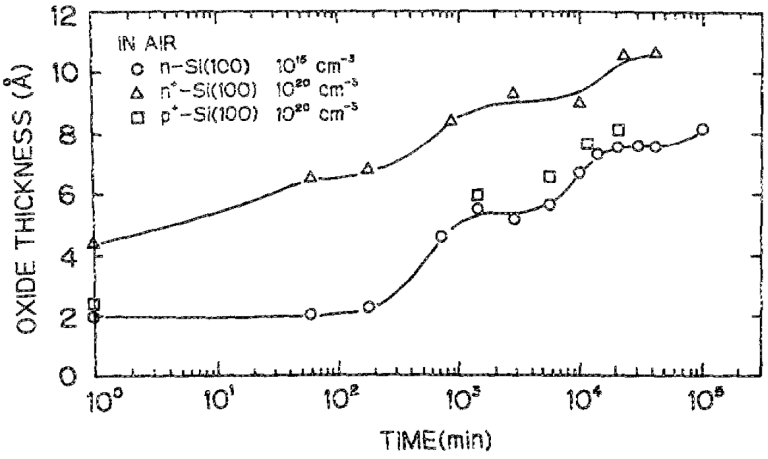

Figure 2.5.2: Oxide thickness on n-, n^+- and p^+-silicon wafers as a function of exposure to air [15].

The experimental results presented by Niwano *et al.* [4] demonstrated that the oxidation of the surface exposed to high humidity air was quite different from that exposed to O_2. The most probable reaction that occurs is suggested to follow Equation 2.5.1 where water reacts with the Si-H bond at the surface [4].

$$\mathrm{Si{-}H + H_2O \longrightarrow Si{-}OH + H_2} \tag{2.5.1}$$

Figure 2.5.3 gives a linear illustration of the layer-by-layer growth of an oxide layer on the silicon surface. The Si-Si bonds on the surface are broken by the oxygen species present to produce Si-O bonds. The oxygen species are produced by the coexistence of O_2 and H_2O near the Si-Si bonds [15]. The Si-Si bonds of the underlayer are broken to produce Si-O bonds when the Si-atoms at the overlayer are oxidised.

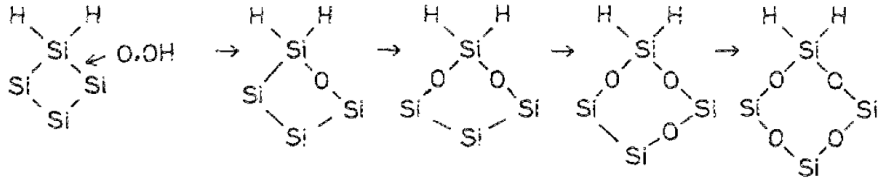

Figure 2.5.3: A model of the layer-by-layer growth of native oxide on a silicon surface exposed to air. Oxidation species, oxygen or OH, breakes the Si-Si bonds to produce Si-O bonds [15].

Cerfolini and Meda [16] proposed a mechanism to describe the oxidation of silicon wafers in air, where the rate limiting step was electron transfer from negatively charged silicon at the Si-SiO_2 interface to adsorbed O_2 at the SiO_2 surface. They reported that for oxidation in humid air, the thickness of the growing oxide (measured by XPS) did not increase steadily with time, t, but had a relative maximum immediately after the completion of the first layer [16]. This observation was deduced from an inspection of XPS data. XPS analysis from a previous work performed by Nymark [5] stated that the oxide layer did not increase with increasing exposure to humid air, but rather showed a maximum constant value.

A previous study done by Nymark [5] showed that exposing silicon powder to humid air at 22°C, giving a vapor pressure of 0.026 atm, affected the oxidation of silicon in water compared to powder stored at dry conditions. When silicon reacts with water hydrogen is formed as a consequence of the oxidation process, as seen in Equation 2.1.2. By exposing the silicon powder to humid air before reacting it with water Nymark [5] concluded that the hydrogen evolution was affected, which was seen both in the onset time for hydrogen evolution and the total amount of hydrogen evolved in a four hour long experiment. For powder exposed to humid air for 35 days before reaction with water, the onset time for hydrogen evolution was later compared to powder exposed only for two days to air with the same humidity. On the basis of these experiments it was believed that an oxide layer builds up during storage, resulting in later onset time for hydrogen evolution because the oxide layer formed must dissolve before silicon reacts with the solution. The procedure used for these experiments has later shown not to be adequate, raising some questions to these conclusions.

2.5.3 Aqueous oxidation of silicon

The reaction between silicon and water will be dependent on the oxide layer formed on the particle surface of silicon. The silioxane links (Si-O-Si) at the silica surface will react with water at ambient temperatures [10], as seen in Equation 2.2.1, giving silanol groups at the surface. If silica is exposed to water for longer times hydrolysis can result in dissolution of the silica layer exposing the underlaying silicon to water. When silicon is mixed with water it oxidises forming silicon dioxide and hydrogen gas according to Equation 2.5.2.

$$\mathrm{Si(s)} + 2\,\mathrm{H_2O(l)} \longrightarrow \mathrm{SiO_2(s)} + 2\,\mathrm{H_2(g)} \tag{2.5.2}$$

Surface area analysis of silicon powder reacted with water, performed by Jørgensen [13] showed that the surface area increased as the total hydrogen evolution increased. The results were believed to display the surface area of the silica particles attached to the silicon particle, rather than the surface area of the whole silicon particle with a silica layer. SEM analysis of the oxidised silicon particles revealed that the powder was covered with an oxide layer, while the non-oxidised powder was not [13]. The non-oxidised powder consisted of particles with smaller particles attached, while the oxidised powder seemed to be covered with a "mud-like" layer which Jørgensen [13] thought to be the oxide layer consisting of small silica particles. Jørgensen [13] concluded that the measured surface area and the SEM investigation agreed with the assumption that oxidation of silicon in water led to the formation of silica on the silicon powder.

From the oxidation experiment performed by Jørgensen [13], it was found that the amount of oxygen increased as the total amount of hydrogen evolved increased. It was also observed that the formation of silicic acid was the dominant reaction early in the oxidation process, following Equation 2.5.3. When the amount of hydrogen evolved increased a shift in the dominating reaction was observed, and silica was formed, following Equation 2.5.2. Jørgensen [13] believed that this shift was liable

since the silicic acid reaches a solubility limit [10] and the formation of colloidal silica through condensation would be the dominating reaction.

$$\mathrm{Si(s) + 4\,H_2O(l) \longrightarrow Si(OH)_4(aq) + 2\,H_2(g)} \tag{2.5.3}$$

2.5.4 Thermal oxidation of silicon

Thermal oxidation of silicon has been extensively studied in relation to the semiconductor industry, and passivation of the silicon surface. Exposing silicon to an oxidising environment of O_2 or H_2O at elevated temperatures will result in an oxide layer at the silicon surface. Since silicon spontaneously form a stable oxide layer even at room temperature if oxidising species are present, the elevated temperatures used in thermal oxidation primarily serves as an accelerator of the oxidation process. This results in a thicker oxide layer per unit of time [17].

Either water vapour or molecular oxygen can be used as oxidants in the thermal oxidation, known as wet or dry oxidation, given in Equation 2.5.4 and 2.5.5 respectively. Wet oxidation usually gives a higher oxide growth rate than dry oxidation, and is therefore preferred when growing thick oxides. Thermal oxidation is usually performed in furnaces at 800 - 1200°C. The oxides formed by wet and dry thermal oxidation are comparable in terms of quality [18].

$$\mathrm{Si(s) + 2\,H_2O(l) \longrightarrow SiO_2(s) + 2\,H_2(g)} \tag{2.5.4}$$

$$\mathrm{Si(s) + O_2(g) \longrightarrow SiO_2(s)} \tag{2.5.5}$$

Liu *et al.* [19] used Raman spectroscopy to study silicon nanowires (Si-NW) before and after annealing at 800 °C in O_2, for different times, to get at clearer picture of the oxidation mechanism and its inpact on the structure of the Si-NWs. Crystalline silicon will appear as a narrow symmetrical peak at 521 cm^{-1} i present in the sample. After annealing, is was observed that this peak was shifted from a narrow symmetrical peak to a broad asymmetrical peak at 480 cm^{-1} corresponding to amorphous silicon. Liu *et al.* [19] concluded that the spectra obtained after annealing showed an amorphous layer composed of both amorphous silicon and amorphous silica. According to this, the spectrum can be decomposed into the crystalline component and amorphous component induced by the large stress at the Si/oxide interface.

In Figure 2.5.4, a schematic illustration based on this theory shows a hypotesis of the oxidation process that is believed to occur. The first figure show a crystalline silicon core surrounded by an amorphous layer of silicon and a surface layer of amourphous silica. Based on this hypotesis, it is believed that the formation of an amorphous silicon layer could be necesarry for an amorphous silica layer to form. When the grains oxidise more crystalline nano-inclusion is believed to form in the amorphous silicon matrix as the crystalline silicon core is consumed. This is shown in the second figure.

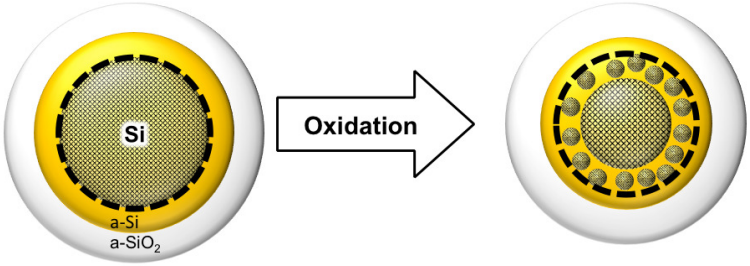

Figure 2.5.4: Hypotesis and schematic illustration of the oxidation process of crystalline silicon. Si refers to crystalline silicon, a−Si to amorphous silicon and a−SiO_2 to amorphous silica. The small grey dots illustrates crystalline nano inclusions [20].

2.6 Stabilisation of silicon in water

The stability of the dispersion of silicon and water is a very important parameter for obtaining a dense green body. The suspension properties of silicon powders are influenced by the oxide layer formed on the surface and the storing history of the powders [9].

Most oxide surfaces are hydrated [12], therefore when silicon is introduced into a acid or basic solution the silicon surface will be charged because of adsorption of ions onto the surface. In acid solutions, adsorption of H^+ ions produces a positively charged surface, Equation 2.6.1, whereas in basic solution, adsorption of OH^- ions leads to a negatively charged surface, Equation 2.6.2. This is illustrated in Figure 2.6.1.

$$SiOH + H^+ \longrightarrow SiOH_2^+ \tag{2.6.1}$$

$$SiOH + OH^- \longrightarrow SiO^- + H_2O \tag{2.6.2}$$

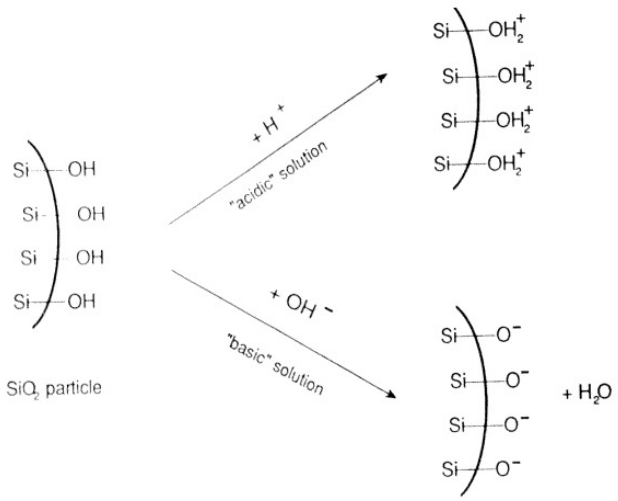

Figure 2.6.1: The production of surface charges on SiO_2 particles by adsorption of ions from acidic or basic solutions [12].

The pH at which the adsoption of H^+ and OH^- on the particle surface is balanced is called the point of zero charge (PZC), where the surface is effectively neutral. Acidic oxides like SiO_2 have a low PZC and basic oxides like Al_2O_3 have high PZC, 2 and 8-9 respectively [12]. However, according to Rahman [12] it is more convenient to measure the potential at short distance from the particle surface to describe the charge of a particle when dealing with ceramic suspensions. This layer is called the Stern layer, shown in Figure 2.6.2. The potential at the Stern layer is called the zeta-potential, and the pH giving zero zeta potential is the isoelectric point (IEP). According to Figure 2.6.3 the zeta-potential of silicon in water is found to be zero at pH 4.1.

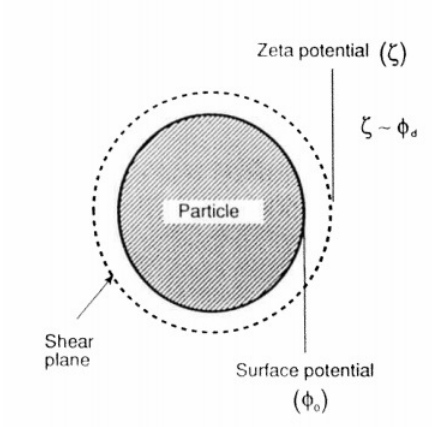

Figure 2.6.2: The zeta-potential (ζ) is taken to be the electric potential at the plane of shear between the particle and the electrolyte solution [12].

From Figure 2.6.3 it can be seen that the zeta potential for silicon particles decreases with increasing pH. Thus, increasing the pH result in a charge on the particle surface, leading to a more stable suspension because of the repulsion between the particles. According to Richerson [1] high pH results in excellent dispersions and low viscosity for silicon particles, where a pH of about 9 is judged to be optimum. In the slip cast forming method of ceramics where the slip is poured into a mould, low viscosity is important. The viscosity as a function of pH for different slips with 30 vol% silicon is shown in Figure 2.6.4. For pH 9 the viscosity is independent of the shear rate, and the dispersion is said to show a Newtonian behaviour [12], which yields the most stable dispersions.

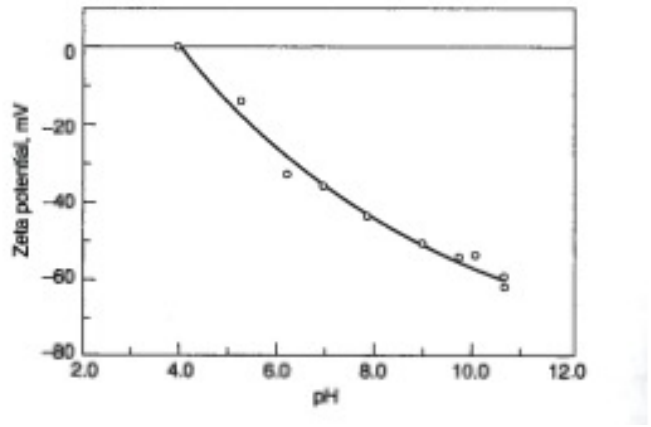

Figure 2.6.3: Zeta potential as a function of pH for silicon particles in water showing a lowering in zeta potential as the pH is increased [1].

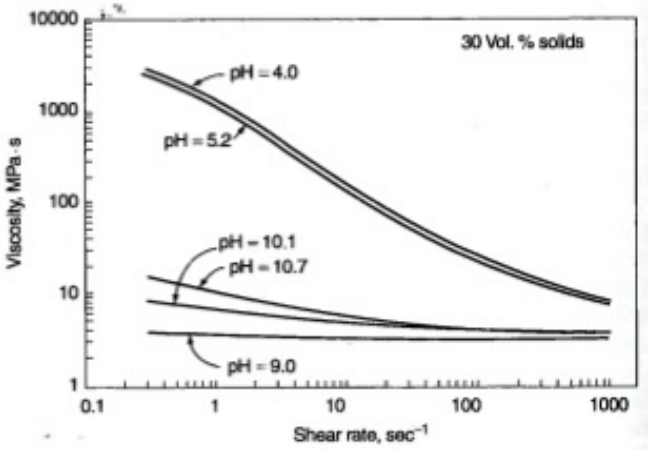

Figure 2.6.4: Viscosity as a function of pH for slips containing 30 vol% silicon in water [1]. For pH 9 the viscosity shows a Newtonian behaviour.

The system, consisting of particles and the electrolyte must be electrically neutral. Thus, there must exist an equal and opposite counter charge in the solution because of the charged particle surface. This give rise to a diffuse electrical double layer of charges between the particles. An illustration of the electrical double layer is given in Figure 2.6.5. As two particles approach one another in the liquid, the diffuse double layers starts to overlap.

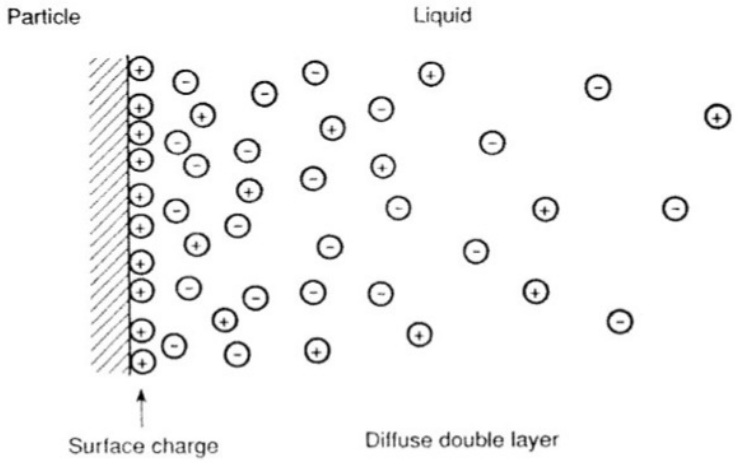

Figure 2.6.5: Electrical neutrality of the system give rise to a diffuse electrical double layer outside the particles [12].

In ceramic suspensions there exists attractive Van der Waal forces and electrostatic- or steric repulsive forces between the particles. In Figure 2.6.6 the potential energy between two particles in a liquid resulting from the net effect of the attractive- and repulsive forces is illustrated. If the attractive forces are large enough they will lead to coagulation (*M1*) or flocculation (*M2*) of the particles. To obtain a stable dispersion, this must be avoided. To hinder the particles to "stick" together, the repulsive forces between the particles must therefore be larger than the attractive forces [12]. This can be achieved by for instance increasing the double layer repulsion between the particles. There are three common methods of stabilising a suspension; Electrostatic stabilisation, Polymeric stabilisation or Electrosteric stabilisation, which is a combination of the two. Theory discussing this is beyond the scope of this thesis. For readers interested in these topics a more detaild description can be found in "Ceramic processing and sintering" by Rahman [12].

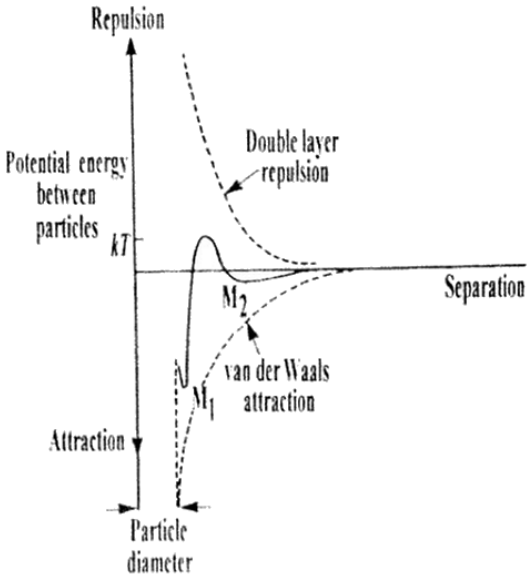

Figure 2.6.6: Potential energy between two particles in a liquid resulting from the net effect of repulsive- and attractive forces [12].

2.7 X-ray photoelectron spectroscopy

X-ray photoelectron spectroscopy is a non-destructive surface analysis technique used to obtain chemical information about the surface of solid materials [21].

The sample is irradiated by an X-ray photon of energy hv, which leads to ionisation and ejection of an core electron. The kinetic energy (E_k) of the electron is measured and then analysed by the electron spectrometer, resulting in a graph of intensity vs. electron energy. An illustration of the process of photoemission is shown in Figure 2.7.1 [22], where an electron is ejected from the atom.

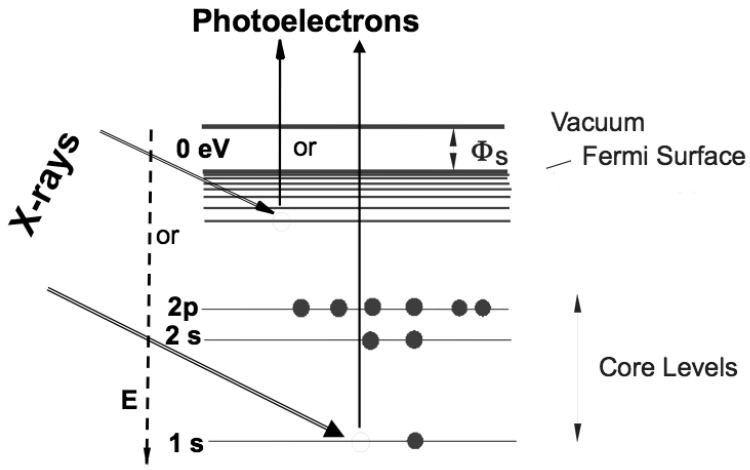

Figure 2.7.1: Schematic diagram of the XPS process, showing irradiation of an core electron by an X-ray photon leading to photoionisation of the atom by the ejection of a 1s electron [23].

The kinetic energy of the electrons measured is not an intrinsic material property since it is dependent on the photon energy of the X-rays employed. The electron is rather identified by its binding energy (E_B), and the relationship between the parameters involved in the XPS analysis is shown in Equation 2.7.1

$$E_B = hv - E_k - W \tag{2.7.1}$$

The photon energy is given as hv, E_K is the kinetic energy of the electron, and W is the work function of the spectrometer. All of the quantities on the right-hand side of the equation are known or measurable, thus the binding energy of the electron can easily be calculated.

The ability to distinguish between different oxidation states and chemical environments of the sample [21] is one of the major strengths of the XPS analysis technique. Atoms bonded to different chemical species exhibit different binding energies. The difference in binding energies can be seen by shifts of peak positions between the two different chemical environments, known as a chemical shift [24]. In a study of the oxidations states of Si performed by Thøgersen *et al.* [24] XPS was used to identify and detect the amount of elemental Si present in SiO_2. Five oxidation states were reported to be present in Si/SiO_2 systems, corresponding to five chemical states Si^0, Si_2O, SiO, Si_2O_3 and SiO_2. Figure 2.7.2 gives a suggestion of how oxygen is bonded to silicon for Si_2O, SiO, Si_2O_3.

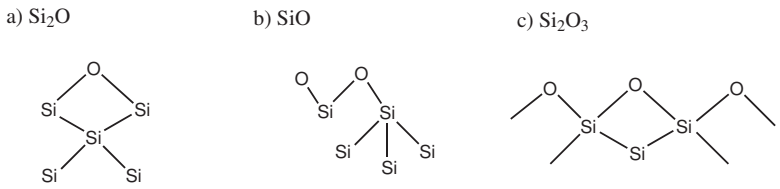

Figure 2.7.2: Schematic illustration of how the oxygen are bonded to silicon. a) Si_2O, b) SiO and c) Si_2O_3 with the valences Si^{1+}, Si^{2+}, Si^{3+} respectively [25].

A possible approach on how to estimate the thickness of the oxide on the silicon surface is described by Watts and Wolstenholme [22]. This approach is based on the SiO_2/Si intensity ratio and refers to oxide grown on flat samples.

2.7.1 The photoelectron spectrum

The calculated binding energy found from the measured energy of the ejected electron is shown in a photoelectron spectrum vs. the measured intensity. The photoelectron spectrum will reproduce the electronic structure of an element quite accurately since all electrons with a binding energy less than the photon energy will feature in the spectrum. The characteristic peaks appearing in the spectrum are the contribution from electrons which are excited without energy loss, whereas the electron that suffers energy loss contribute to the *background* of the spectrum [21].

2.7.2 Analysis depth

The analysis depth of XPS analysis is determined by the attenuation length (λ) of the electrons, which is related to the inelastic mean free path (IMFP), and varies with the kinetic energy of the electrons under consideration. 95% of the signals will emanate from a depth of d$\cong 3\lambda$. The typical analysis depth are between 5 and 10 nm. XPS is a very surface sensitive technique because emitted photoelectrons have very short inelastic mean free path [21].

2.8 Raman Spectroscopy

Raman spectroscopy is a spectroscopic technique used to study vibrational or rotational modes in solid, liquid or gaseous samples. The sample is irradiated by a monochromatic light source, and the incident photons interacts with the material of the sample.

The interaction can lead to absorption, reflection or scattering of photons. The scattering can be either elastic, known as Rayleigh scattering, or inelastic, known as Raman scattering. It is the inelastically scattered photons that is utilised in Raman Spectroscopy. The energy of the inelastically scattered photons can be shifted up or down in comparison with the incident energy. This shift in energy is

known as the Raman effect [26] and provides chemical and structural information about the molecules in the sample. Rayleigh scattering is filtered out because it do not provide any information about vibrational changes [26].

For the Raman scattering, the interaction between photons and the material leads to distortion of the electron cloud around the nuclei to form a short-lived state called a 'virtual state' [27], thus the photons are excited from the initial state (ν_0) to a virtual energy state. This state is not stable and the photons are quickly re-raditated [27], which gives a shift in energy that is either higher or lower than the incident energy. If the final vibrational state of the molecule is more energetic ($\nu_0 - \nu_m$) than the initial state the emitted photons will be at a lower frequency in order for the total energy of the system to remain balanced. This is called a Stokes shift. If, on the other hand, the final vibrational state of the material is less energetic ($\nu_0 + \nu_m$) than the initial state the emitted photons will be at a higher frequency, designated as an Anit- Stokes shift. In Figure 2.8.1 the different scatterings are shown.

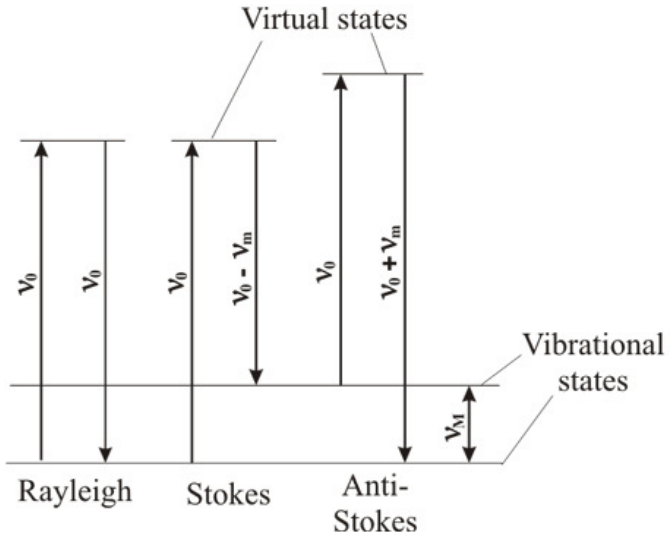

Figure 2.8.1: Schematic illustration of the different scattering processes. Rayleigh scattering, Stoke scattering and Anti-Stoke scattering are shown [26].

At room temperature the population state of a molecule is in the ground vibrational state. Because Stokes scattering is the most probable scattering process this isusually preferred. Stokes scattering is recorded in the low-energy side and Anti-Stokes scattering is recorded in the high-energy side, as illustrated in Figure 2.8.2. The intensity obtained for Stoke scattering is higher than for Anti-Stoke scattering, giving cleared peaks in the Raman spectra.

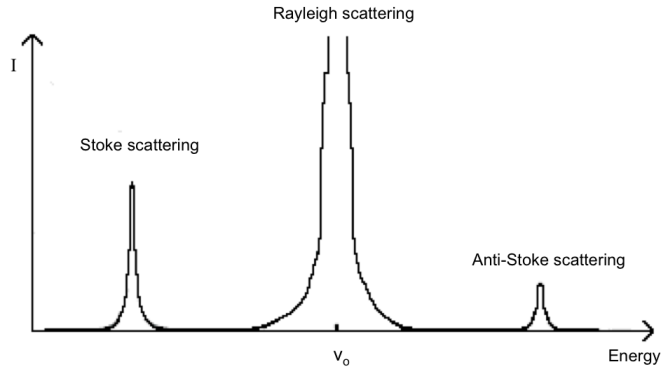

Figure 2.8.2: Illustration of intenisty as a function of Energy. Rayleigh scattering at υ_0, Stoke scattering shifted to lower energies and Anti-Stoke scattering shifted to higher energies [20].

The amount of energy change, either loss or gain, of a photon is characteristic of the nature of each vibrational mode present in the sample. It therefore provides a fingerprint by which the material can be identitied. The monochromatic light used is usually from a laser in the visible, near infrared or near ultraviolet range. The Raman shift are typically expressed in wave-numbers. The crystalline silicon peak can be found at 521 cm^{-1} and the amorphous silicon is shown as a broad, weak 'bump' at 480 cm^{-1}.

Chapter 3

Experimental

3.1 Silicon powder and overview of experimental methods

The silicon powder investigated was delivered by Elkem. The powder was jet milled in August 2011 and stored in a plastic bottle before any further process was performed.

Table 3.1.1 gives an overview over particle size and mechanical and chemical treatment of the silicon powder. The chemical analysis is given in Table 3.1.2. The powder was Jet milled which can affect the crystallinity of the material. Acid treatment of the powder may also affect the surface properties of the material.

Table 3.1.1: Mechanical and chemical treatment of the silicon powder delivered by Elkem.

Sample	*Size*	*Mechanical treatment*	*Chemical treatment*
Silicon powder	0-75µm	Jet milled	Acid treated

Table 3.1.2: Chemical analysis of the silicon powder. Measurements performed by Elkem.

Sample	*Si%*	*Fe%*	*Al%*	*Ca%*	*Ti%*
Silicon powder	99.54	0.12	0.20	0.024	0.012

Before the silicon powder was examined it was divided into three batches. For convenience, it is named Batch A, Batch B and Batch C. The storing history of the different batches is given below.

- Batch A: exposed to humid atmosphere at different temperatures for different time periods directly after storage in the plastic bottle.

- Batch B: stored in a desiccator for several months after storage in the plastic bottle. It was then exposed to humid atmosphere at different temperatures for different time periods.

- Batch C: stored in a desiccator for three weeks after storage in the plastic bottle and not exposed to humid air

Powder from Batch A and Batch B were exposed to humid air at 10 °C and 22 °C. Batch C was only used for a reproducibility tests for the hydrogen measurements.

After storage and exposure to humid air the powder was mixed with water in a purpose built apparatus and oxidised. The amount of hydrogen formed in the aqueous oxidation reaction was measured as a function of how long the powders were aged in humid air. Selected samples from the reacted powders were further analysed by SEM and by measuring the BET surface area and the oxygen content. For comparison, powder not exposed to humid air was reacted with water and analysed. Thermal treatment of silicon powder was also performed. XPS analysis was performed on selected unreacted samples exposed to humid air or thermally treated to give an idea about how storage and thermal treatment affects the growth of a possible oxide layer. Figure 3.1.1 summaries the experimental methods and which powders that were analysed by the different methods.

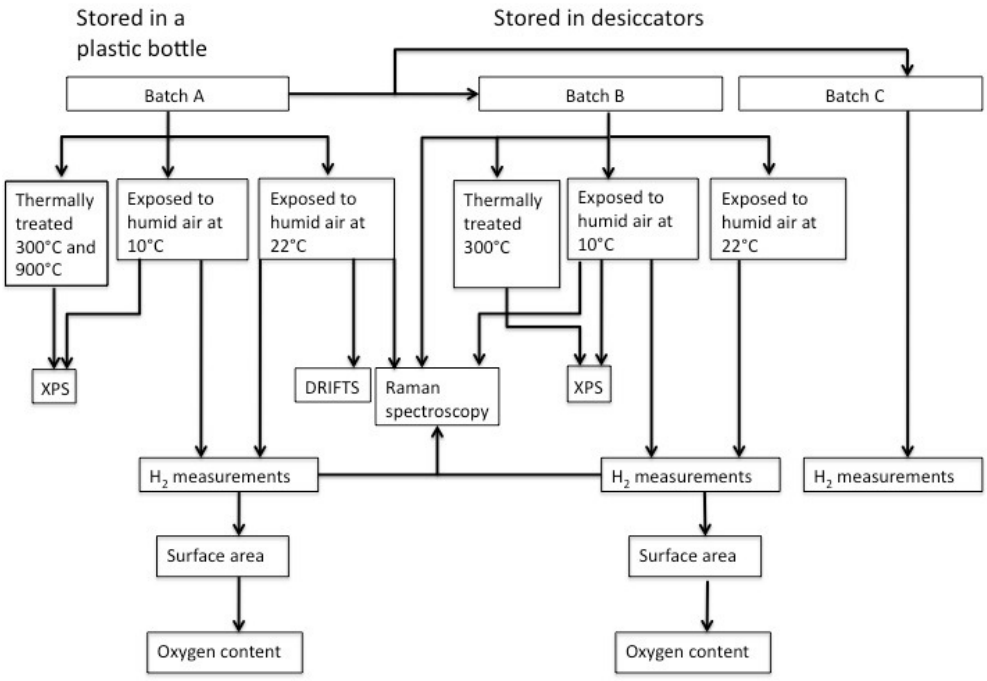

Figure 3.1.1: Overview of powder batches, ageing of silicon powder and experimental methods used to analyse the silicon powder.

3.2 Oxidation of silicon powder

3.2.1 Ageing of silicon powder and exposure to humid air

About 2 grams of silicon powder were weighed, put in open petri dishes and put into tight containers containing a beaker with water giving a humid atmosphere. The containers were then placed into either a incubator to obtain a controlled temperature of 22 °C (±1 °C), or in a wine cooler to obtain a controlled temperature of 10 °C (±1 °C). This gave a saturation vapour pressure of 0.026 atm in the incubator and 0.012 atm in the wine cooler. The calculations for the saturated vapour pressures can be found in Appendix B. The powders were not in contact with the water. An overview of the ageing history is given in Table 3.2.1 and Table 3.2.2. The samples were taken out after a certain time of exposure to humid atmosphere and reacted with water. The sample code tells how many days the powders were exposed to humid air and which temperature it was aged at.

All the samples from Batch A are indicated by *A*, samples form Batch B are indicated by *B* and samples from Batch C are indicated by *C* a at the start of the sample code. As an example, A-D8.1-10C is powder from Batch A, aged 8 days in humid air at 10 °C before it was taken out. Sample B-D0.1 is powder from Batch B not exposed to humid air. If several parallels of powders with the same storing history have been examined a number will be given after the dot, as 1 and 3 in A-D8.1-10C and A-D8.3-10C indicates parallel 1 and 3 of powders from Batch A aged 8 days at 10 °C. Four samples from Batch A, sample A-D2-10C, A-D49-10C, A-TO-300C and A-TO-900C were only analysed by XPS and not reacted with water. Sample A-D57-22C, B-D30-10C and B-D0.2 was only analysed by Raman Spectroscopy and not reacted with water. Sample A-D21.2-22C was only analysed by DRIFTS and not reacted with water. For Batch B there are one sample code, B-D1-10C-hpH, which has an extra note at the end, *hpH*, indicating that a higher pH was used in the aqueous oxidation experiment for this sample.

Table 3.2.1: Overview of the ageing history of the silicon powders from Batch A[1] and Batch B[1].

Sample batch	*Atmosphere exposed to*	*Sample code*	*Exposure to humid air [days]*
Batch A	10 °C - 0.012 atm	A-D2-10C	2
		A-D8.1-10C	8
		A-D8.3-10C	8
		A-D10.1-10C	10
		A-D14.1-10C	14
		A-D21.1-10C	21
		A-D35.1-10C	35
		A-D49-10C	49
	22 °C - 0.026 atm	A-D1.1-22C	1
		A-D7.1-22C	7
		A-D7.2-22C	7
		A-D15.1-22C	15
		A-D21-22C	21
		A-D23.1-22C	23
		A-D35.1-22C	35
		A-D57-22C	57
	22°C - Dry	A-D0.1	0
		A-D0.2	0
	300°C - Air	A-TO-300C	-
	900°C - Air	A-TO-900C	-
Batch B	10 °C - 0.012 atm	B-D1.1-10C	1
		B-D3.1-10C	3
		B-D3.2-10C	3
		B-D5.1-10C	5
		B-D5.2-10C	5
		B-D7.1-10C	7
		B-D14.1-10C	14
		B-D14.2-10C	14
		B-D28.1-10C	28
		B-D30-10C	30
		B-D1-10C-hpH	1
	22 °C - 0.026 atm	B-D1.1-22C	1
		B-D3.1-22C	3
		B-D5.1-22C	5
		B-D5.2-22C	5
		B-D7.1-22C	7
		B-D14.1-22C	14
		B-D14.2-22C	14
		B-D28.1-22C	28
	22°C - Dry	B-D0.1	0
		B-D0.2	0
	300°C - Air	B-TO-300C	-

[1] Batch A - powder exposed to humid air directly after storage in a plastic bottle. Batch B - powder that in addition is stored in a desiccator in several months before exposure to humid air.

Table 3.2.2: Overview of silicon powder from Batch C[1] not exposed to humid air.

Sample batch	*Atmosphere exposed to*	*Sample code*	*Exposure to humid air [days]*
Batch C	22°C - Dry	C-D0.1	0
		C-D0.2	0
		C-D0.3	0

[1] Powder from Batch C is stored in a desiccator for three weeks after storage in a plastic bottle and not exposed to humid air.

3.2.2 Thermal treatment of silicon powder

Thermal treatment of the silicon powder was carried out in a LabStar 1200/4 chamber furnace. Each heat treatment was executed at the desired temperature for 1 hour. The heating and cooling rate vas 200 °C/h to avoid unfortunate reactions within the powder. Figure 3.2.1 shows the temperature profile 1 and 2 used for powders heat treated at 300 °C and 900 °C, respectively.

The silicon powder (2 g) was placed into alumina crucibles and mounted into the furnace. The heating program was set and the heating started.

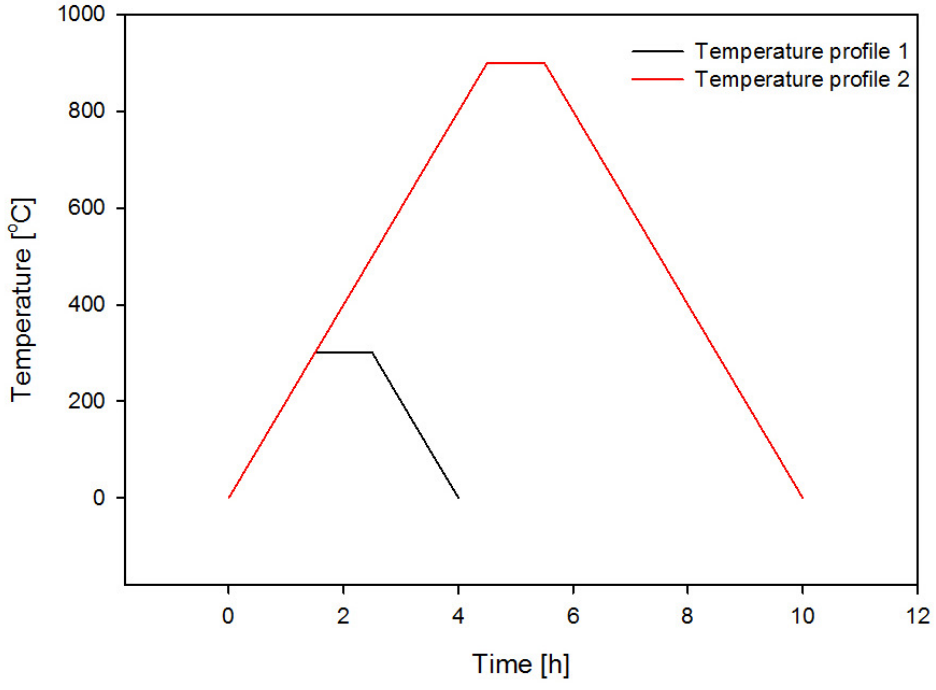

Figure 3.2.1: Temperature profiles for the thermal treatment of silicon powder.

3.2.3 Hydrogen evolution measurements

The apparatus used for the hydrogen evolution measurements was built by Rune Nilsen [28] and Jan Otto Hoel from Elkem, and modified by Håkon Trygve Strøm

Jørgensen [13]. But since the results done by author [5] in the project thesis showed some scattering and variations with respect to the hydrogen flow and onset-time some modification was needed. The modified apparatus is shown in Figure 3.2.2. Before any experiments were started both flow meters were calibrated according to a procedure described more detailed in Appendix A.

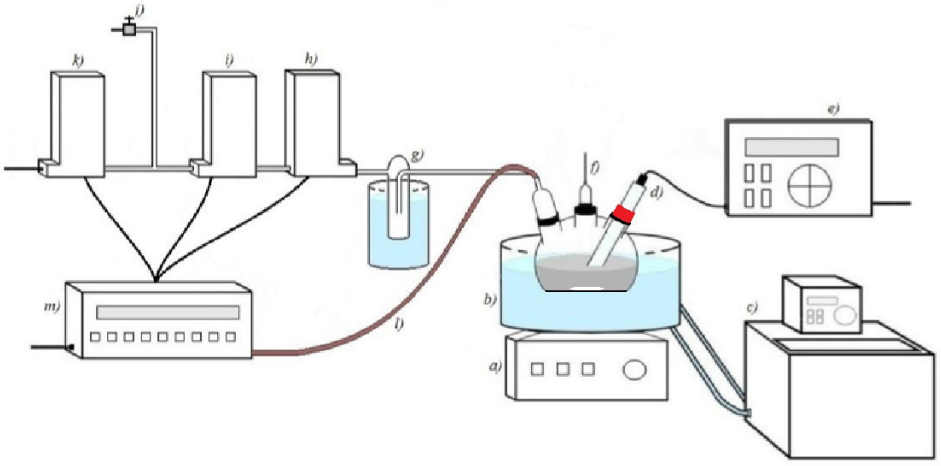

Figure 3.2.2: The modified apparatus used for the oxidation of silicon powder. a) Magnet stirrer, b) Water bath - 60 °C, c) Heat circulator, d) pH-electrode, e) pH-meter, f) N_2-input, g) Cold trap - liquid N_2, h) Pressure sensor, i) Flow meter - large range, j) Valve, k) Flow meter - small range, l) Thermocouple - type K, m) Data logger.

All measurements were carried out as equal as possible to ensure comparable results, and to avoid possible sources of error. The pH was raised to 9.4 and the temperature in the water bath was 60 °C. Before each experiment the pH-electrode was calibrated using buffer solutions at pH 7.01 and pH 10.01. This is described more detailed in Appendix A. The duration of hydrogen evolution was set to 90 minutes for all experiments.

The procedure is described in detail below.

- About two grams of silicon powder (dry, exposed to humid air or thermally treated) were weighed out and mixed with 50 mL distilled water.
- The slurry was poured into a three necked bottle with a flat bottom, and put into a preheated water bath *(b)* placed on a magnet stirrer *(a)*, which was used to agitate the slurry. The same rotation speed was used for all experiments. The water in the water bath covered the height of the slurry in the bottle. A heat circulator *(c)* from Julabo was used to preheat the water bath.
- The cold trap *(g)* was led into the container with liquid nitrogen.
- The apparatus was flushed with nitrogen through input *(f)* before logging to remove air.

- When the temperature of the slurry reached 60 °C, ammonia was added through input *(f)* to give a pH of 9.4. It took about ten minutes from the powder was mixed with water until the pH adjustment was finished. The pH was measured by an Inlab 413SG pH-electrode *(d)* and registered by a Seven Easy S20 pH-meter *(e)* from Mettler Toldeo.

The gas flow was led through a cold trap *(g)* cooled with liquid nitrogen to ensure that water vapour and ammonia gas was removed before the gas flow entered the pressure sensor *(h)* and the flow meters *(i* and *k)*. The pressure was measured by a pressure sensor *(h)* delivered by Ellison sensors International, and the gas flow was measured by flow meters delivered by Bronkhorst High Tech. Flow meter *(i)* had a capacity of 170 mL/min, and flow meter *(k)* had a capacity of 3.7 mL/min. Only flow meter *(i)* was used during the experiments, valve *(j)* was therefore always open. The gas flow was logged by an Agilent 34970A data acquisition/switch unit *(m)* connected to a computer with a Benchlink logging software. The temperature of the slurry was measured by a type K thermocouple *(l)*.

During the experimental work problems with noise and scattering were identified. This led to a change in the experimental routine, which is further described in Appendix A. The result of the change was that the cold trap was led into the liquid nitrogen *after* the apparatus had been flushed with nitrogen gas, rather than *before*. A lower gas flow was measured for most of the samples and consequently only the fine flow meter *(k)* was used, valve *(j)* was therefore closed. The pH electrode suffered high wear when it was exposed to the agitated slurry. It was therefore decided that the electrode only should be used in the start and at the end of the experiment, it was therefore taken out during the experiment to increase its lifetime.

3.2.4 Drying of the slurry

After the aqueous oxidation reaction the slurry containing reacted silicon powder and water was poured into a beaker and dried in a furnace at about 100 °C, leaving the dried powder. The powder was collected and mortared to give a homogeneous mixed powder before further analysis.

3.3 Thermogravimetric analysis

Thermogravimetric analysis (TG-analysis) is a method where weight loss is measured as a function of temperature. However, if the material reacts with the surrounding atmosphere it can also gain weight.

TG-analysis of the silicon powder was measured with a Netzsch STA449 C Jupiter J, and was carried out by Eli Beate Larsen. First, a background analysis of an empty alumina crucible was performed using the same heating program and air atmosphere that would be used in the analysis of the powder samples. The background analysis was later used as a correction of the actual analysis to obtain a

correct result for the samples. The powder samples were heated 1.67 °C/min up to 1600 °C in air in an alumina crucible.

3.4 Surface area measurements

The surface area of selected reacted powders from both Batch A and Batch B were examined by nitrogen adsorption using a Tristar 3000 from Micromeritics. First the sample holder was weighed, then the powder was added and the sample holder was weighed again. The sample holder was then degassed overnight under vacuum at 250 °C. The following day the sample holder was again weighed in case any weight was lost due to volatile species. The mass of the powder was then determined. The sample tubes were mounted into the Tristar 3000 machine and liquid nitrogen was added to a cold-bath inside the machine before the measurements started. The data was logged and the surface area was determined by the 5-point BET method [29].

3.5 Oxygen analysis

The oxygen content was measured by performing a LECO analysis. Selected samples from both Batch A and Batch B were analysed. The samples were weighed in a tin capsule. The capsule was closed and the air was removed before it was placed into the apparatus. Before the analysis started both the sample and the furnace chamber were flushed with helium. A graphite crucible was placed between two electrodes working as a heating element. After all of the oxygen in the chamber was removed the sample was put into the graphite crucible. The oxygen in the sample reacted with the carbon and CO and CO_2 were formed. The amount of CO and CO_2 was measured and the oxygen content could be determined [30]. The analysis was performed by Anne Støre at SINTEF.

3.6 Scanning electron microscopy analysis

Selected powder samples from Batch A and Batch B were analysed by Scanning electron microscopy (SEM). The powder samples analysed had been exposed to different humidity, reacted with water at pH 9.4 and 60 °C and dried. It is important to mention that the hydrogen evolution time was not the same for the samples from Batch A. However, the humid samples from Batch B have the same hydrogen evolution time. A Hitachi SU6600 SEM was used for all measurements.

The silicon powders analysed were prepared in two ways;

1. Ethanol was added to some material and mixed in an ultra sound bath to separate fine and coarse particles. Coarse particles sediment, while fine particles flow. A couple drops of the mixture were dried on a carbon tape and analysed.

2. The particles, as received, were sprinkled onto a stub or carbon tape and analysed

The analysis of powder from Batch A was performed by Anne Grete Forwald at Elkem Solar [31].

3.7 X-ray Photoelectron Spectroscopy

X-ray photoelectron spectroscopy (XPS) was performed on selected samples from Batch A by Spyros Diplas at SINTEF Materials and Chemistry, Oslo. The instrument used was a KRATOR AXIS ULTRA^{DLD} spectrometer using monochromatic Al Kα radiation (hν =1486.6 eV) at 15kV and 10 mA.

The samples were mounted on Cu sample holder and inserted into the spectrometer fast entry lock where they remained overnight until a vacuum level of approximately 5×10^{-7} mbar was established. This was in case of gas emission from the sample. The samples were transferred into the analysis chamber for XPS analysis the following day.

Pass energies of 160 eV and 20 eV were used for the survey scans and the high resolution scans respectively. The samples were focused, and charge neutralisation was applied to compensate for the non-conducting sample. The charge compensation was achieved with the use of low energy electrons driven by a magnetic field towards the sample surface. The peaks were later shifted to their correct positions during data processing, to correct for the overcompensation. This was done by correcting the energy of the spectrum by placing the C 1s at 285 eV. During analysis the vacuum in the analysis chamber was 5×10^{-9} mbar. The same procedure was followed for every sample and the same energies were used [32].

To estimate the oxide thickness the approach described by Watts and Wolstenholme [22] was used, which refers to oxides grown on flat samples. Curvature effects and surface roughness were not taken into account, and only the SiO_2/Si-ratios were considered for the estimation calculations. The thickness of the oxide layer on the α-Si wafer is estimated to 0.6 nm as a reference [32].

3.8 Diffuse Reflectance Infra-red Fourier Transform

Diffuse Reflectance Infra-red Fourier Transform analysis (DRIFTS) was performed on a powder sample A-D21-22C, from Batch A, exposed to humid atmosphere for three weeks. The analysis was performed by Tina Kristiansen at the Department of Chemistry.

3.9 Raman spectroscopy

Raman spectroscopy was performed on selected silicon powder samples from Batch A and Batch B. The instrument was a Horiba Jobin Yvon, LabRam HR800 UV. Powders exposed to humid air at both 22 °C and 10 °C not reacted with water, dry powders from Batch B and two aqueous oxidised samples were analysed. The samples were prepared by mounting small amounts of powder in an XRD-sample holder and put into the laser beam path of the instrument. The UV laser, at 325 nm, was used for all samples.

Chapter 4

Results

4.1 Powder characterisation

The powder characterisation is meant to give an overview of the powders, and especially in order to be able to compare the results from the different analysis methods.

The BET surface area of the silicon powder was measured in a previous work by the author [5] and found to be 0.69 m^2/g. The 5-point BET surface area plot can be found in Appendix C. The particle size distribution of the powder can be seen in Figure 4.1.1, and the cut-off values are given in Table 4.1.1.

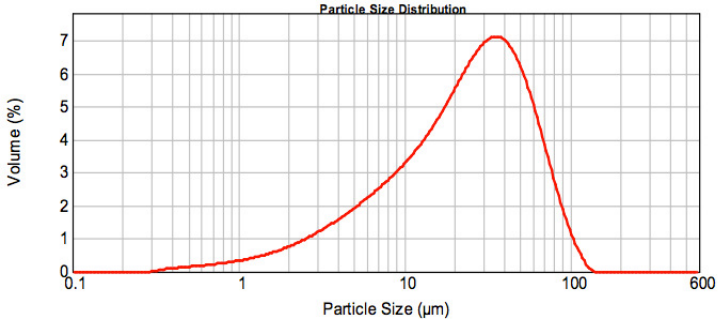

Figure 4.1.1: Particle size distribution of silicon powder. Measurements performed by Elkem.

Table 4.1.1: Cut-off values from the particle size distribution of the silicon powder. Measurements performed by Elkem.

Sample	*d(0.1)* (μm)	*d(0.5)* (μm)	*d(0.9)* (μm)
Silicon powder	4.05	18.98	45.45

4.1.1 Air oxidation behaviour

The result from the Thermogravimetric analysis (TGA) of silicon powder from Batch A is shown in Figure 4.1.2, describing how the mass changes with temperature. It can be seen from the figure that mass gain starts at about 800 °C, indicating the growth of an oxide layer.

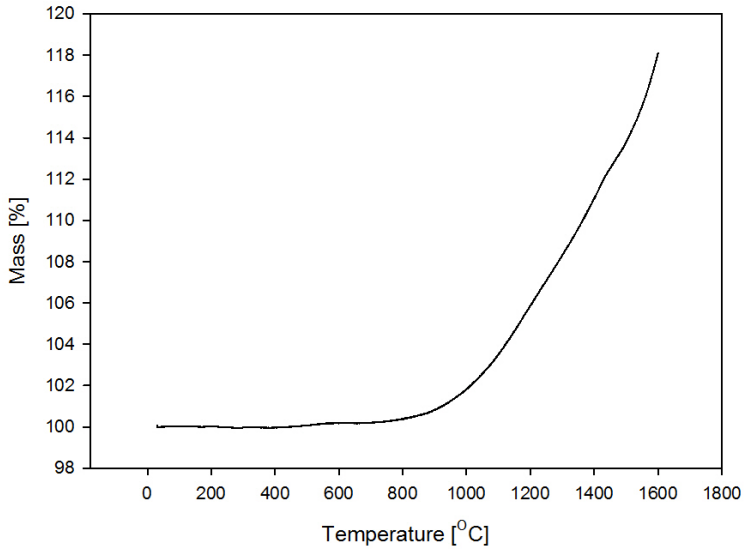

Figure 4.1.2: Thermogravimetric analysis of silicon powder from Batch A.

4.2 Characterisation of silicon powder aged in humid air at 10°C

4.2.1 XPS analysis

Selected samples of powder from Batch A were stored in humid air at 10 °C for different periods of time and analysed with XPS. Powder A-D2-10C and A-D49-10C exposed to humid air at 10°C for 2 and 49 days, respectively, were analysed. These XPS results are plotted together with samples exposed to humid air at 22 °C for 2 and 35 days from a previous study by the author [5].

Figure 4.2.1 shows the survey scan taken from the two samples stored in humid air at 10°C, showing the various elements present on the samples surface. Sodium, oxygen, copper, carbon and silicon are observed. Presence of copper in sample A-D49-10C could be attributed to signals from the sample holder, while the sodium content, found in both samples, can be due to inhomogeneous powder from the sample batch. No apparent difference in Si 2s and Si 2p intensity can be seen between the two samples, but it appears like the intensity for the O 1s peak for sample A-D49-10C is higher than for sample A-D2-10C. This indicates higher oxygen content in sample A-D49-10C.

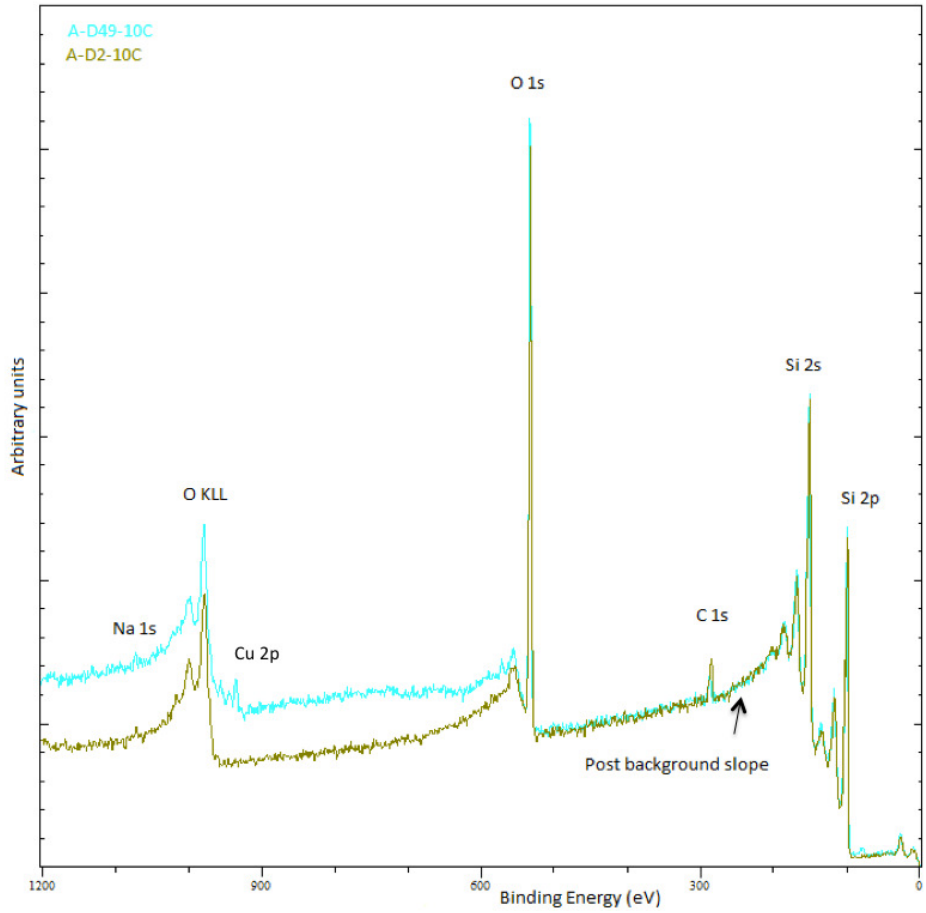

Figure 4.2.1: Survey scan of sample A-D2-10C and A-D49-10C. Presence of oxygen, carbon, sodium and silicon are observed.

Figure 4.2.2 shows the high resolution O 1s spectra. The broadness of the peaks indicates strong presence of suboxides and OH^-. Additional bands are observed for sample A-D2-10C, A-D2-22C and A-D35-22C, located at the high energy side of the O 1s peak. The intensity for suboxides and OH^- for sample A-D35-22C and A-D2-22C is slightly higher compared to the intensity for sample A-D2-10C. From this figure the O 1s intensity seems to be higher for sample A-D2-10C compared to sample A-D49-10C. This is opposite of what is observed by the curves in the survey spectra, Figure 4.2.1.

In Figure 4.2.3 the high resolution Si 2p spectra of the same samples are shown. For sample A-D2-22C and A-D2-10C no apparent difference in peak intensity can be seen. A clear difference can however be observed for sample A-D49-10C and A-D35-22C. The SiO_x/Si peak intensity ratio is larger for sample A-D49-10C compared to sample A-D35-22C. The broadness of the Si ground state peaks, $Si^0 2\,p_{3/2}$, denotes that the underlaying silicon does not have a typical crystalline form. A shift of the peaks can also be seen. This is probably due to charge referencing, which is not important in this matter [33].

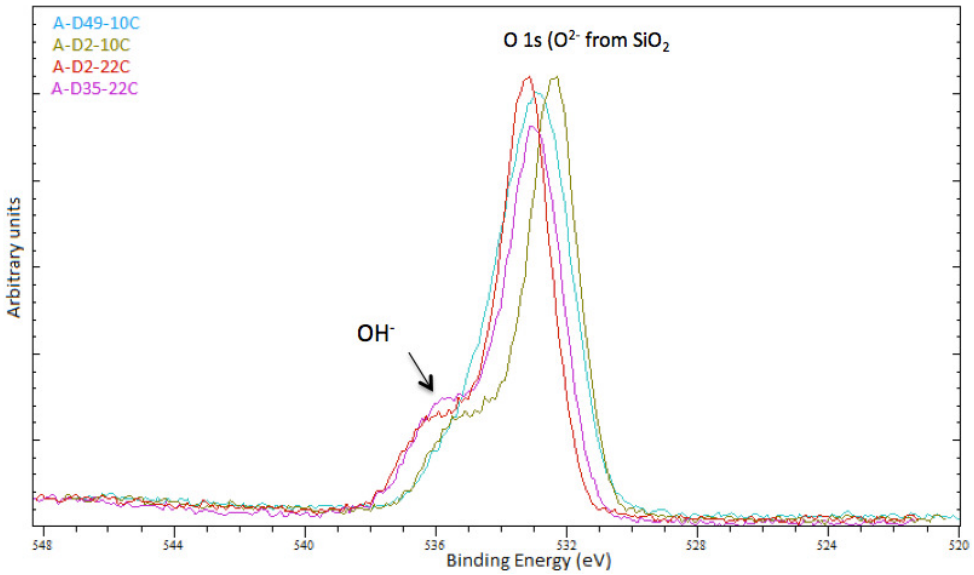

Figure 4.2.2: High resolution O 1s spectra of different silicon samples A-D2-10C, A-D49-10C, A-D2-22C and A-D35-22C. Hydroxide present is shown as a broadening of the O 1s peak on the high energy side.

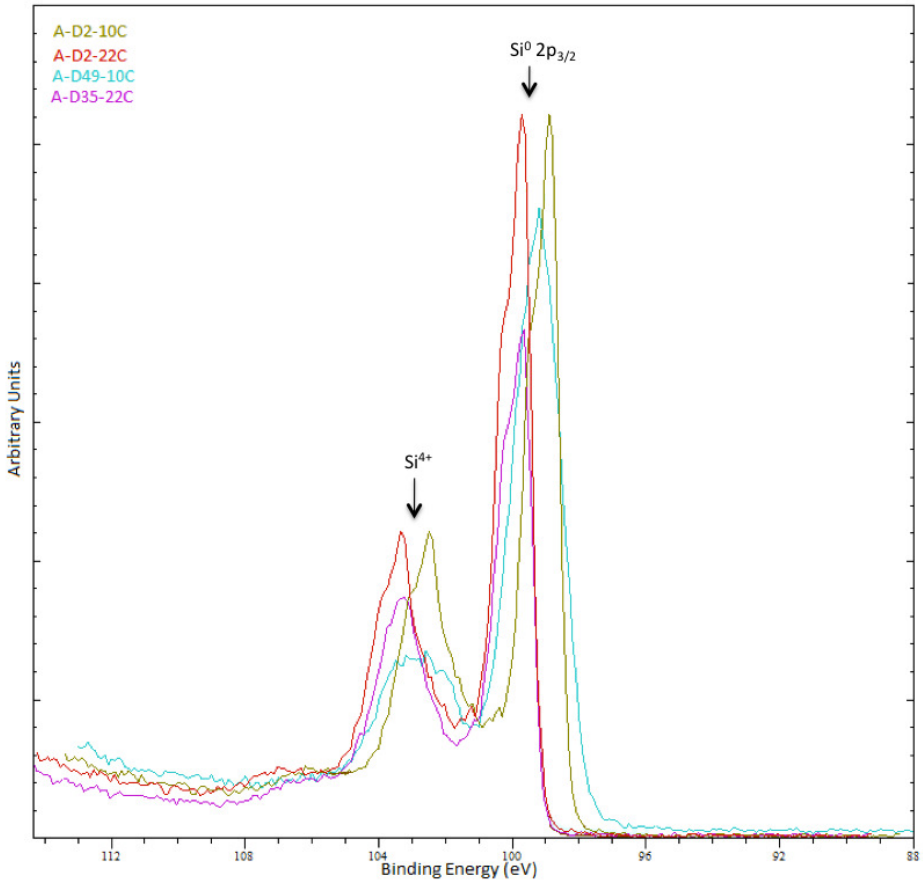

Figure 4.2.3: High resolution Si 2p spectra of silicon samples A-D2-10C, A-D49-10C, A-D2-22C and A-D35-22C. $Si^0 2\,p_{3/2}$ and Si^{4+} peaks are shown for all samples.

The estimated oxide thickness of sample A-D2-10C and A-D49-10C are given in Table 4.2.1 together with oxide thickness estimations of samples stored at 22°C. The oxide thickness estimated for samples exposed to 10 °C are lower compared to the estimated oxide thickness of samples exposed to 22 °C.

Table 4.2.1: Estimated oxide thickness of powders aged in humid air at 10 °C and 22 °C [5].

Storing conditions	*Sample code*	*Days of exposure to humid air*	*Estimated SiO_x thickness [nm]*
10°C - 0.012 atm	A-D2-10C	2	0.9
	A-D49-10C	49	0.6
22°C - 0.026 atm	A-D2-22C	2	1.5
	A-D7-22C	7	1.5
	A-D14-22C	14	1.5
	A-D35-22C	35	1.7
	A-D56-22C	56	1.6

4.2.2 Raman Spectroscopy

Four selected silicon powder samples were analysed by Raman spectroscopy. Sample B-D0.2 not exposed to humid air, sample B-D30-10C and B-D57-22C exposed to humid air and sample B-D5.1-22C, aqueous oxidised. The Raman spectra are given in Figure 4.2.4 showing the whole energy range. The curve for a silicon wafer is included for comparison. A sharp peak can be observed around 500 cm^{-1} for all samples.

Figure 4.2.5 shows an enlargement of the peaks observed in Figure 4.2.4. The crystalline bulk silicon peak appear at 521 cm^{-1} and a shift in peak position to lower energy is evident for all analysed samples. The peak for sample B-D0.2 is broad and seems to consist of two peaks, one at 515 cm^{-1} and one at 504 cm^{-1}. For sample B-D30-10C two peaks appear, one at 493 cm^{-1} and one at 517 cm^{-1} and for sample A-D57-22C one broad peak is seen at 505 cm^{-1}. The peak for sample B-D5.1-22C has lower energy and is much broader compared to the other samples. It appear to consist of two peaks, one at 488 and one at 517 cm^{-1}.

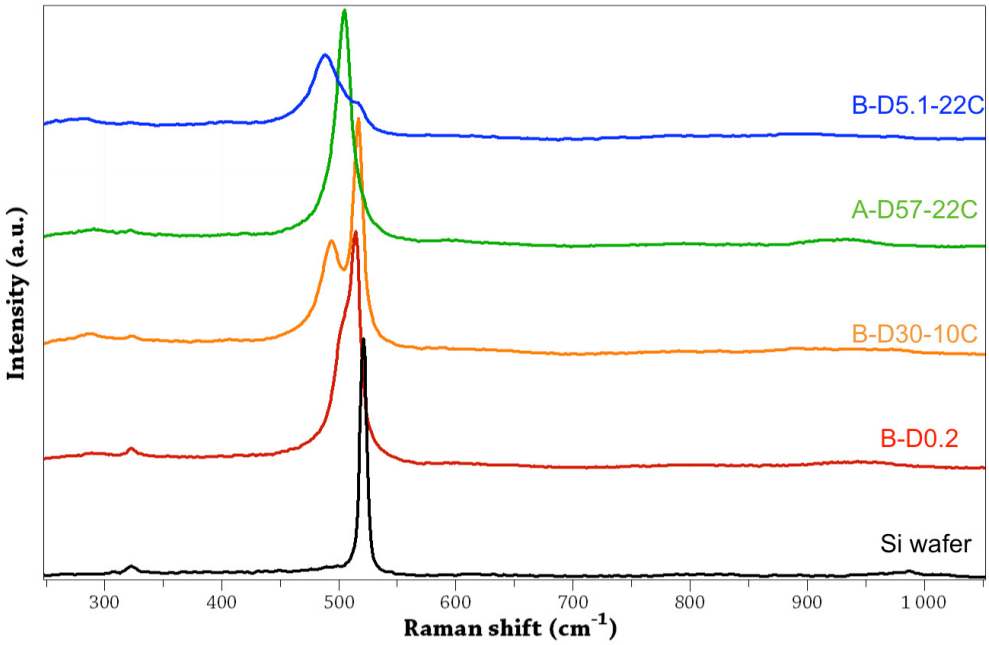

Figure 4.2.4: Raman spectra for sample B-D0.2, B-D30-10C, B-D57-22C, B-D5.1-22C. The curve for a silicon wafer is included for comparison [20].

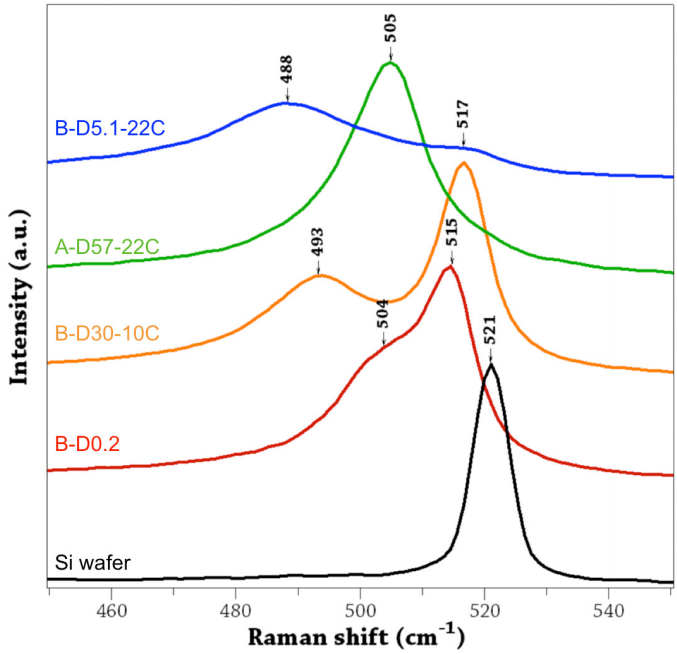

Figure 4.2.5: Enlarged Raman spectra showing the silicon peak for sample B-D0.2, B-D30-10C, B-D57-22C, B-D5.1-22C. The curve for a silicon wafer is included for comparison [20].

4.3 Characterisation of thermally treated silicon powder

4.3.1 XPS analysis

Powder from Batch A were thermally treated and analysed by XPS. The powder was heated at 300°C and 900°C, A-TO-300C and A-TO-900C respectively.

Figure 4.3.1 shows the survey spectra obtained from the XPS analysis showing the presence of oxygen, silicon and sodium for both samples. The sodium content can be due to inhomogeneous powder from the sample batch. The change in the Si 2p post peak background slope for sample A-TO-900C compared to sample A-TO-300C represents the presence of an oxide layer thicker than 10 nm on the surface. The most evident difference between the two spectra is the O 1s peak, which is much larger for sample A-TO-900C, verifying high oxygen content in the sample.

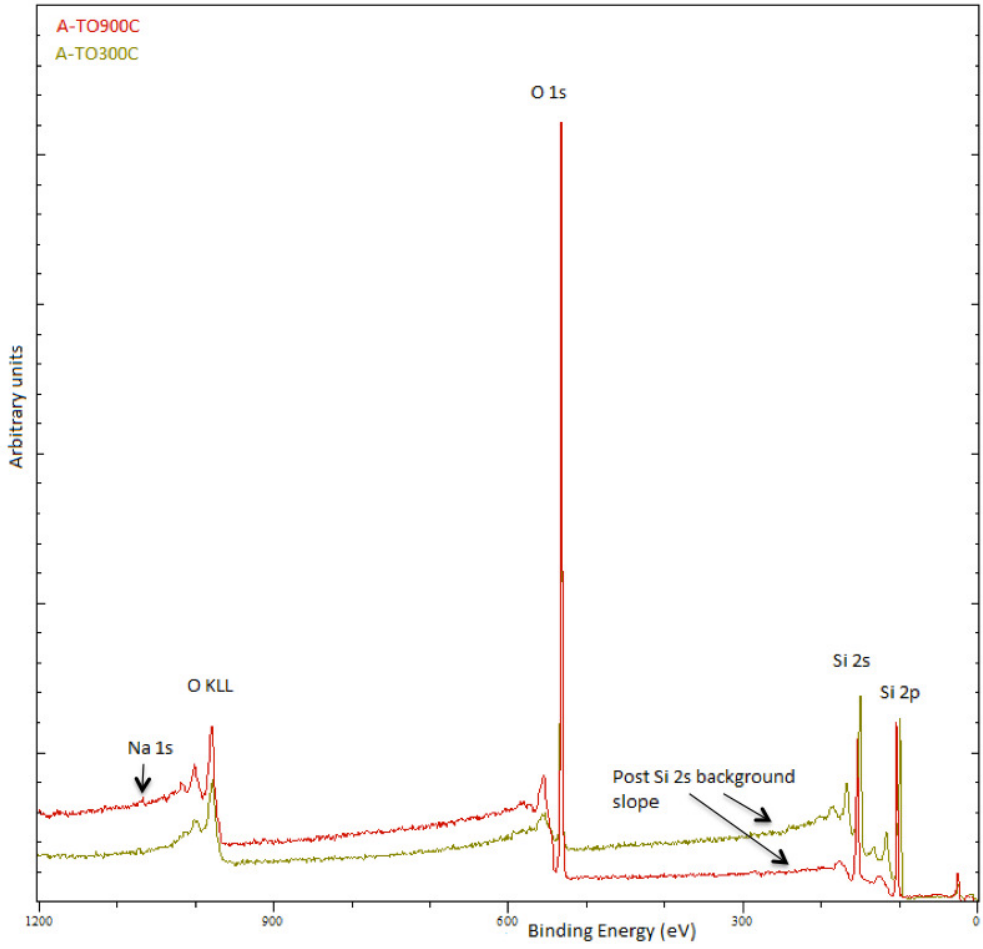

Figure 4.3.1: Survey scan for the thermally treated samples, A-TO-300C and A-TO-900C, showing the elements present on the samples surface.

The high resolution O 1s peaks are shown in Figure 4.3.2, showing a well defined sharp peak for sample A-TO-900C indicating a more stoichiometric nature of this

oxide compared to the sample treated at 300 °C. The O 1s intensity for sample A-TO-300C is much lower than for A-TO-900C, indicating a lower oxygen content. The signal for OH^- is not detected for neither of the thermal oxidised samples. The spectrum for sample A-D49-10C, exposed to humid air at 10 °C, is included in the figure for comparison. This curve is much broader on the high energy side, indicating OH^- present at the surface as expected. In Figure 4.3.3 a comparison of the high resolution Si 2p spectra are shown. No peak for $Si^0 2p_{3/2}$ is present for sample A-TO-900C because the oxide thickness is larger than the detection depth for XPS. Thus, the Si 2p spectra for this sample consists only of the oxide component. The amount of suboxides is significant for both samples. The SiO_x/Si intensity ratio for sample A-TO-300C is comparable to that of sample A-D49-10C.

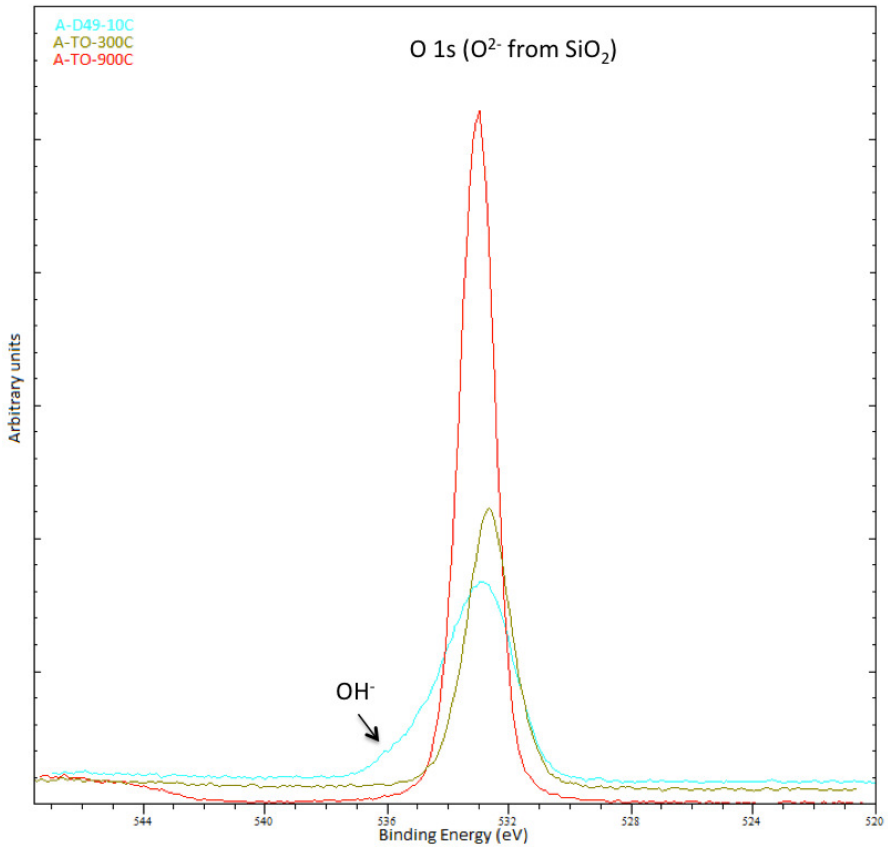

Figure 4.3.2: High resolution O 1s spectra of sample A-TO-300C and A-TO-900C. The spectrum of sample A-D49-10C is included for comparison, showing the presence of hydroxide on the high energy side of the O 1s peak.

The estimated oxide thickness for the thermally treated samples are shown in Table 4.3.1. The estimated oxide thickness is much higher for sample A-TO-900C than for sample A-TO-300C. The oxide thickness of sample A-TO-300C can be comparable to the oxide thickness estimated for the samples exposed to humid air.

Table 4.3.1: Estimated oxide thickness of powders thermally treated at 300 °C and 900 °C.

Ageing conditions	*Sample code*	*Temperature [°C]*	*Estimated SiO_x thickness [nm]*
Thermal treament	A-TO-300C	300	0.7
	A-TO-900C	900	>10

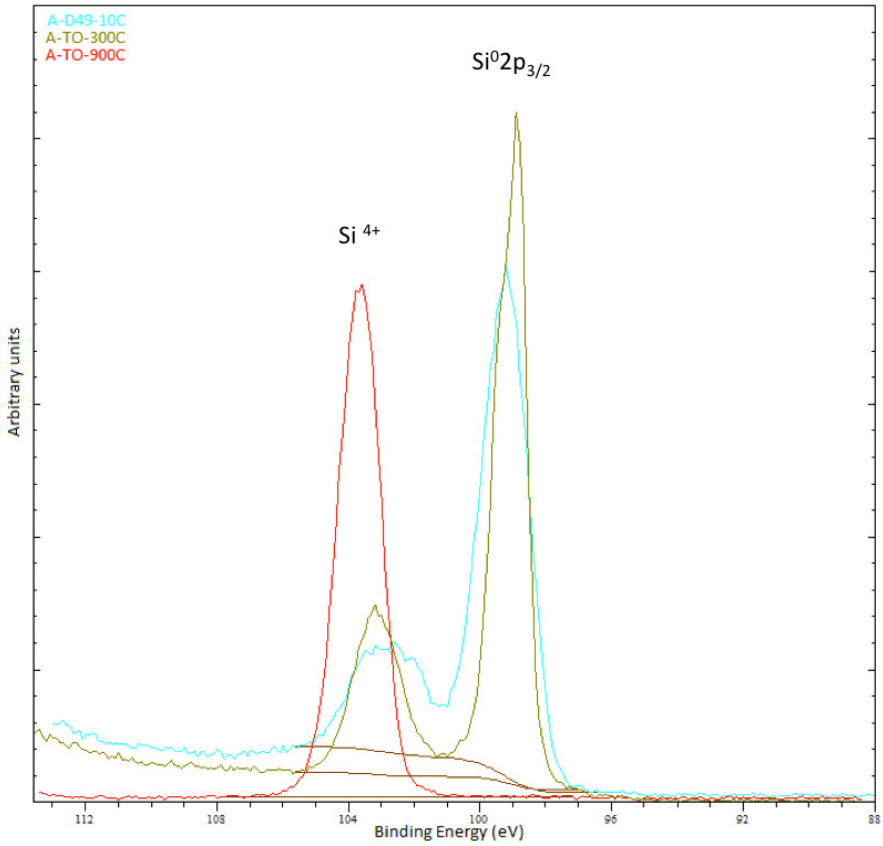

Figure 4.3.3: High resolution Si 2p spectra of sample A-TO-300C and A-TO-900C. The curve for sample A-D49-10C is included for comparison.

4.4 Aqueous oxidation of silicon powders

In this section the results from the aqueous oxidation of silicon powder will be presented.

4.4.1 Reproducibility of the aqueous oxidation of silicon powder

In order to verify the hydrogen measurements from the aqueous oxidation a series of experiments on silicon powder, not exposed to humid air, were performed. Three powder samples, from Batch C, were analysed and the results are presented in Figure 4.4.1. The powder samples analysed were first stored in a plastic bottle

then stored in a desiccator for about 3 weeks. Onset time for hydrogen evolution, total amount of hydrogen gas measured and the pH at the end of the experiment (pH-end) are given in Table 4.4.1. From the table it can be seen that the measured values are approximately the same, verifying a good reproducibility of the hydrogen measurements. The onset time for hydrogen evolution is defined as the time from addition of ammonia until hydrogen was first measured. The total amount of hydrogen formed during the experiment is calculated using the trapezoidal method. The hydrogen evolution was set to 90 minutes for all experiments.

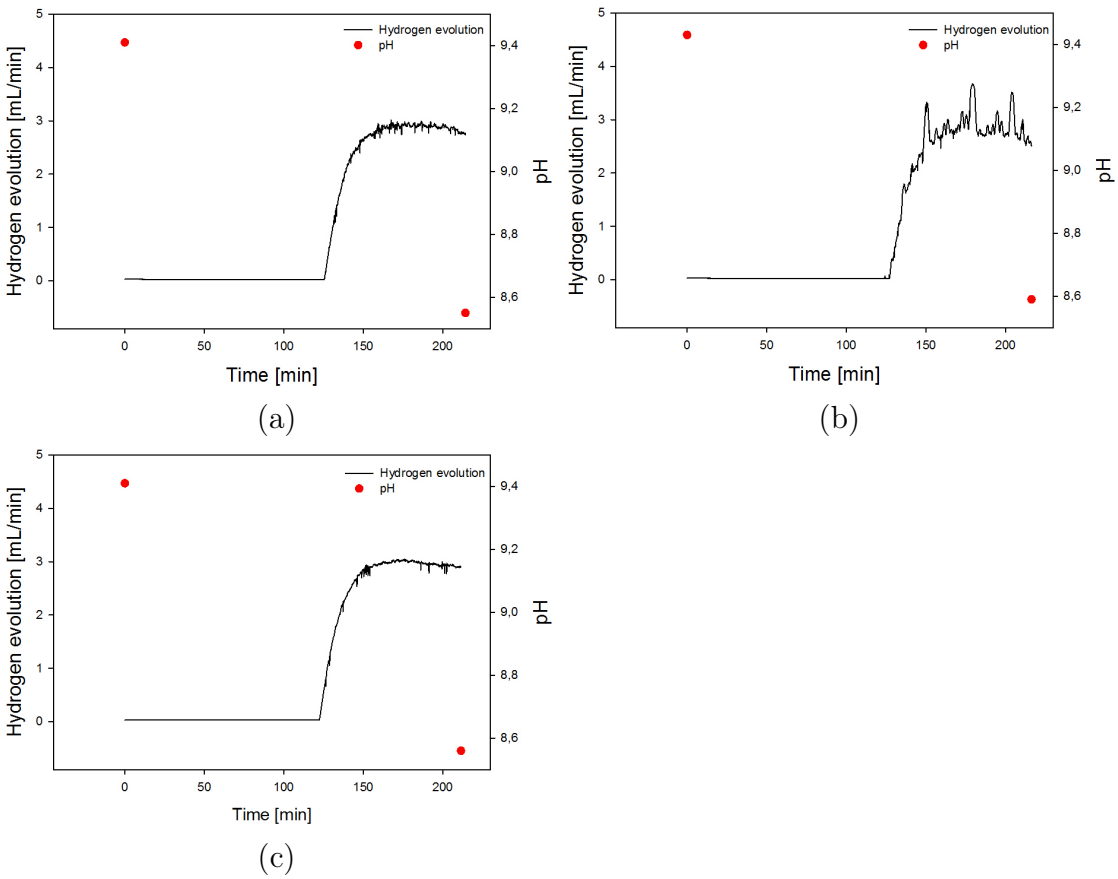

Figure 4.4.1: Results from the aqueous oxidation experiments of silicon powder from Batch C. The red dots show the pH at the start and at the end of the experiment and the black curve show the hydrogen gas flow. Three parallels of the same powder were performed. a) C-D0.1 b) C-D0.2 c) C-D0.3

Table 4.4.1: Overview of the results from the reproduction series of the aqueous oxidation of silicon powder from Batch C. Onset time for hydrogen evolution, total amount of hydrogen gas measured and the pH at the end of the experiment are given.

Sample code	*Onset time for H_2 evolution [min]*	*Total amount of H_2 evolved [mL]*	*pH-end*
C-D0.1	126	230	8.55
C-D0.2	127	231	8.59
C-D0.3	122	237	8.56

4.4.2 Aqueous oxidation of silicon powders stored at ambient conditions

Aqueous oxidation of silicon powders from Batch A[1] were performed in order to measure the amount of hydrogen formed in the reaction as a function of storing history. The reacted powders were later analysed by measuring BET surface area and oxygen content. All aqueous oxidation experiments were performed at 60 °C and at a start pH of 9.4. However, during the experimental work uncertainties in the hydrogen measurements for most samples were identified, thus only the measured BET surface area and the oxygen content for these samples will be presented. Illustration of selected hydrogen flow curves can be found in Appendix D. All experiments presented in this section were performed before the experimental routine was changed.

Table 4.4.2: Overview of the results from the aqueous oxidation of silicon powder from Batch A, showing the pH-end, BET surface area and oxygen content.

Storing conditions	*Atmosphere exposed to*	*Sample code*	*pH-end*	*Surface area [m^2/g]*	*Oxygen content [%]*
Batch A	10°C - 0.012 atm	A-D8.1-10C	8.70	28.1	8.4
		A-D8.3-10C	8.97	73.1	-
		A-D10.1-10C	8.80	77.7	21.1
		A-D14.1-10C	8.75	39.8	11.3
		A-D21.1-10C	8.58	33.8	9.7
		A-D35.1-10C	8.57	23.8	7.5
	22°C - 0.026 atm	A-D1.1-22C	8.92	7.8	-
		A-D7.1-22C	8.89	53.2	12.1
		A-D7.2-22C	8.94	64.1	14
		A-D15.1-22C	9.23	55.3	13.1
		A-D23.1-22C	8.57	-	-
		A-D35.1-22C	8.67	-	-
	22°C - Dry	A-D0.1	8.70	47.1	-

[1]Powders from Batch A were stored in a plastic bottle after milling until it was exposed to humid air.

The surface area for powders exposed to humid air at 10 °C and 22 °C are shown as a function of oxygen content in Figure 4.4.2 and Figure 4.4.3, respectively.

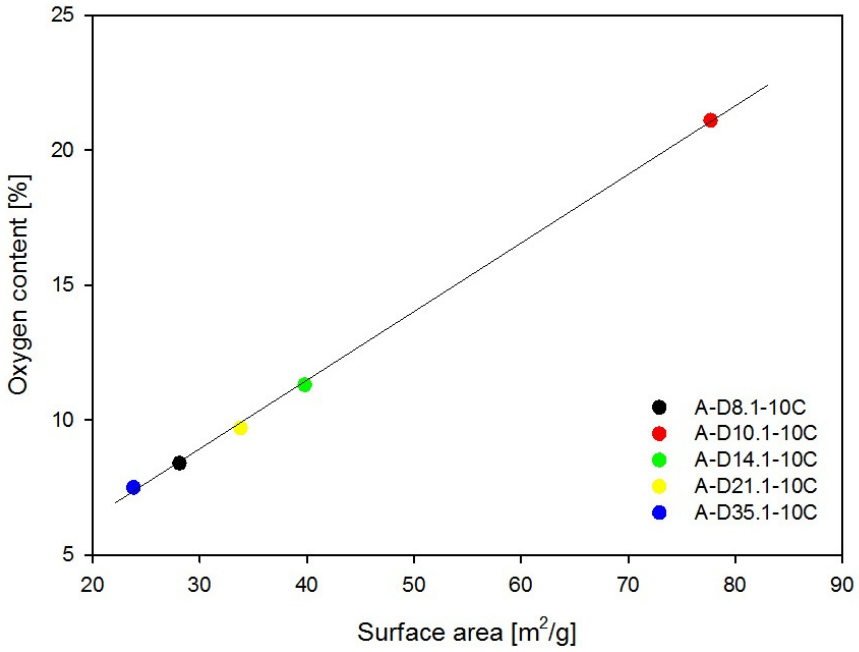

Figure 4.4.2: BET surface area as a function of oxygen content for silicon powders from Batch A, exposed to humid air at 10 °C. The line is included only as a guide for the eye.

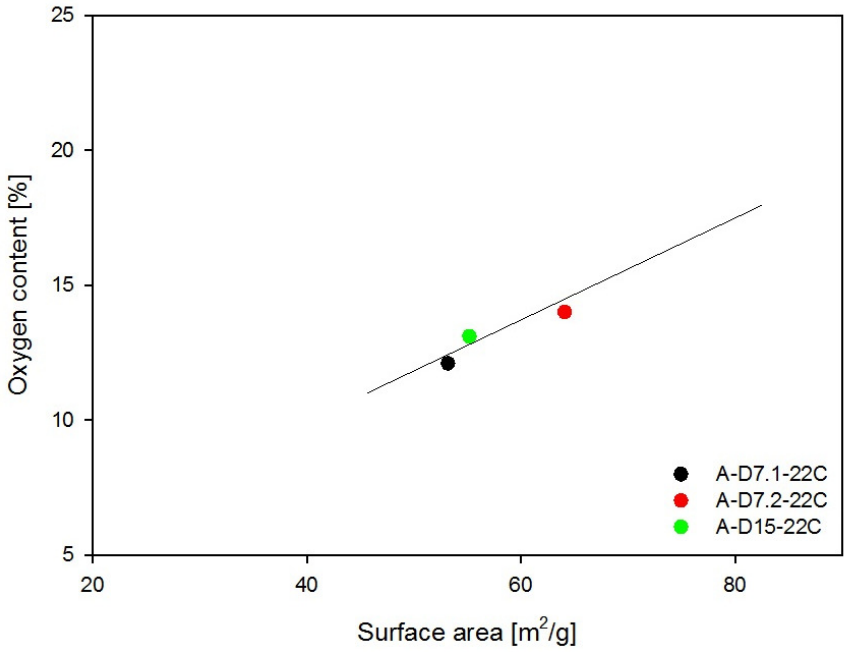

Figure 4.4.3: Surface area as a function of oxygen content for silicon powders from Batch A exposed to humid air at 22 °C. The line is included only as a guide for the eye.

A linear relation between surface area and oxygen content can be seen from both figures. It is believed that colloidal silica forms on the surface of the silicon particles during the aqueous oxidation, and as the surface area increases more colloidal silica is formed. The high oxygen content measured in the samples confirms this. The linear relation is more evident for the samples exposed to humid air at 10 °C compared to samples exposed to humid air at 22 °C. An unbroken line is included in both figures only as a guide for the eye.

The pH at the end of the experiment is shown as a function of the total time of experiment for powders exposed to humid air at 10 °C and 22 °C in Figure 4.4.4 and Figure 4.4.5, respectively. The unbroken line shows a decreasing trend in pH as the experiment time increases. This is clear for powders exposed to humid air at both 10 °C and 22 °C. Some variations in the results are found for both samples, and sample A-D10.1-10C in Figure 4.4.4 was not included when implementing the line (since this pH is believed to be erroneous). The measured value for sample A-D0.1, not exposed to humid air, is lower compared to sample A-D8.3-10C. This can be explained by the formation of a thicker oxide layer during ageing in humid air for sample A-D8.3-10C, and therefore the need of more hydroxide to dissolve the oxide layer.

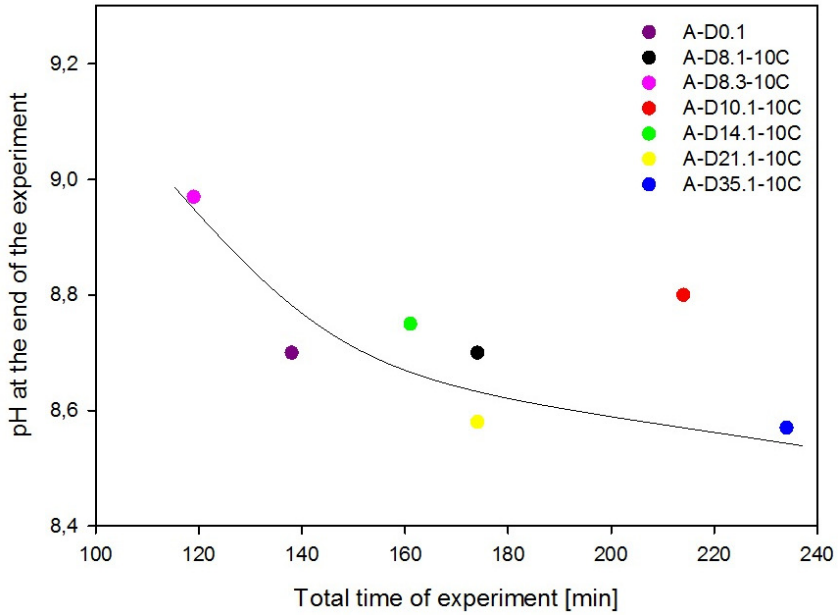

Figure 4.4.4: pH at the end of the experiment as a function of the total time of experiment for silicon powders exposed to humid air at 10 °C. The line is included only as a guide for the eye. Sample A-D10.1-10C was not taken into account when implementing the line.

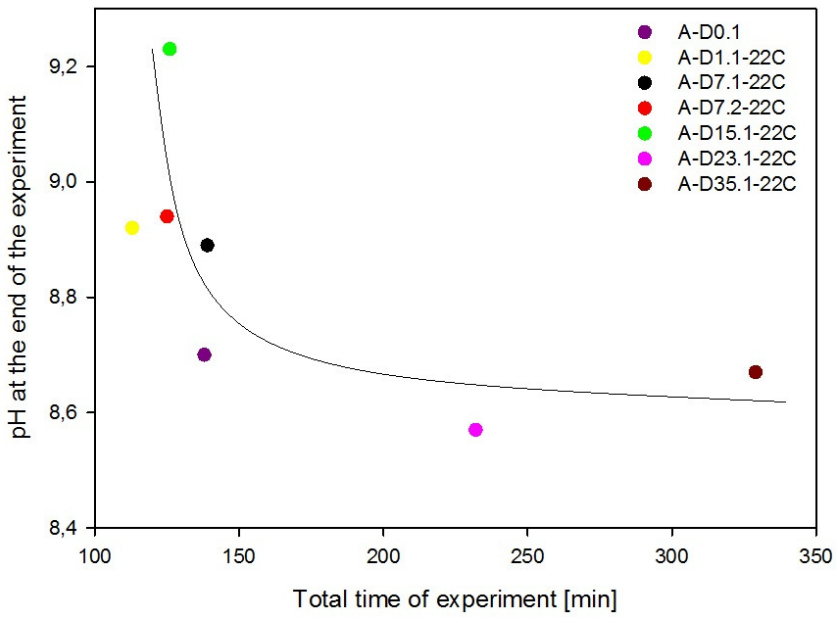

Figure 4.4.5: pH at the end of the experiment as a function of the total time of experiment for for silicon powders exposed to humid air at 22 °C. The line is included only as a guide for the eye.

4.4.3 Aqueous oxidation of silicon powders stored at dry conditions

Silicon powders from Batch B[1] were used in the aqueous oxidations presented in this section. The oxidation experiments were performed in order to measure the amount of hydrogen formed in the reaction as a function of ageing history. The reacted powders were later analysed by SEM and BET surface area as well as oxygen content were measured. All experiments were performed after the experimental routine was changed. The aqueous oxidation were performed at 60 °C and a start pH of 9.4 was used. The duration for hydrogen evolution was set to 90 minutes.

The results from the aqueous oxidation of humid powders from Batch B are divided into two parts because two different pH-electrodes were used (pH-electrode I and II). Replacing the pH-electrode resulted in very different values and because a shift in trends were observed, it was necessary to separated the results obtained. The results are presented in the same figures for comparison. It is important to mention that the fine flow meter was used for the experiments using pH-electrode I and both the fine- and the coarse flow meters were used for the experiments using pH-electrode II. The coarse flow meter is less accurate than the fine flow meter, more scattering and noise are therefore expected in these measurements. The scattering observed influenced the total amount of hydrogen measured, and the given values are therefore less accurate than the values calculated for the series where pH-electrode I was used.

[1]Powders from Batch B were stored in a desiccator after storage in a plastic bottle, before exposure to humid air.

Silicon powders exposed to humid air at 10 °C and 22 °C were oxidised in reaction with water. For comparison, powders not exposed to humid air was also investigated. The hydrogen flow curves for three selected samples will be presented, the rest can be found in Appendix D. In Table 4.4.3 there is an overview of the total amount of hydrogen measured, the onset time for hydrogen evolution, the pH at the end of the experiment (pH-end), the BET surface area and the oxygen content measured.

The hydrogen flow curves for sample B-D5.1-10C, B-D5.1-22C and B-D14.2-22C are shown in Figure 4.4.6, Figure 4.4.7 and Figure 4.4.8 respectively. pH-electrode I was used for sample B-D5.1-10C and B-D5.1-22C and pH-electrode II was used for sample B-D14.2-22C. The pH at the start and at the end of the experiments are shown as red dots and the black line is the hydrogen gas flow curve. The curves have a similar form with a steep increase when hydrogen evolution starts, then it levels out as a maximum hydrogen flow is reached. It seems like the gas flow curve for sample B-D5.1-10C and B-D14.2-22C decreases slightly after the maximum flow is reached, compared to the curve for sample B-D5.1-22C. An earlier onset time for hydrogen evolution is observed for sample B-D14.2-22C compared to the two other samples and the maximum hydrogen flow is much higher. The pH at the end of the experiment is also much higher for this sample compared to the other two. Since a higher gas flow was measured for sample B-D14.2-22C, the coarse flow meter was used. This flow meter is less accurate than the fine flow meter, as can be seen by the noise in the hydrogen flow curve for this sample.

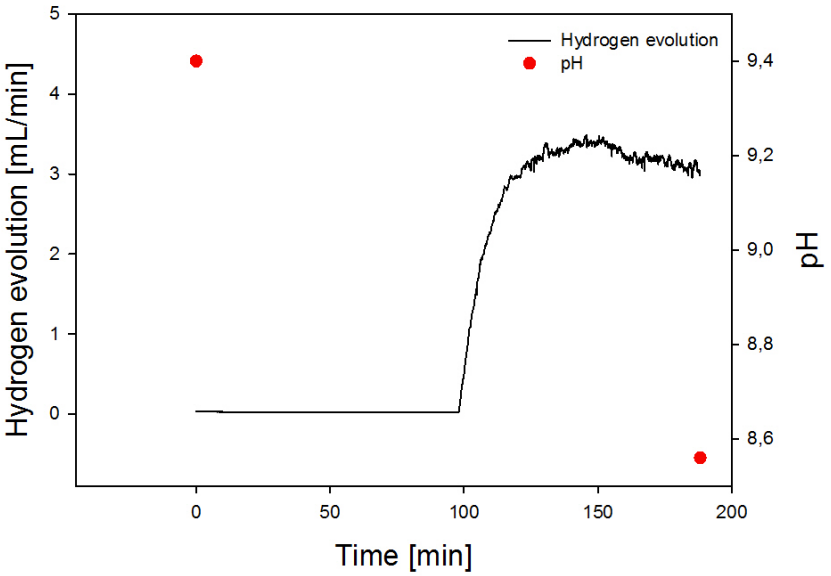

Figure 4.4.6: Hydrogen flow and pH for powder exposed five days to humid air at 10 °C, B-D5.1-10C. pH-electrode I was used. The pH at the start and at the end of the experiments are shown as red dots and the black line is the hydrogen gas flow curve

Table 4.4.3: Overview of the results from the aqueous oxidation of silicon powder, from Batch B. Results for powder aged in humid air, stored at dry conditions and powder thermally treated are included.

Storing conditions	*Atmosphere exposed to*	*Sample code*	*Onset time for H_2 evolution [min]*	*Total amount of H_2 evolved [mL]*	*pH-end*	*Surface area* [m^2/g]	*Oxygen content* [%]
Batch B	10 °C - 0.012 atm	B-D1.1-10C	108	260	8.61	36.8	7.4
		B-D1-10C-hpH	55	400	8.72	-	-
		B-D3.1-10C	96	128	8.55	33.8	7.0
		B-D3.2-10C	78	296	8.56	48.4	12.4
		B-D5.1-10C	98	267	8.56	42.3	9.2
		B-D5.2-10C	42	794	8.69	77.2	14
		B-D7.1-10C	113	222	8.56	38.4	8.7
		B-D14.1-10C	158	196	8.54	26.1	9.7
		B-D14.2-10C	47	555	8.68	77.3	15.3
		B-D28.1-10C	64	455	8.69	67.4	13.3
	22 °C - 0.026 atm	B-D1.1-22C	95	245	8.62	38.2	7.4
		B-D3.1-22C	113	231	8.62	39.6	8.1
		B-D5.1-22C	123	239	8.55	37.6	8.2
		B-D5.2-22C	55	731	8.71	68.4	13
		B-D7.1-22C	-	-	-	9.2	-
		B-D14.1-22C	108	156	8.55	37.5	8.5
		B-D14.2-22C	47	808	8.70	69.9	12.9
		B-D28.1-22C	58	656	8.70	66.8	12.5
	22 °C - Dry	B-D0.1	78	234	8.51	39.1	-
	Thermally treated	B-TO-300C	-	-	1.1	0.38	

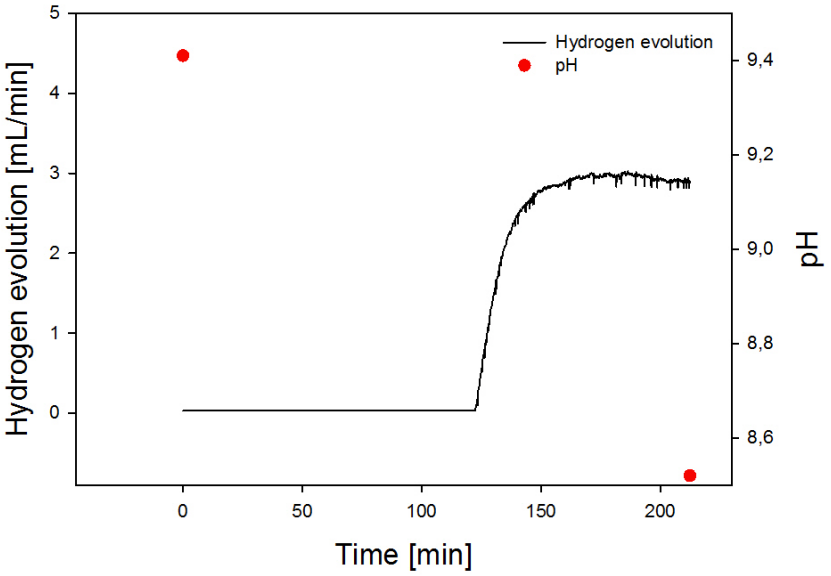

Figure 4.4.7: Hydrogen flow and pH for powder exposed five days to humid air at 22 °C, B-D5.1-22C. pH-electrode I was used. The pH at the start and at the end of the experiments are shown as red dots and the black line is the hydrogen gas flow curve

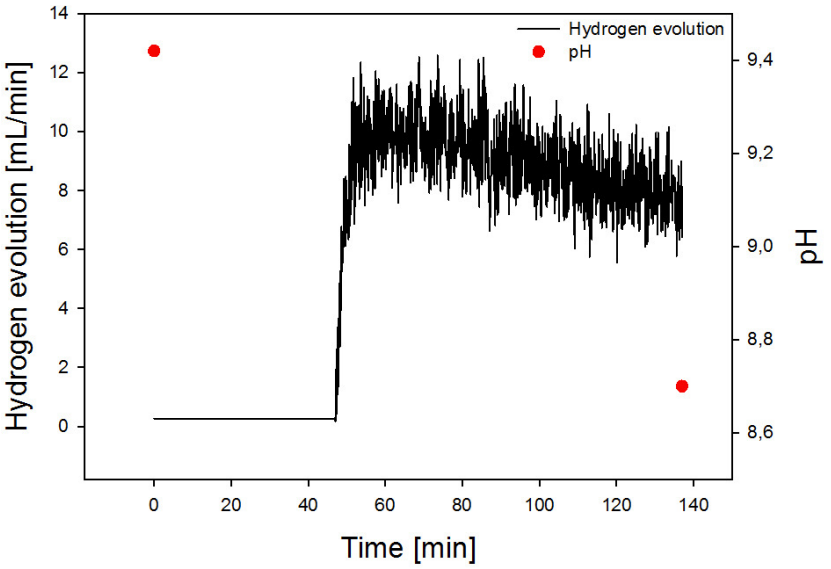

Figure 4.4.8: Hydrogen flow and pH for powder exposed 14 days to humid air at 22 °C, B-D14.2-22C. pH-electrode II was used. The pH at the start and at the end of the experiments are shown as red dots and the black line is the hydrogen gas flow curve

For Figure 4.4.9, 4.4.10, 4.4.11, 4.4.12, 4.4.13 and 4.4.14 the results from the experiments using both pH-electrode I and II are shown in the same figures. The dots represents pH-electrode I and the cross represents pH-electrode II. As a guide for the eye, dotted and unbroken lines are implemented in some of the figures showing the expected trend. It is important to emphasis that the lines does not

have any mathematical relation. Unbroken lines represents pH-electrode I and dotted lines represent pH-electrode II.

The onset time for hydrogen evolution for samples exposed to humid air at 10 °C is shown in Figure 4.4.9. For pH-electrode I, some variations in the results are observed, but the general trend show a later onset time as the exposure time to humid air increases. This is expected as a thicker oxide layer is believed to form on the silicon surface during ageing. For pH-electrode II, only three measurements were performed and less variations are observed. However, a slightly later onset time as the exposure time to humid air increases can be seen. This is the same trend as observed for pH-electrode I. The onset time for pH-electrode I seems to be more dependent on exposure time to humid air compared to pH-electrode II. This is shown by the implemented lines.

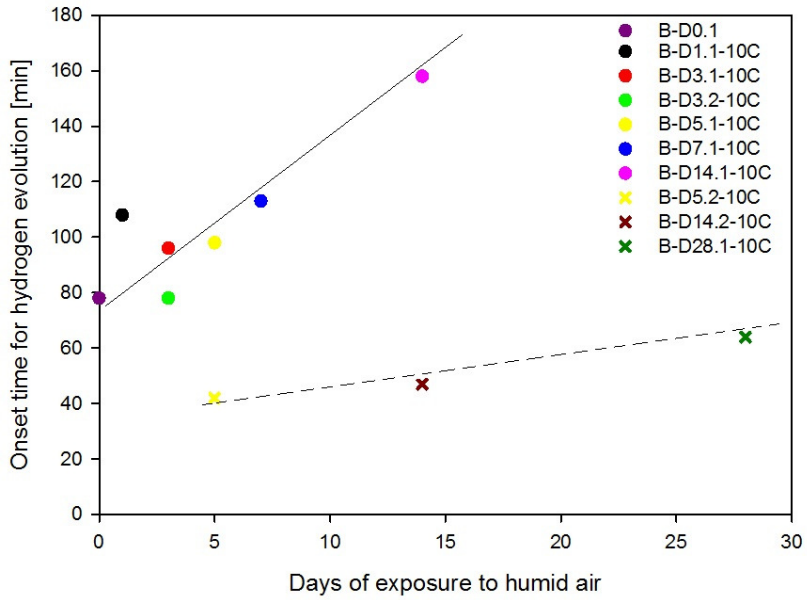

Figure 4.4.9: Onset time for hydrogen evolution for samples exposed to humid air at 10 °C. The dots represents pH-electrode I and the cross represents pH-electrode II. The dotted and the unbroken lines in the figure are implemented only as a guide for the eye, showing a later onset time as the exposure to humid air increases.

The total amount of hydrogen measured for samples exposed to humid air at 10 °C is shown in Figure 4.4.10. The trends are very different for the two series. For pH-electrode I an almost constant amount of hydrogen is measured as exposure to humid air increases. However, an increase in amount of hydrogen is measured for sample B-D3.2-10C before it seems to decrease again. Sample B-D3.1-10C was not taken into account when the unbroken line was implemented since the measured hydrogen amount was much lower compared to the other samples. For pH-electrode II a large decrease in amount of hydrogen is seen between sample B-D5.2-10C and B-D14.2-10C, before it seems to level out for sample B-D28.1-10C. Since the coarse flow meter, which is less accurate than the fine flow meter, was used for the experiments using pH-electrode II, it is expected that the deviations in measured amount are larger compared to the fine flow meter for these results. The expected trend shown by the dotted line for pH-electrode II has not taken into

account the large amount measured for sample B-D5.2-10C, since a more linear relation is expected.

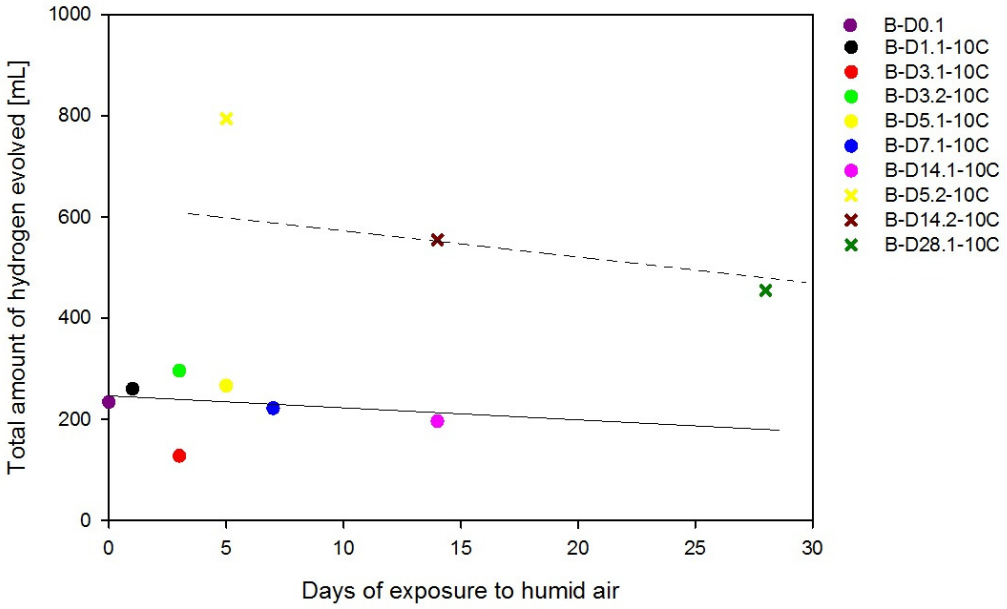

Figure 4.4.10: The total amount of hydrogen measured for samples exposed to humid air at 10 °C. The dots represents pH-electrode I and the cross represents pH-electrode II. The dotted and the unbroken lines in the figure are implemented only as a guide for the eye, showing the expected trends.

The pH at the end of the experiment (pH-end) for samples exposed to humid air at 10 °C is shown in Figure 4.4.11. For pH-electrode I a large decrease in pH is seen from sample B-D0.1, not exposed to humid air, to the samples exposed to humid air. For powders exposed to humid air the pH seems to decrease slightly as the exposure time increases. This is expected as a thicker oxide layer is believed to form during ageing. For pH-electrode II the variations in the measured pH-end values are small and is about 8.7 for all samples. However, as shown by the dotted line, a decrease is expected as the exposure to humid air increases, but more experiments are necessary to state this.

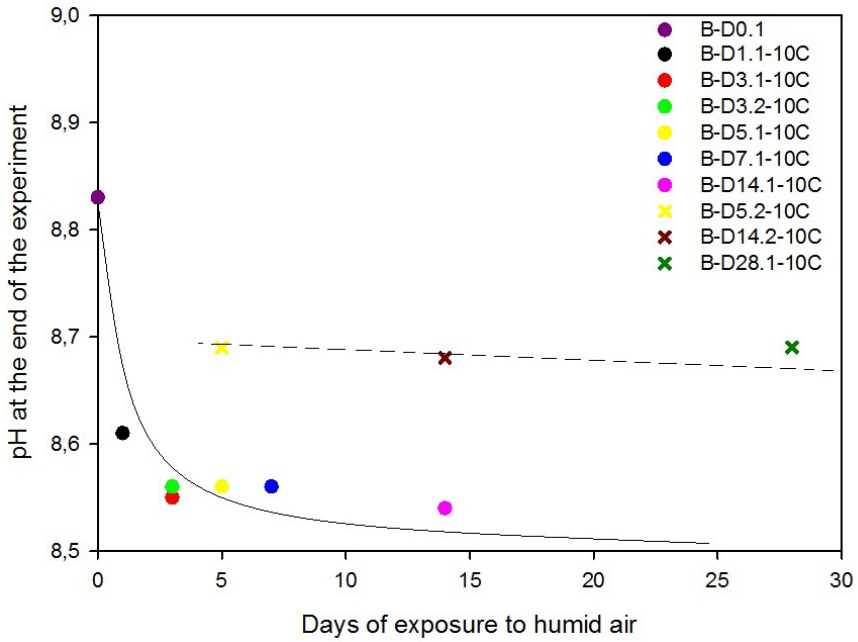

Figure 4.4.11: pH at the end of the experiment for for samples exposed to humid air at 10 °C. The dots represents pH-electrode I and the cross represents pH-electrode II. The dotted and the unbroken lines in the figure are implemented only as a guide for the eye, showing the expected trends.

The onset time for hydrogen evolution for samples exposed to humid air at 22 °C is shown in Figure 4.4.12. For both series the onset time is observed to be later as the exposure time to humid air increases. A much steeper relation is seen for the samples using pH-electrode I compared to pH-electrode II, where the measured values are about the same for all samples. However, as indicated by the dotted line, an increase is expected as the exposure time to humid air increase. Sample B-D14.1-22C was not included when the unbroken line was implemented for the series using pH-electrode I, because it is believed that the onset time found does not fit with the expected trend. Since no hydrogen was measured for sample B-D7.1-22C, during 4.5 hours experiment duration, it is not included in this figure.

The total amount of hydrogen measured for samples exposed to humid air at 22 °C is shown in Figure 4.4.13. For both series a slight decrease in the amount of hydrogen measured as the exposure time to humid air increases can be seen. The variations in the results using pH-electrode I is small and for samples exposed 1, 3 and 5 days to humid air the total amount of hydrogen measured is more or less the same. Thus, it seems like the total amount measured does not vary with time of exposure to humid air for short ageing. However, for sample B-D14.1-22C the total amount measured is lower than for the other samples and may indicate a decreasing trend. For pH-electrode II, the amount measured for sample B-D14.2-22C is higher than for sample B-D5.2-22C, which is contrary to what is expected and shown by the dotted line. Based on the trend observed for pH-electrode I a small decrease in total amount of hydrogen is expected as the exposure time to humid air increase. However, more experiments are needed to verify this

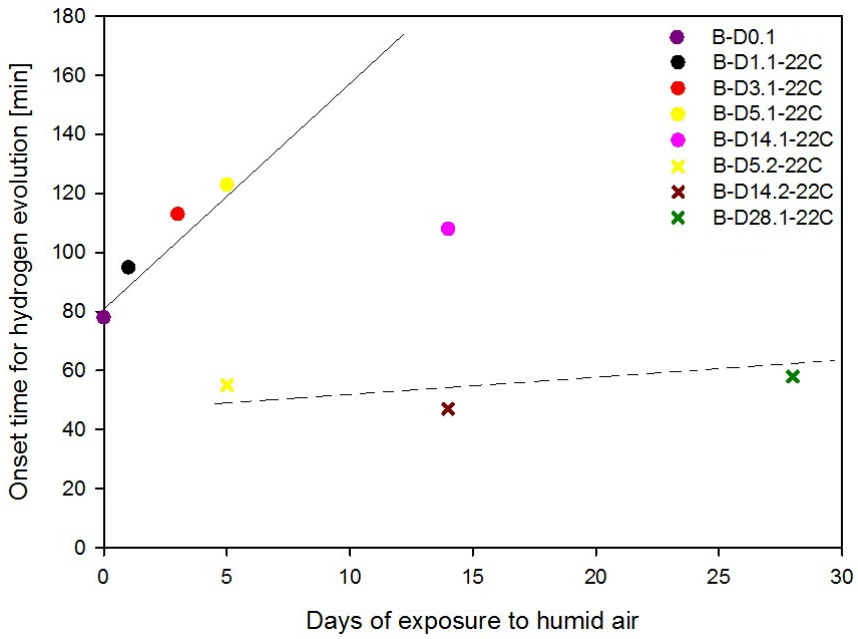

Figure 4.4.12: Onset time for hydrogen evolution for samples exposed to humid air at 22 °C. The dots represents pH-electrode I and the cross represents pH-electrode II. The dotted and the unbroken lines in the figure are implemented only as a guide for the eye, showing the expected trends.

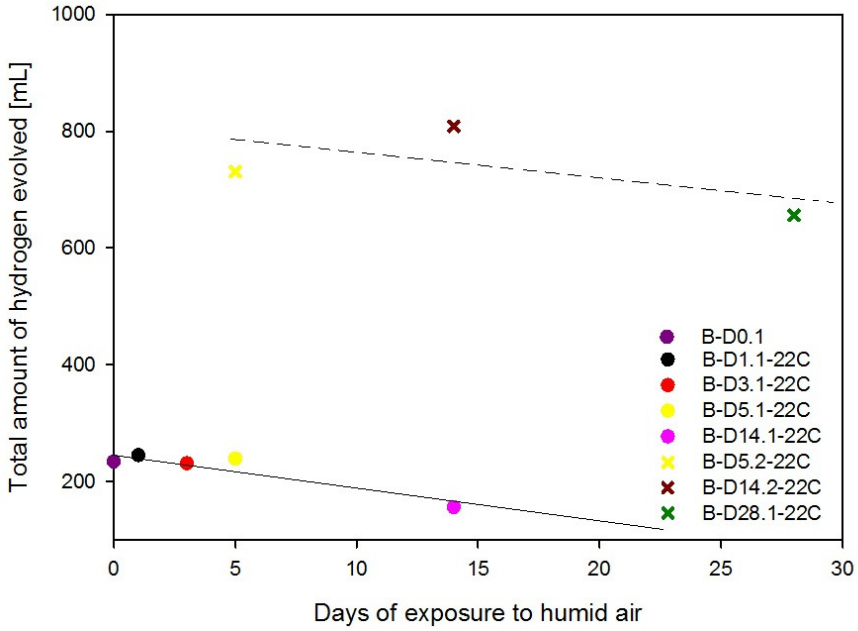

Figure 4.4.13: Total amount of hydrogen measured for samples exposed to humid air at 22 °C. The dots represents pH-electrode I and the cross represents pH-electrode II. The dotted and the unbroken lines in the figure are implemented only as a guide for the eye, showing the expected trends.

The pH at the end of the experiment for samples exposed to humid air 22 °C is shown in Figure 4.4.14. The results using pH-electrode I shows a decrease in pH as the exposure time to humid air increases. The pH appears to level out as the

exposure time to humid air increases, as seen by the unbroken line. For the results using pH-electrode II a linear trend is seen and the pH seems not to be affected by the ageing time in humid air. This was also observed for the powders exposed to humid air at 10 °C.

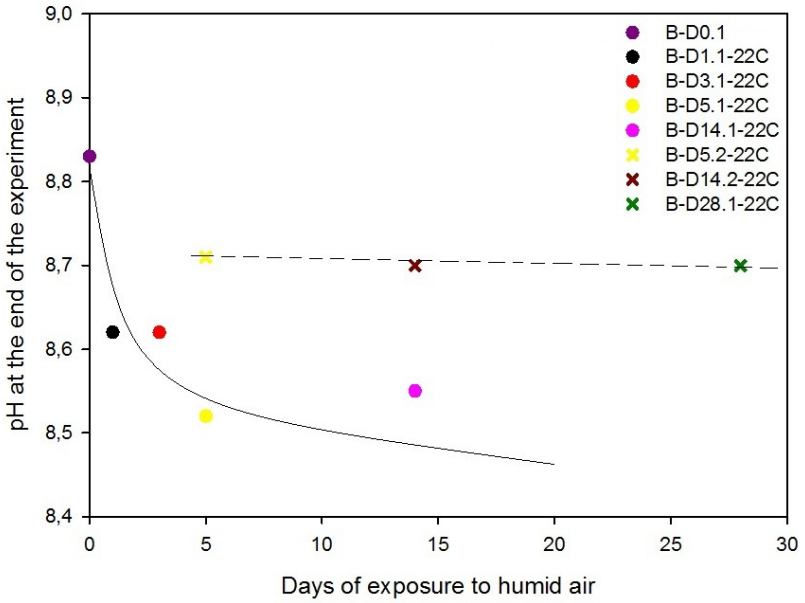

Figure 4.4.14: pH at the end of the experiment as a function of exposure to humid air. Samples exposed to humid air at 22 °C is shown, the dots representing pH-electrode I and the cross representing pH-electrode II. The dotted and the unbroken lines in the figure are implemented only as a guide for the eye.

To make it easier to compare the effect of high (22 °C) and low (10 °C) humidity for the hydrogen measurements the results for powders exposed to humid air at both 10 °C and 22 °C are presented in the same figures. Only results using pH-electrode I are presented in these figures. The red dots corresponds to powder exposed to humid air at 10 °C and the black triangles corresponds to powder exposed to humid air at 22 °C. The dotted and the unbroken lines in the figures are implemented only as a guide for the eye, representing 10 °C and 22 °C respectively.

A comparison of the onset time for hydrogen evolution for samples exposed to humid air at 10 °C and 22 °C is shown in Figure 4.4.15. It seems like the onset time for hydrogen evolution is higher for powders exposed to 22 °C compared to powders exposed to 10 °C. As can be seen from the figure the onset time for hydrogen evolution is higher for powder exposed to 22 °C than for powder exposed to 10 °C, shown by the lines. This is expected because a thicker and more stable oxide layer is expected to form on the surface for ageing in higher humidity (22 °C) air. However, the most aged powder in the black triangle series have a much earlier onset time compared to the expected trend and is therefore not included in the implemented line showing the expected trend. There are also some variations in the red dots series, especially for short ageing, but based on the trends from the least to the most exposed sample, an increasing trend is expected.

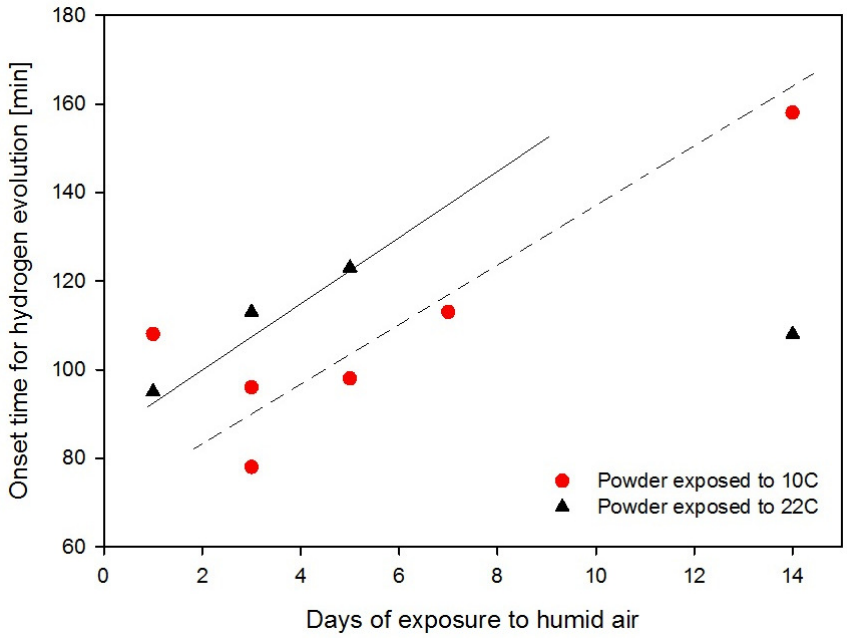

Figure 4.4.15: Onset time for hydrogen evolution for samples exposed to humid air at 10 °C and 22 °C, shown as red dots and black triangles respectively. The dotted and the unbroken lines in the figure are implemented only as a guide for the eye, showing an increase in onset time as the exposure time to humid air increases.

The total amount of hydrogen measured is shown in Figure 4.4.16. The hydrogen amount measured for samples exposed to 10 °C seems to be slightly higher compared to powders exposed to 22 °C. There are small variations in the hydrogen amount measured for powders exposed short times to humid air at 22 °C and it seems like it is more or less independent on ageing time in humid air. However, the amount measured for the most aged sample is much lower compared to the least aged sample and it can therefore look like the amount measured eventually will decrease if the exposure time to humid air is long enough. For the dotted line representing powders exposed to humid air at 10 °C, a decreasing trend can be observed as the exposure time increases. The amount of hydrogen measured for one of the least aged sample in the series is much lower than expected, based on the other results, and is therefore not taken into account when the dotted line was implemented.

In Figure 4.4.17 the pH at the end of the experiments is shown. The trend for both series is the same showing a decrease in pH with increasing exposure to humid air as expected, since a thicker oxide layer is believed to form during ageing. The pH decrease seems to level out for longer ageing times for both series. However, more results are needed to verify this. No apparent differences can be observed from the two series. Some variations in the results are seen, and the pH for samples with only a few days different exposure time, does not appear to be very affected by this. Still, the variations in the measured values are small (between 8.52 and 8.62 for all samples).

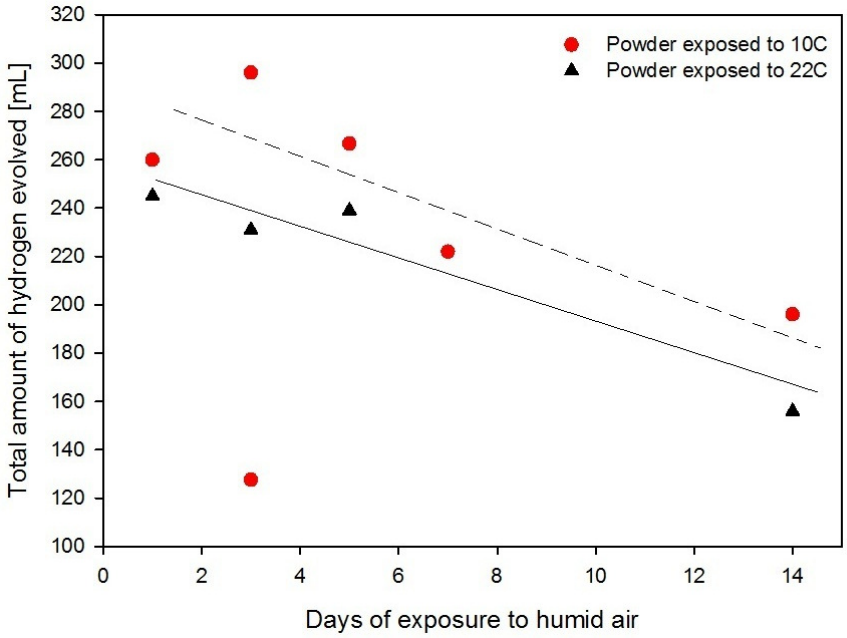

Figure 4.4.16: Total amount of hydrogen measured for samples exposed to humid air at 10 °C and 22 °C, shown as the red dots and the black triangles, respectively. The dotted and the unbroken lines in the figure are implemented only as a guide for the eye.

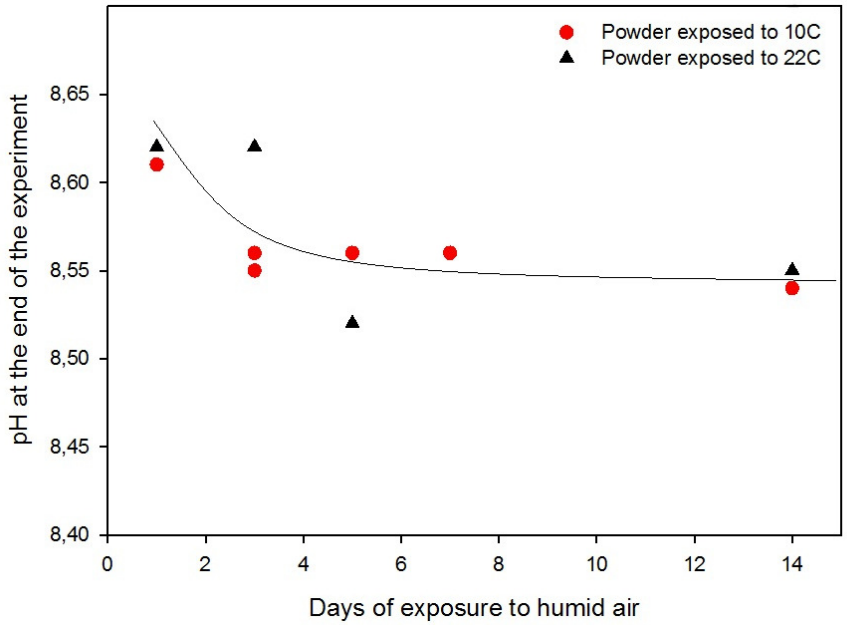

Figure 4.4.17: pH at the end of the experiment for samples exposed to humid air 10 °C and 22 °C, shown as the red dots and the black triangles, respectively.The dotted and the unbroken lines in the figure are implemented only as a guide for the eye, showing a decrease in pH as the exposure to humid air increase for both series.

The BET surface areas and oxygen content measured for selected samples are

presented in Table 4.4.3. In Figure 4.4.18 and Figure 4.4.19 the surface area as a function of days of exposure to humid air are shown for samples exposed to humid air at 10 °C and 22 °C, respectively. Results from both pH-electrodes are presented in the same figures. pH-electrode I are presented as dots and pH-electrode II is presented as cross. From Figure 4.4.18 it is clear that the surface area measured for samples where pH-electrode II were used is much higher compared to the series where pH-electrode I was used. Some variations is seen for both series, but this is especially evident for the series where pH-electrode I was used. Based on the samples that had been aged the longest, a decrease in surface area (for both series) as exposure time to humid air increases was expected. This is shown by the implemented lines.

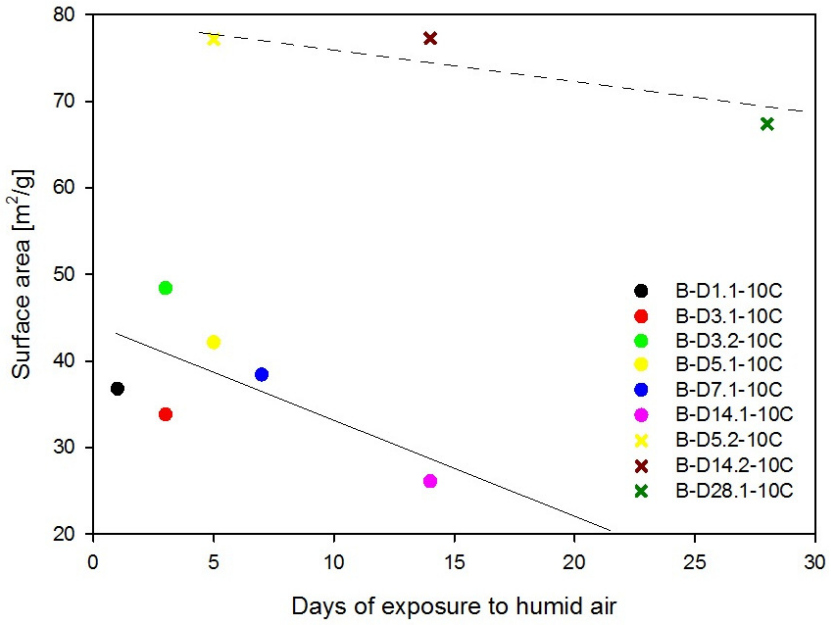

Figure 4.4.18: The surface area as a function of days of exposure to humid air for samples exposed to humid air at 10 °C. The dots represents pH-electrode I and the cross represents pH-electrode II. The dotted and the unbroken lines in the figure are implemented only as a guide for the eye.

In Figure 4.4.19, showing the results from the powder exposed to high humidity (22 °C) the same trends are seen. However, the decrease in the measured surface area is much smaller, and seems to be less dependent on exposure time to humid air compared to the results from the powder exposed to low humidity (10 °C). Some variations in the results can be seen, but these seem smaller than for powders exposed to humid air at 10 °C. For sample B-D7.1-22C the surface area are very low, 9.2 m^2/g, which is expected because no hydrogen gas was measured during the aqueous oxidation experiment. This sample is not included in Figure 4.4.19.

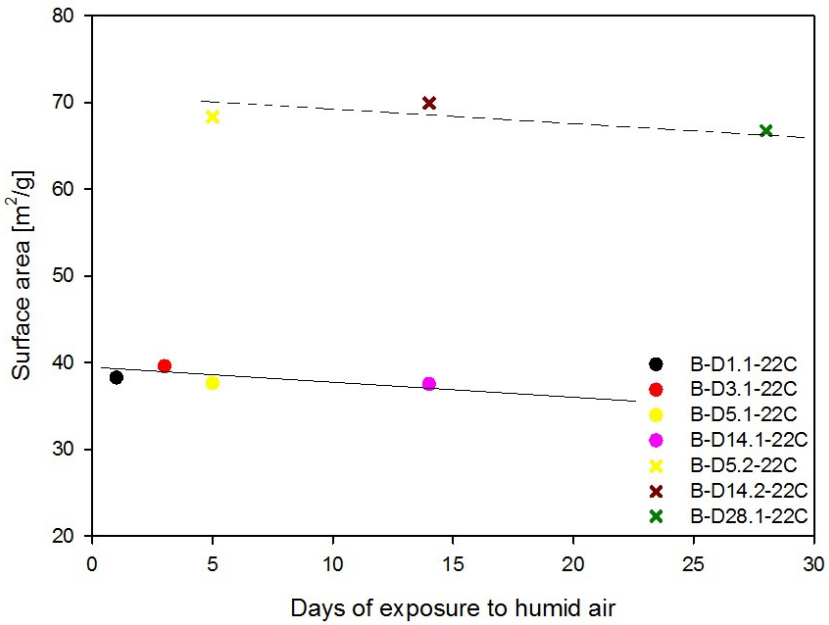

Figure 4.4.19: The surface area as a function of days of exposure to humid air for samples exposed to humid air at 22 °C. The dots represents pH-electrode I and the cross represents pH-electrode II. The dotted and the unbroken lines in the figure are implemented only as a guide for the eye.

The surface area as a function of oxygen content are shown in Figure 4.4.20 for samples exposed to humid air at 10 °C and in Figure 4.4.21 for samples exposed to humid air at 22 °C. Except from sample B-D14.1-10C, a more or less linear relation is shown for both series. The oxygen content measured for sample B-D14.1-10C is much higher than expected based on the surface area and the measurements of the other samples in the series for pH-electrode I. For pH-electrode II, sample B-D5.2-10C has lower oxygen content compared to sample B-D14.2-10C with regards to the measured surface area. For samples exposed to humid air at 22 °C the measured surface areas and oxygen content are about the same for all samples where pH-electrode I was used. The surface area of sample B-D5.1-22C and B-D14.1-22C is about the same as for sample B-D1.1-22C. It was therefore expected that the oxygen content for these samples were the same, but it was rater slightly higher for sample B-D5.1-22C and B-D14.1-22C. For samples where pH-electrode II were used, a small linear increase between surface area and oxygen content was observed. The values measured are about the same for these samples.

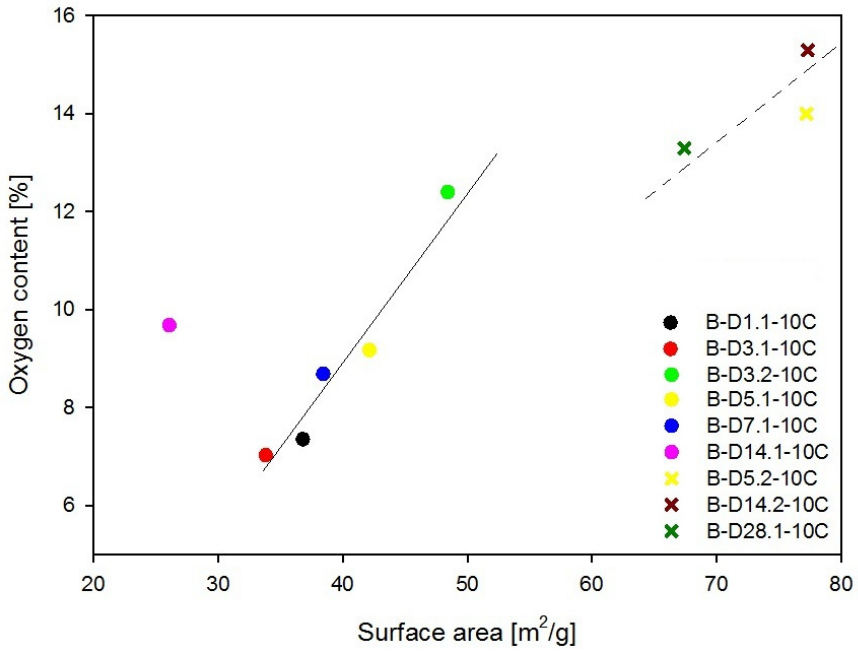

Figure 4.4.20: The surface area as a function of oxygen content for samples exposed to humid air at 10 °C. The dots represents pH-electrode I and the cross represents pH-electrode II. The dotted and the unbroken lines in the figure are implemented only as a guide for the eye.

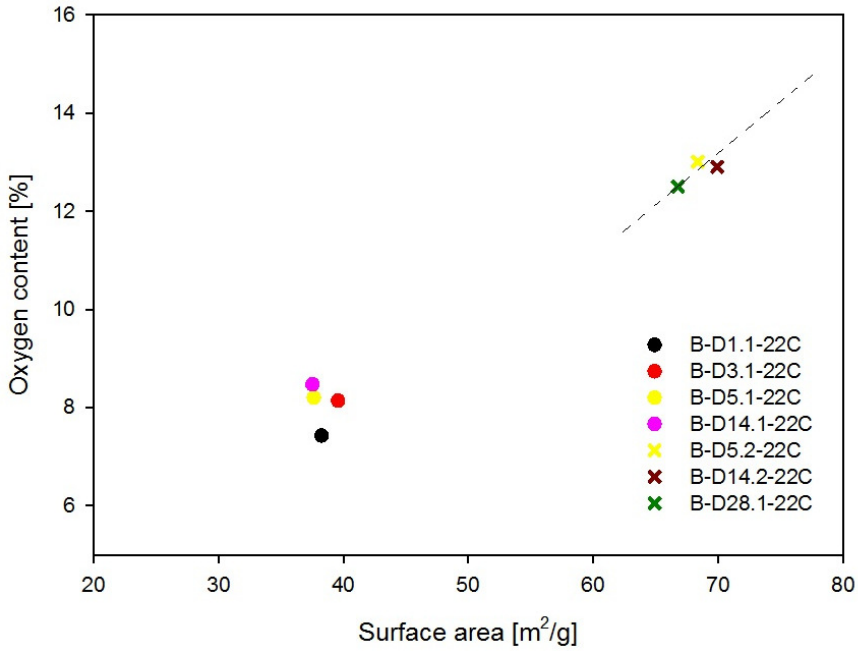

Figure 4.4.21: The surface area as a function of oxygen content for samples exposed to humid air at 22 °C. The dots represents pH-electrode I and the cross represents pH-electrode II. The dotted line in the figure are implemented only as a guide for the eye.

4.4.4 Effect of replacing the pH-electrode

Because the pH-electrode suffered hard wear during the experiments it had to be replaced, which resulted in different results in the hydrogen measurements. This seemed to be because the amount of base added to the slurry before the experiment was much higher after replacing the pH-electrode. To give a clearer picture of how the results were affected by varying the amount of base added, the results using the two different pH-electrodes are presented in the same figures. It is important to emphasise that the pH measured in each experiment was the same, around 9.4. The pH-electrodes were calibrated before each experiment, a detailed description of the calibration process is given in Appendix A. In Figure 4.4.22 and Figure 4.4.23 the amount of base added as a function of onset time for hydrogen evolution is presented for powders exposed to humid air at 10 °C and 22 °C, respectively. The black dots represents the results where pH-electrode I were used and the blue cross represents the results where pH-electrode II were used.

The onset time for hydrogen evolution is much earlier when the amount of base added is higher, as can be seen from the figures. This is most evident for powders exposed to humid air at 22 °C. In Figure 4.4.22, a clear trend between amount of based added and onset time can be seen. From Figure 4.4.23 it is clear that the onset time is much earlier for larger amounts of base added. It is evident that the amount of base added and thus the concentration of hydroxide in the solution, has a large effect on the onset time for hydrogen evolution, and may therefore influence the hydrogen measurements more than the exposure to humid air.

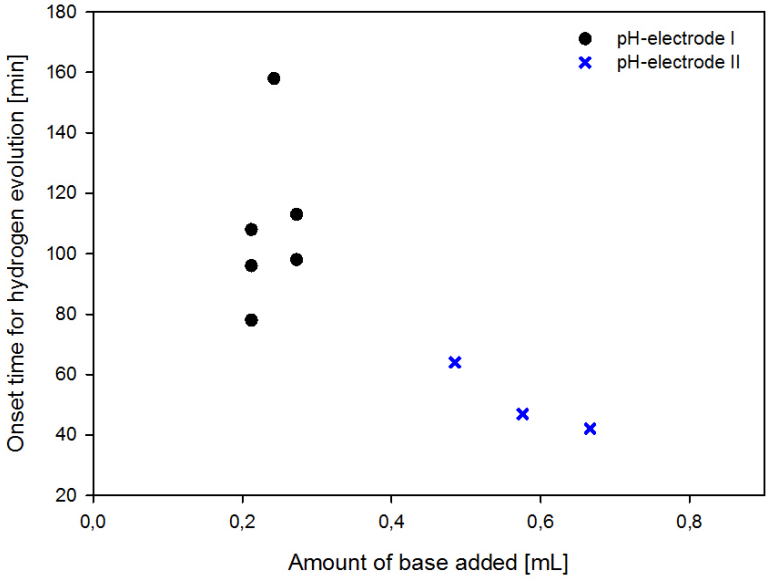

Figure 4.4.22: The onset time for hydrogen evolution as a function of the amount of base added for powders exposed to humid air at 10 °C.

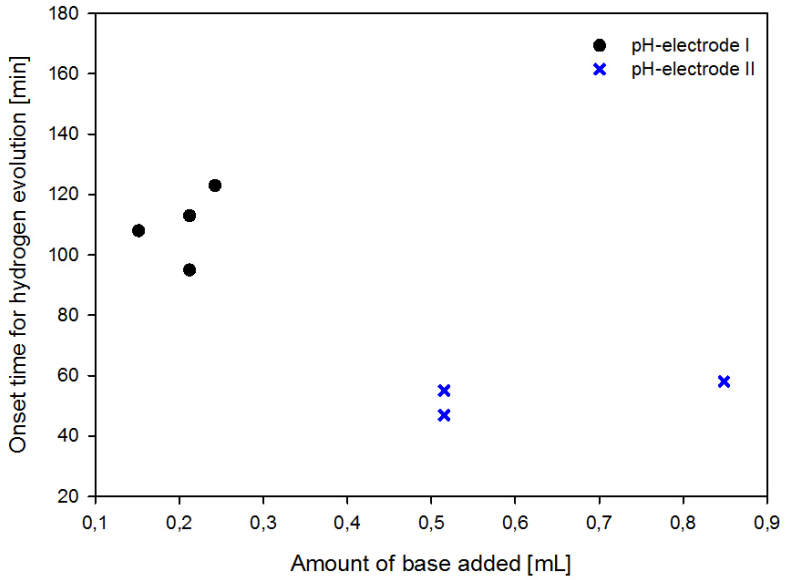

Figure 4.4.23: The onset time for hydrogen evolution as a function of the amount of base added for powders exposed to humid air at 22 °C.

4.4.5 Effect of high pH on aqueous oxidation of silicon powder

Powder exposed to humid air at 10 °C for one day was investigated, sample B-D1-10C-hpH. The start pH for this experiment was raised to 9.65. The onset time for hydrogen evolution was about 50 minutes earlier than expected, compared to sample B-D1.1-10C which also was exposed to humid air at 10 °C for one day. The maximum flow measured was about 5.5 mL/min for sample B-D1-10C-hpH, compared to about 3 mL/min for sample B-D1.1-10C.

The hydrogen flow curve is shown in Figure 4.4.24. The hydrogen gas flow was first measured in the fine flow meter, but because of a higher flow compared to the other measurements, the coarse flow meter had to be used. The hydrogen flow curve therefore consists of the first part measured by the fine flow meter and the second part measured by the coarse flow meter. Measurements done by the fine flow meter shows little noise, whereas the measurements done by the coarse flow meter shows higher hydrogen flow and more noise and scattering. The total amount of hydrogen is difficult to calculate due to much noise and scattering, the change in flow meter will also give a error parameter. However, the total hydrogen flow can be estimated to be around 400 mL, which is about twice the amount compared to the total hydrogen amount measured for sample B-D1.1-10C. The pH at the end of the experiment is 8.72, which is slightly higher compared to the other experiments, where the pH lies around 8.56 at the end of the experiments.

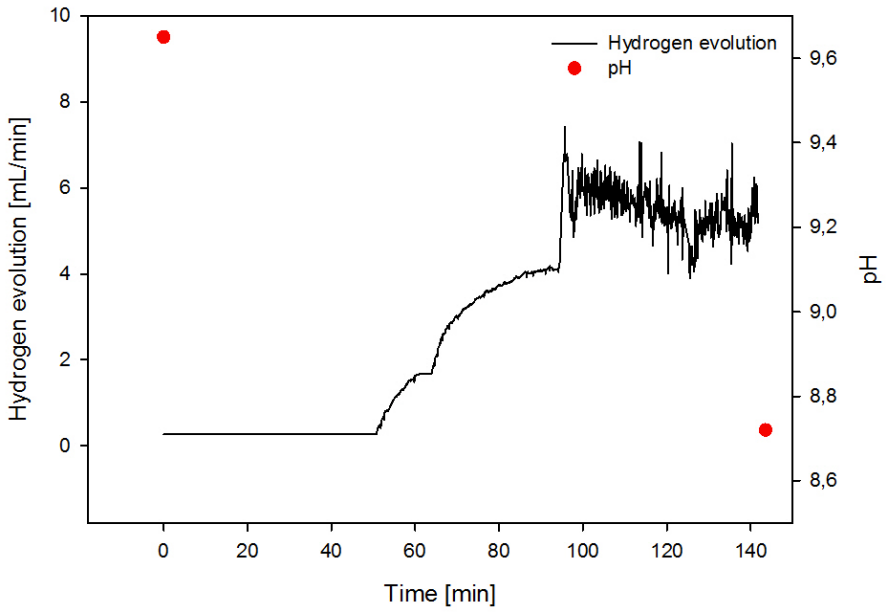

Figure 4.4.24: Hydrogen flow and pH for sample B-D1-10C-hpH, exposed one day to humid air at 10 °C. The pH at the start and at the end of the experiment is shown as red dots. The hydrogen flow is given by the black line. The start pH was raised to 9.65 compared to 9.4 for the other experiments.

4.4.6 Aqueous oxidation of thermally treated silicon powder

Silicon powders from Batch B were thermally treated in order to see if this influenced the aqueous oxidation process. The TG-analysis of untreated silicon powder, Figure 4.1.2, shows that the weight gain of heated silicon power starts at about 800°C. On the basis of this result two different temperatures, 300°C and 900°C, were chosen for the thermal treatment. The aqueous oxidation of powders thermally treated at 300°C did not give any hydrogen evolution during a 6 hours long experiment. It was therefore decided not to do the aqueous oxidation experiment on powder thermally treated at 900°C, since these powders most likely have a thicker oxide layer and therefore are less reactive.

Because no hydrogen was measured for sample B-TO-300C only the BET surface area and the oxygen content will be presented. Table 4.4.4 shows the results.

Table 4.4.4: Overview of the results from the aqueous oxidation reaction of thermally treated powder, presenting BET surface area and oxygen content measured.

Storing conditions	*Temperature exposed to*	*Sample code*	*Surface area* $[m^2/g]$	*Oxygen content [%]*
Batch B	300°C	B-TO-300C	1.1	0.38

The small surface area measured indicates that the thermally grown oxide layer was not dissolved during 6 hours of reaction with water. The underlaying silicon

was therefore not exposed to the solution, thus no oxidation yielding hydrogen was detected. This is verified by the low oxygen content measured, which indicates a small amount of colloidal silica formed.

4.5 SEM analysis

Selected samples from Batch A and Batch B were analysed by SEM. Table 4.5.1 give an overview of the analysed samples.

Table 4.5.1: Overview of the samples analysed by SEM.

Storing conditions	*Atmosphere exposed to*	*Sample code*
Batch A	22 °C - 0.026 atm	A-D2.2-22C
	22 °C - Dry	A-D0.3
Batch B	10 °C - 0.012 atm	B-D3.2-10C
		B-D14.1-10C
	300 °C	B-TO-300C

Only selected pictures will be presented, however all the pictures can be found in Appendix E.

First results from Batch A will be presented, which were prepared by method 1, presented in Chapter 3.6. The hydrogen evolution time for sample A-D0.3 is longer than for sample A-D2.2-22C, it is therefore expected that sample A-D0.3 is more oxidised than sample A-D2.2-22C. Overview pictures of the fine fraction from the ultra sound bath are shown in Figure 4.5.1 for both samples. If present, nano particles will probably be seen in this fraction. The pictures shows that there are more particles with dark colour for A-D0.3, Figure 4.5.1b, than for A-D2.2-22C, Figure 4.5.1a. This indicates oxides or other species with low average atomic number. A clear difference between the samples can be observed. In Figure 4.5.1c-d a larger magnification is used, and oxide-grains can be observed for sample A-D0.3, Figure 4.5.1d. This can be hydroxide, but another method is needed to prove this. For both samples it seems like smaller particles are attached to the surface of the larger particle.

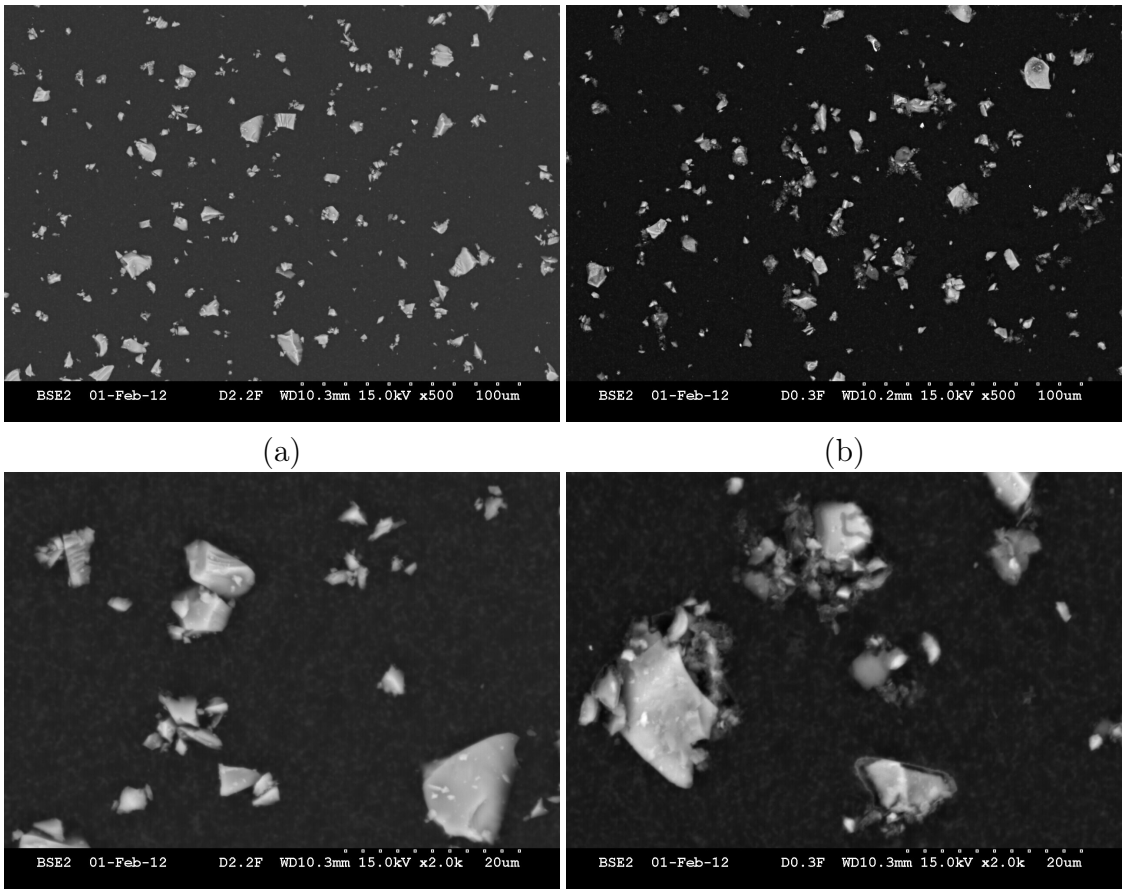

Figure 4.5.1: Pictures of fine fractions of both samples at different magnifications. Oxides are shown as dark areas. a) D2.2, X500 b) D0.3, X500 c) D2.2, 2.0k d) D0.3, 2.0k [31].

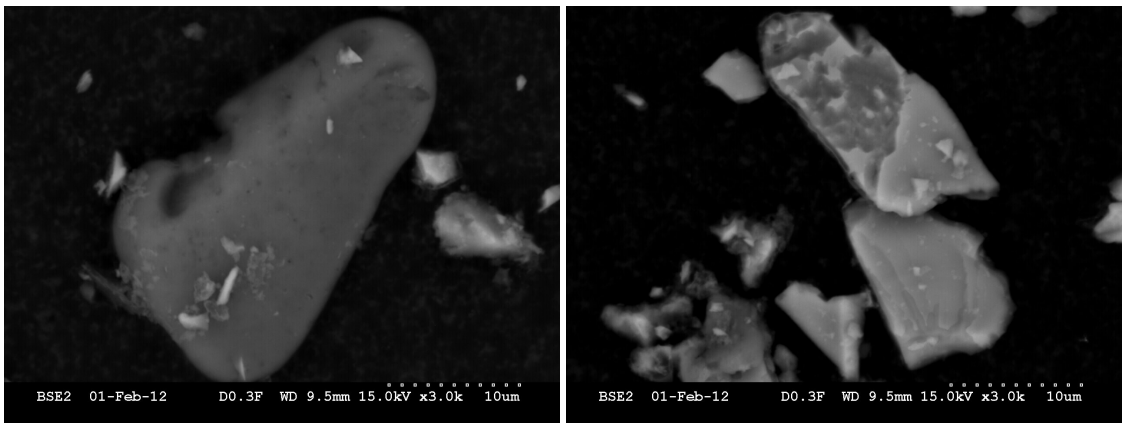

Figure 4.5.2: SEM images of the fine fractions of sample A-D0.3. Two different areas where oxide particles are observed as dark areas is shown [31].

Figure 4.5.2 shows two different areas of the fine fraction of sample A-D0.3 where oxide particles are found, shown as dark areas. Smaller particles attached to

the surface of larger particles can be seen and dark areas containing oxides are evident.

The powders from Batch B is prepared by method 2, presented in Chapter 3.6. No clear difference was seen for the samples exposed to humid air. In Figure 4.5.3 a) and b) images of sample B-D3.2-10C and B-D14.1-10C is shown, respectively. Some dark and bright particles are seen in both samples, but no clear difference is observed from these images. In Figure 4.5.3 c) and d) larger magnification is used. From these images it is clear that some particles are oxidised as seen by the darker areas indicating oxides. Smaller particles seems to be attached to the surface of larger particles for both samples. Cracks can be observed on some of the particles for both samples, as shown by the red arrows. This is believed to be cracks formed in the layer of nano silica particles covering the silicon surface.

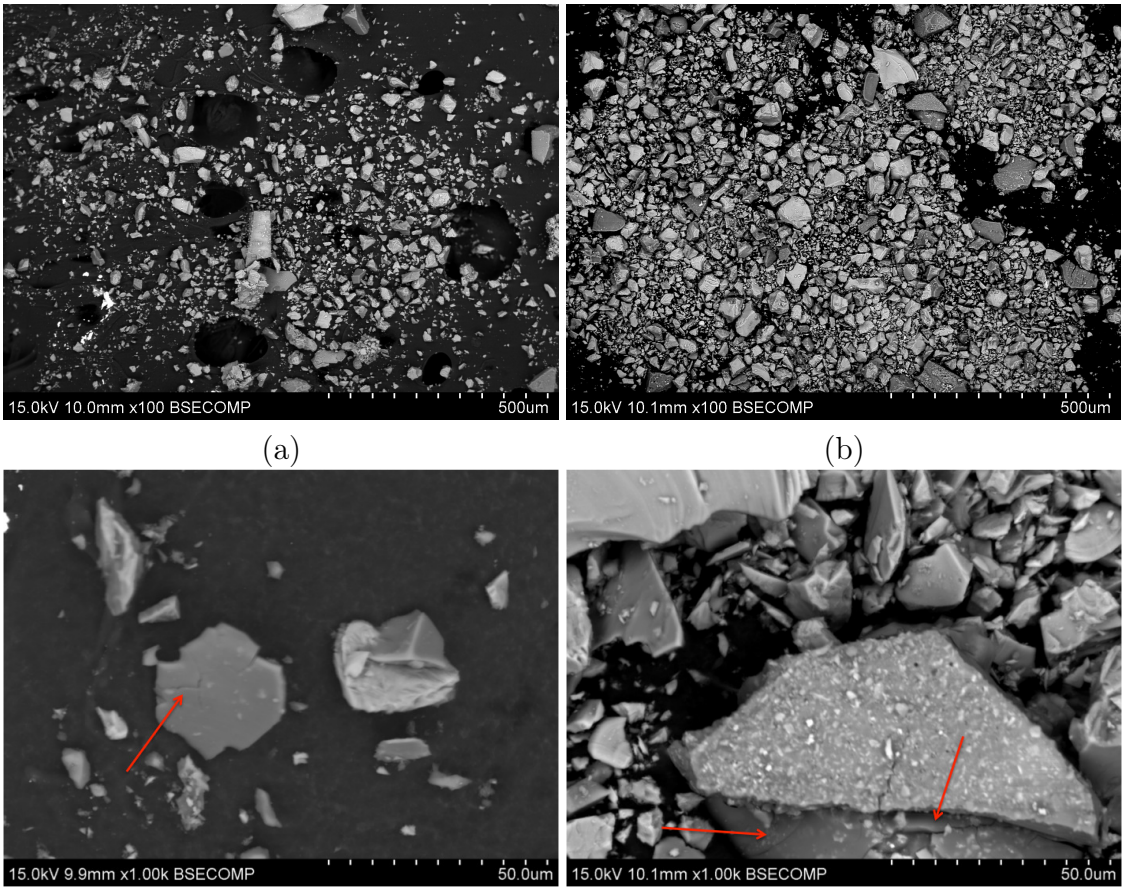

Figure 4.5.3: SEM images of a) B-D3.2-10C, 100X b) B-D14.1-10C, 100X d) B-D3.2-10C, 1.0k e) B-D14.1-10C, 1.0k [31]. The images are showing cracks in the layer of nano silica particles on the surface of silicon particles, indicated by red arrows.

The SEM images of the thermally treated sample, B-TO-300C was different from the images of the humid aged samples. In Figure 4.5.4a an overview image of the sample is shown. Most of the particles have the same grey-colour and small contrast differences can be observed from the image. Based on the small contrast

differences seen, the oxidation of the particles is believed to be more homogeneous, forming an oxide layer of nano silica particles on the surface of the silicon particles. In Figure 4.5.4b larger magnification is used, and it is clear that the contrast difference is small. However, the edges seems to be brighter, which can indicate either silicon or a charging effects. Small particles are attached to the surface of the larger particles also for this sample. No cracks in the nanoscale oxide layer is observed.

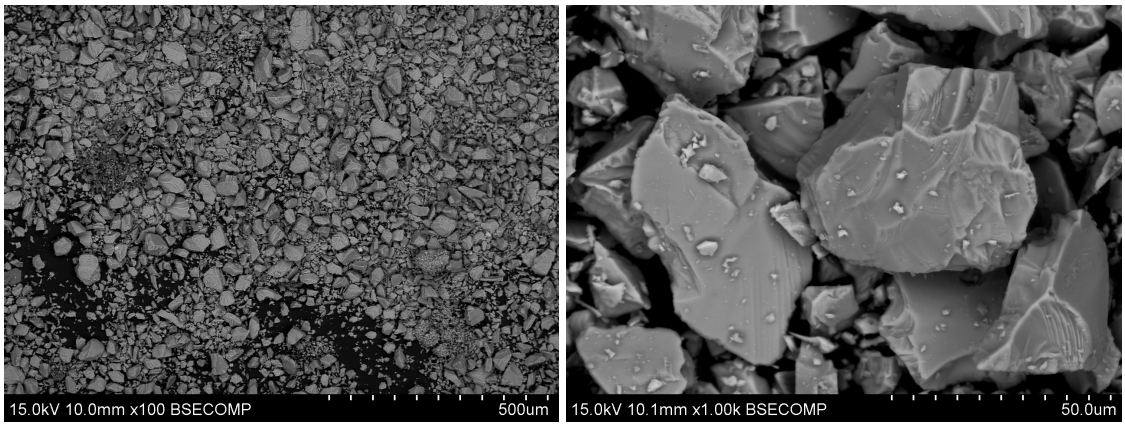

(a) (b)

Figure 4.5.4: Pictures of a) B-D3.2-10C, 100X b) B-D14.1-10C, 100X d) B-D3.2-10C, 1k e) B-D14.1-10C, 1k

4.6 Diffuse Reflectance Infra-red Fourier Transform

Diffuse Reflectance Infra-red Fourier Transform (DRIFTS) was performed on a powder sample A-D21-22C, from Batch A, exposed to 22°C for three weeks. The analysis was performed by Tina Kristiansen at the Department of Chemistry. The signal from hydroxides should appear between 3000 and 3500 cm^{-1}. As can be seen from Figure 4.6.1 no signal was detected from the analysis.

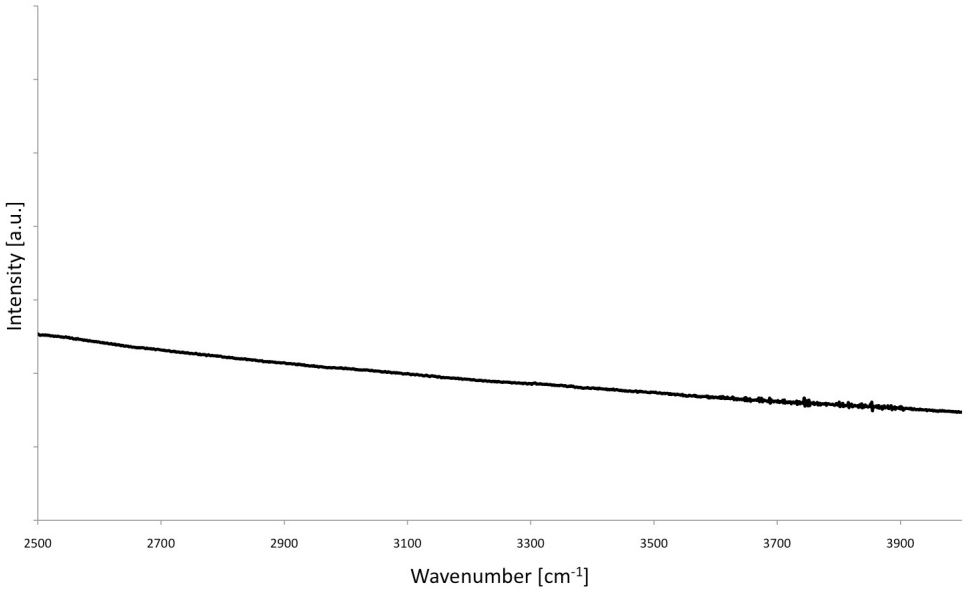

Figure 4.6.1: The spectrum from the DRIFTS analysis of silicon powder exposed to humid air and 22°C for three weeks. No signal was detected.[34].

Chapter 5

Discussion

5.1 Characterisation of silicon powder

XPS proved to be, in a previous study by the author [5], a very suitable method to study the formation of the oxide layer as a function of exposure to humid atmosphere. It was therefore also used to analyse powders stored in a less humid atmosphere and thermally treated powders to obtain a more complete study of the oxide growth. The silicon powders analysed were from Batch A, exposed 2 and 49 days to humid air at 10 °C and powder thermally treated at 300 °C and 900 °C were analysed.

The intensity of the O 1s peaks in the high resolution oxygen spectra is slightly higher for sample A-D2-10C compared to sample A-D49-10C. This is contrary to what was expected. The ageing time in humid air for sample A-D49-10C was longer than for sample A-D2-10C, thus a thicker oxide layer would form. Since a higher O 1s peak indicates a higher oxygen content it was therefore believed that the O 1s peak would be highest for sample A-D49-10C. The oxygen peak for the sample aged 49 days is broader than the peak for the sample aged 2 days, which is thinner and additional bands are located at the high energy side. Because the shape of the curves are very different it is difficult to compare the hydroxide contents in the two samples. It seems like the hydroxide content in sample A-D2-10C is higher than for sample A-D49-10C because of the additional bands observed, which is directly opposite of what is expected. However, the overall broader peak for sample A-D49-10C may also indicate a high hydroxide content. The hydroxide content for sample A-D2-10C is nevertheless lower than for samples exposed to humid air at 22 °C because of ageing in a less humid atmosphere. This is shown in the reprint of Figure 4.2.2 in 5.1.1.

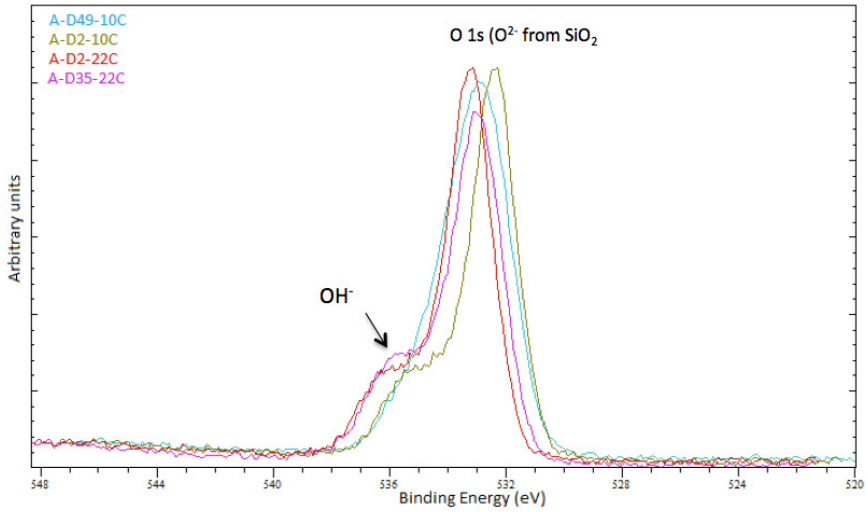

Figure 5.1.1: High resolution O 1s spectra of different silicon samples A-D2-10C, A-D49-10C, A-D2-22C and A-D35-22C. Hydroxide present is shown as a broadening of the O 1s peak on the high energy side.

These results are supported by findings in the literature, which states that exposure to higher humidity results in retardation of oxidation of $Si-H_2$ bonds [4]. The effect on humidity on the formation of the oxide layer is believed to be smaller in low humidity compared to high. The high resolution Si 2p spectra showed no obvious difference in oxide thickness, since the SiO_x/Si intensity ratios were similar for the two samples exposed to humid air at 10 °C. Sample A-D2-10C and A-D2-22C were exposed 2 days to low and high humidity, respectively. They showed no apparent difference in SiO_x/Si intensity ratio. The powders A-D49-10C and A-D35-22C, that were stored for longer times, showed no significant difference in SiO_x/Si intensity ratios either, but a broader Si^{4+} peak was observed for sample A-D49-10C. The broadness of the peak for sample A-D49-10C can be because of stronger charging effects, indicating a more insulating nature of the underlaying silicon. Silicon suboxides and/or Si-H bonds may also contribute to broadening of the peak.

Powders thermally treated at 900 °C showed a much higher oxygen content than powder thermally treated at 300 °C. The O 1s peak for powder exposed 49 days to humid air at 10 °C is broader compared to the thermally treated powders. This suggest a presence of hydroxide on the surface after exposure to humid air. The O 1s peaks are higher for the thermally treated powders, indicating more oxygen. The SiO_x/Si intensity ratio is also larger, which would suggest a thicker oxide layer. Only the Si^{4+} peak could be measured for sample A-TO-900C indicating a thick oxide layer.

The oxide thickness was estimated to be 0.7 nm for powders exposed to humid air at 10 °C, about 1.5 nm for samples exposed to humid air at 22 °C, 0.7 nm for sample A-TO-300C and >10 nm for sample A-TO-900C. From the estimated oxide thickness of the humid silicon powders it may appear like the thickness is dependent on the level of humidity in the ageing atmosphere. More analysis of powders exposed to low (10 °C) and high (22 °C) humidity are needed to verify this. The estimated oxide thickness for sample A-TO-300C was expected to be much

larger than for the powders exposed to humid air, but this was not the case for all samples. The reason for why the oxide layer for sample A-TO-300C was not much larger than this can be explained by the result from the TG analysis. It was found that no apparent weight gain appeared before 800 °C, which can explain the small oxide thickness measured, indicating that the oxide has not grown significantly during heating. In addition, the structure of the thermally grown oxide may be different from the oxide formed in humid air. This might have an impact on the measurements. It is important to mention that the oxide thickness estimation is based on that the oxide grows on a flat surfaces. Therefore the effects of curvature and surface roughness are not accounted for. The oxide thickness calculations gave an oxide layer thicker than 10 nm for sample A-TO-900C, which is much thicker than the analysis depth for XPS.

In short, XPS analysis can give valuable information about the oxide layer formed during ageing. The oxide layer is estimated to be thicker for powders aged at high humidity compared to low. On the basis of this results, ageing in higher humidity will give a less reactive silicon surface regarding the water based slip casting process.

Raman Spectroscopy, using the UV-laser at 325 nm, was performed on both aqueous oxidised silicon powder and silicon powder aged in humid air, to determine if the method was suitable for the study of the development of an oxide layer on the silicon particle surface. The main reason for trying the Raman analysing was in order to identify the presence of hydroxide ions on the surface. If present, OH^- ions would appear as a peak between 3000 cm^{-1} and 3500 cm^{-1}, which was not observed for these samples. However, a shift and broadening of the silicon peak was observed for the analysed samples, which can give information about the oxidation process. The broad peak for sample B-D0.2 is believed to consist of two peaks, one at 515 cm^{-1} and one at 504 cm^{-1}. One hypothesis explaining the appearance of these peaks is that the crystalline silicon peak originating from the silicon core is shifted to lower energy due to strain effects, and appear at 515 cm^{-1}. The peak at 504 cm^{-1} is also believed to be crystalline silicon, but originating from nano-inclusions within the amorphous silica matrix. Because of size effects this peak is shifted to event lower energy. For sample A-D57-22C one peak appear at 505 cm^{-1}, which, based on the hypothesis is believed to be from the crystalline nano-inclusions. For sample B-D5.1-22C a broad and weak peak appear at 488 cm^{-1}. This may be amorphous silicon, which can be found around 480 cm^{-1}.

Diffuse Reflectance Infra-red Fourier Transform was performed on one unreacted, humid sample, B-21.2-22C, in desire to observe hydroxide ions. The method seems to be unsuitable to measure the presence of hydroxide ions on the silicon particle surface.

5.2 Aqueous oxidation of silicon powders

In all of the aqueous oxidation experiments a slurry of silicon powder mixed with water was used. The slurry was dried and the powder was mortared before any further analysis of the powder was performed. The powder can reveal a lot of

information about the oxidation process and was therefore studied by SEM and measurements of surface area and oxygen content.

To verify the reproducibility of the hydrogen measurements a number of tests on dry powder were conducted. The result was promising, giving about the same onset time for hydrogen evolution, total amount of hydrogen measured and pH at the end of the experiment. Based on these results, the reproducibility is believed to be good and the experimental method and routine is acceptable with regards to measuring the hydrogen formation in the aqueous oxidation of silicon powder.

During the aqueous oxidation reaction the pH in the slurry decreased from the start of the experiment to the end. For pH-electrode I the decrease in pH seemed to be dependent on the exposure time to humid air, because the pH decrease was larger for powders aged longer in humid air. This can be explained by the formation of a thicker oxide layer during ageing. As the oxide layer grows thicker more hydroxide is needed from the solution to dissolve the silica layer formed, which can explain that the decrease in pH was larger for thicker oxide layers. A thicker oxide layer was believed to form on samples exposed to humid air at 22 °C compared to samples exposed to humid air at 10 °C, yielding a larger pH decrease. This was however not the case, and the end- pH for some of the samples exposed to humid air at 10°C was even observed to be slightly higher than for samples exposed to humid air at 22 °C. An explanation of this observation can be that the particle surface is believed to become more hydrated in higher humidity (22 °C) compared to lower (10 °C), thus needing less hydroxide from the solution to dissolve the formed oxide layer. The difference in pH was small and no conclusion regarding the hydrated surface can be given based on the pH alone. However, XPS analysis of humid powders showed that the hydroxide content increased with increasing exposure to humid air. This was most evident for powders exposed to humid air at 22 °C. In order to give a conclusion regarding the hydration of the silicon surface as a function of humidity, more measurements are necessary. It would also be useful to find a suitable method for measuring the hydroxide content more accurately.

For experiments were pH-electrode II was used, the pH decrease was about the same for all samples and seemed to be more or less independent on exposure time to humid air. The initial concentration of hydroxide was higher for these samples, which can explain the different observation regarding the pH decrease. The difference between pH-electrode I and pH-electrode II will be discussed more later.

The onset time for hydrogen evolution was dependent on the storing history of the silicon powers. As the exposure to humid air increased the onset time was delayed. This indicated that a thicker oxide layer had formed during ageing leading to a longer dissolution process. Hydrogen is believed to form first *after* the silica layer is dissolved and the underlaying silicon is exposed to the solution. This can explain the dependence between onset time and thickness of the oxide layer, and thus also the dissolution process. However, some deviations can be seen from the results regarding the onset time. For powders exposed to humid air at 10 °C variations in the onset time is clearly seen, especially for powders with short ageing time. Sample B-D1.1-10C has a later onset time than samples B-D3.1-10C, B-D3.2-10C

and B-D5.1-10C, which is difficult to explain. No obvious trend can be observed for these samples. However, as the ageing time increases to more than five days the onset time is clearly later. In Figure 5.2.1 a reprint of Figure 4.4.9 is given, showing the relation between onset time for hydrogen evolution and ageing time in humid air.

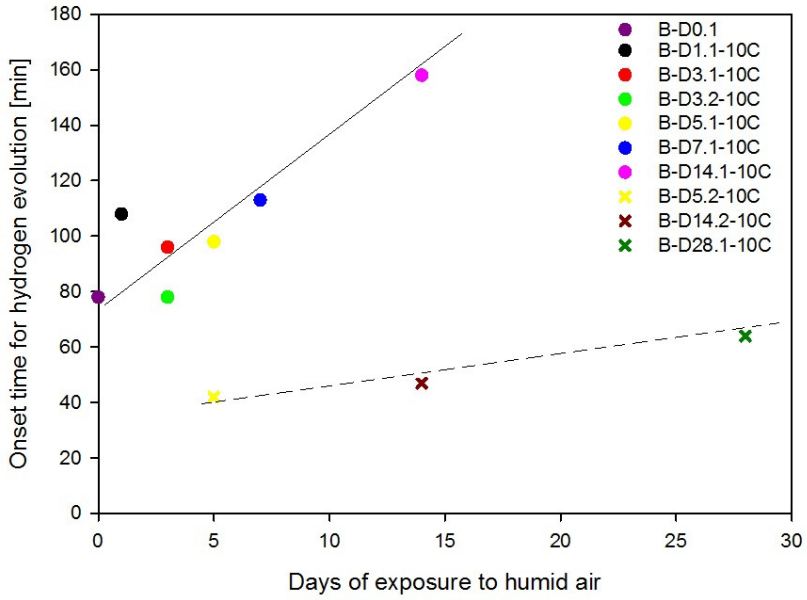

Figure 5.2.1: Onset time for hydrogen evolution for samples exposed to humid air at 10 °C. The dots represents pH-electrode I and the cross represents pH-electrode II. The dotted and the unbroken lines in the figure are implemented only as a guide for the eye, showing a later onset time as the exposure to humid air increases.

For powders exposed to humid air at 22 °C a linear relation between onset time is seen for short ageing. However, the onset time for sample B-D14.1-22C, aged 14 days in humid air, is much earlier than expected and is about the same as for sample B-D3.1-22C. The variations in onset time for short ageing samples for powders exposed 10 °C compared to samples exposed to humid air at 22 °C can be explained by the theory that a thicker and more stable oxide layer will form in a more humid atmosphere. This can result in a more stable and homogeneous oxide layer, showing a clearer tendency with respect to the obtained results from the measurements. An explanation for the deviations in the onset time for powders exposed to humid air at both 10 °C and 22 °C have not been found. However, because the hydrogen measurements for dry powder has found to be reproducible, one theory is that the exposure to humid air influence the samples differently. The sampling of the powder, like for instance the particle size distribution within each sample, can vary and is difficult to control. This will affect both the hydrolysis of the particle surface during ageing and the dissolution process in the aqueous oxidation. Even though the powder samples are exposed to the same humidity conditions it seems difficult to reproduce the ageing in humid air, which can explain the variations in the hydrogen measurements. However, these variations is not expected to result in large deviations (as seen for sample B-D14.1-10C) and no explanation is yet found for the much earlier onset time for this sample. The

hydroxide concentration is however believed to be very important, especially regarding the dissolution process and onset time. This will be discussed further in Chapter 5.3.

The onset time for hydrogen evolution for samples exposed to humid air at 22 °C seems to be later compared to the onset time for samples exposed to humid air at 10 °C. This is shown by the implemented lines in Figure 4.4.15. However, for long exposure time to humid air the onset time is higher for the samples exposed to humid air at 10 °C. The reason for this is not clear, and no deviations was found in the experimental routine. More experiments on powder exposed to high (22 °C) and low (10 °C) humidity are needed to give any conclusion on how the humidity affects the onset time for hydrogen evolution. However, based on the thinner oxide thickness estimated for powders exposed to low humidity the onset time should be earlier than for powder exposed to high humidity. The deviation seen could therefore be errors related to the measurements or the ageing of the powder.

The total amount of hydrogen formed in the aqueous oxidation reactions are calculated using the trapezoidal method. When the silica layer formed on the surface is dissolved, it is believed that the same amount of silicon powder will react with the solution. The amount of hydrogen formed should therefore be approximately the same for most of the powders when the hydrogen evolution time is the same (90 minutes). However, for silicon powder exposed to humid air at 10 °C some variations in the results were observed. This was especially evident for sample B-D3.1-10C and B-D3.2-10C. The two powders were exposed to the same humidity and were expected to give the same amount of hydrogen. A much smaller amount was however measured for sample B-D3.1-10C compared to sample B-D3.2-10C, 128 mL/min and 296 mL/min, respectively. The amount measured for sample B-D3.1-10C was much lower compared to the trend shown for all the samples. The reason for this is not known and there was not discovered any deviations in the experimental routine that could explain this behaviour. For powders exposed to humid air at 22 °C the variations in total amount hydrogen measured was smaller, and for the samples with short ageing time the amount was about the same. For sample B-D7.1-22C no hydrogen was measured during 4 hours of oxidation. For sample B-D14.1-22C, which was aged 14 days, hydrogen onset was much earlier than expected and the total amount hydrogen measured was much less than samples exposed 1, 3 and 5 days to humid air.

The reason for the variations in the results is not known, however it may seem like the total amount of hydrogen formed decreases if the ageing time in humid air is long. The amount of powder weighed out for each sample may vary because of the hydration of the silicon surface leading to a weight gain. The pH in the solution will also affect the hydrogen formation, as higher hydroxide concentration result in more hydrogen according to Equation 5.2.1.

$$\mathrm{Si(s)} + 4\,\mathrm{OH^-} \longrightarrow \mathrm{SiO_4^{4-}}(aq) + 2H_2(g) \tag{5.2.1}$$

To summarise, the pH-end decreases as the exposure time to humid air increases. However, the results from pH-electrode II seems to be more or less independent on ageing history. Only a slight decrease in pH is observed as the ageing time

increases. The onset time for hydrogen evolution is dependent on both the ageing duration and the atmosphere conditions. It seems to be later as the exposure time to humid air increases, and higher humidity seems to have a larger effect on delaying the onset time compared to lower humidity. The total amount of hydrogen evolved is more or less independent on exposure time to humid air for samples having the same hydrogen evolution time.

5.3 The effect of high pH on the aqueous oxidation of silicon powder

The pH for sample B-D1-10C-hpH from Batch B, exposed one day to humid air at 10 °C was raised to 9.65 at the start of the experiment. This resulted in a much earlier onset time for hydrogen evolution than expected. The onset time was about 50 minutes earlier compared to sample B-D1.1-10C, which had the same ageing time and atmosphere. This can be explained by the high concentration of hydroxide ions in the solution contributing to the dissolution process of the silica layer on the silicon surface.

Based on these results, showing a relation between pH and onset time for hydrogen evolution, the deviation for samples where pH-electrode II were used can be explained. Even tough the pH measured was the same as for the other experiments, the amount of base added to these samples were registered to be higher. The higher hydroxide content in these solutions was therefore higher, contributing to the dissolution of the silica layer and giving an earlier onset time for hydrogen evolution. Since both the onset time for hydrogen evolution and the hydrogen flow was affected by this, it is clearly an important parameter and should be carefully controlled to reduce the hydrogen formation in the aqueous oxidation process. In the industry, where the pH is raised in order to give a stable dispersion for the slip casting process, it is crucial to have a accurate control of the hydroxide content in order to be able to control the hydrogen formation.

5.4 Analysis of reacted powder from the aqueous oxidation of silicon powder

The surface area measured for the silicon powders says something about the formation and content of colloidal silica on the silicon particle surface. A larger formation of colloidal silica is believed to give a higher surface area. The surface areas measured for powder samples from Batch A showed a linear relation with increasing oxygen content. This verifies that the surface area measured can be colloidal silica formed on the particle surface, because of the increasing oxygen content with increasing surface area. The linear increase is more clear for samples exposed to humid air at 10 °C compared to samples exposed to humid air at 22 °C, where about the same surface area and oxygen content are measured. The linear relation between measured surface area and oxygen content could also be seen for

powder samples from Batch B. A more clear trend could be observed for samples exposed to humid air at 10 °C compared to samples exposed to humid air at 22 °C. The measured surface area for samples exposed to humid air at 22 °C were about the same, verified by the similar oxygen contents measured for the samples. This confirms the trend seen for powders from Batch A, where surface area and oxygen content is directly related. The surface area for powders from Batch B seems to be more or less independent of the ageing in humid air. This can be explained by the hydrogen evolution time, which is the same for all samples from Batch B. For similar hydrogen evolution times the same amount of silicon powder is believed to oxidise, thus giving the same surface area. Because of uncertainties in the hydrogen evolution time for sample from Batch A, it is difficult to discuss how the surface area is affected by ageing in humid air, but based on the results from Batch B the same trend is expected. The surface area measured seems to be higher for powders exposed to humid air at 10 °C compared to powders exposed to humid air at 22 °C. This indicates a more oxidised surface, which is contrary to the total amount of hydrogen measured.

In short, the surface area and the oxygen content measured for the silicon powder is directly related. The same hydrogen evolution time gives about the same surface area indicating the same degree of oxidation.

In Figure 5.4.1 the amount of oxygen as a function of hydrogen formed in the aqueous oxidation reactions is shown. Trend lines for the amount of oxygen versus hydrogen for the reactions resulting in silica, Equation 5.4.1, and silicic acid, Equation 5.4.2, are included. The experimental values plotted are the total amount of hydrogen measured and the oxygen content measured by LECO. All the experimental data are more or less concentrated around the line for silica. This indicates that the solubility limit for silicic acid is reached for all experiments, resulting in condensation and polymerisation to form colloidal silica. The amount of oxygen measured deviates from the theoretical line at high hydrogen amounts, which can be explained by less accurate measurements by the coarse flow meter giving too high hydrogen amounts.

$$\mathrm{Si(s)} + 2\,\mathrm{H_2O(l)} \longrightarrow \mathrm{SiO_2(s)} + 2\,\mathrm{H_2(g)} \tag{5.4.1}$$

$$\mathrm{Si(s)} + 4\,\mathrm{H_2O(l)} \longrightarrow \mathrm{Si(OH)_4(aq)} + 2\,\mathrm{H_2(g)} \tag{5.4.2}$$

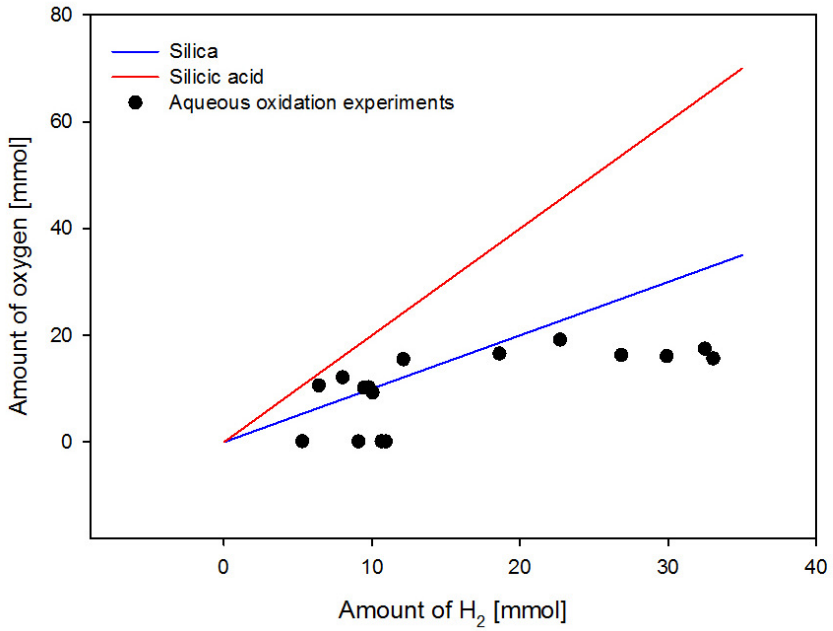

Figure 5.4.1: Amount of oxygen as a function of amount of hydrogen evolved, theoretically, in the aqueous oxidation reactions. All samples from Batch B are included.

Scanning electron microscopy was used to image the particle surface after aqueous oxidation of silicon powder in the hope to see any differences between the reacted powders. Five samples of aqueous oxidised powders were analysed, four samples exposed to humid air and one thermally treated sample. The sample analysis of A-D0.3 and A-D2.2-22C, which had different duration of hydrogen evolution, showed more dark particles for sample A-D0.3. The dark particles indicate silicon oxides in the sample. This was expected because of a longer hydrogen evolution time and thus the formation of more silica. For samples A-3.2-10C and A-D14-10C, which both had 90 minutes of hydrogen evolution, bright and dark particles could be observed for both samples. However, no obvious difference could be observed between the samples. The measured surface area was higher for sample A-D3.2-10C and it was expected to see a small difference even though the hydrogen evolution time was the same, however it was difficult to conclude anything based on the SEM images. The SEM analysis of the thermally treated sample, B-TO-300C, was clearly different from the analysis of the powders exposed to humid air. There were small variations in dark and bright particles indicating a more homogeneous oxidation, as expected.

5.5 Challenges concerning the experimental method and the apparatus

During part one of the aqueous oxidation experiment of powders from Batch A some problems with the hydrogen measurements were identified. Scattering and variations in the results gave reasons to believe that something external affected the

results. On the basis of this it was believed that some of the gas measured in this part actually was evaporated nitrogen from the cold trap that condensed during the nitrogen flush in the start of the experiment. It was therefore difficult to identify the onset time for hydrogen evolution and the amount of hydrogen gas evolved in the aqueous oxidation reaction. If some of the gas measured was nitrogen, this can explain the high gas flow and noise for some of the measurements. A change in the experimental routine was implemented, hindering condensation during flushing of nitrogen, resulting in lower scattering and variations in the experimental results. After changing the experimental routine, the total amount of hydrogen measured corresponded well with both oxygen content and surface area measurements. The problems observed concerning the stirring of the slurry also seemed to disappear when the reaction bottle was replaced with a flat bottom bottle.

The pH- electrode suffered high wear when it was exposed to the agitated slurry, and it needed to be replaced frequently. Even though the pH-electrodes were calibrated before each new measurement with the same calibration solutions, the amount of base needed to obtain the same pH value was different for each experiment. This was especially clear for samples B-D5.2-10C, B-14.2-10C, B-28.1-10C, B-D5.2-22C, B-14.2-22C, B-28.1-22C where the amount was roughly doubled or tripled compared to the other samples. A higher ion concentration was therefore expected in these samples, which was believed to cause the earlier onset time and the higher amount of hydrogen observed. Thus, it is believed that the hydroxide concentration is the critical factor in the hydrogen measurements. To control the reaction, the pH needs to be measured correctly.

Reproduction of hydrogen measurements of powders exposed to humid air was a problem. Since the reproducibility of hydrogen measurements of dry powders was verified, it was believed that the problem lied within the exposure to humid air. Powders exposed to the same humidity, like sample B-D3.1-10C and B-D3.2-10C, gave different results with respect to hydrogen measurements and surface area measured. No difference could be found in the experimental parameters or routine and about the same amount of base was added to the slurry. It is therefore believed that some unknown parameters regarding the ageing in humid air affected the powder differently. As earlier mentioned, it is also believed that the sampling of the different samples can influence the results, for example with regards to the particle size distribution within each sample, which will affect both hydrolysis and dissolution of silica.

5.6 Silicon powders for the water based slip casting process

The formation of a passivating oxide layer on the silicon particle surface seems to be affected by the degree of humidity in the atmosphere and the duration of storing in this atmosphere. Ageing in high humidity is more effective for the the development of a stable oxide layer compared to lower humidity, seen by a later onset time for hydrogen evolution. The total amount of hydrogen seems to be more or less independent on exposure time to humid air. However, both onset

time for hydrogen evolution and the amount of hydrogen formed is dependent on the concentration of hydroxide in the solution. Higher hydroxide concentration yields more hydrogen and an earlier onset time.

To summarise, ageing in humid atmosphere will retard the onset time for hydrogen evolution. The total amount of hydrogen formed, and therefore also the level of defects (as pores) in the green body, seems to be dependent on the hydrogen evolution time and the concentration of hydroxide in the solution. It is therefore suggested that silicon powders, used in the water based slip casting process, should be aged in humid air for some time before processing. To minimise the hydrogen formation the hydroxide concentration must be carefully controlled. This is especially important regarding the suspensions used in the slip casting process, where the pH is raised in order obtain a stable dispersion, giving a dense green body.

Chapter 6

Conclusion

Characterisation of humid and thermally treated silicon powder has been performed with XPS. The analysis of humid powder exposed to 10 °C showed lower oxide content compared to powders exposed to humid air at 22 °C. This indicates that exposure to higher humidity have larger effect on the development of an oxide layer on silicon compared to exposure to lower humidity air. A higher hydroxide content was also found for samples aged at higher humid atmosphere. The estimated oxide thickness for samples exposed to humid air at 10 °C seemed to be smaller than the oxide thickness estimated for powders exposed to humid air at 22 °C. No obvious difference was seen for short and long ageing time in humid air at 10 °C. Analysis of thermally treated silicon powder showed a much higher oxygen content compared to powder exposed to humid air, stating a more effective oxidation process of the surface. No hydroxide was identified.

Powder aged in humid air made the powder less reactive in reaction with water, observed by the later onset time for hydrogen evolution as the exposure time increased. No clear difference in onset time and amount of hydrogen evolved for powders exposed to different humidities were observed from the hydrogen measurements. However, the measured surface area was higher for powders exposed to low humidity compared to powder exposed to higher humidity, indicating a higher reactivity. Based on this observation it is believed that exposure to higher humidity influences the development of an oxide layer more than exposure to lower humidity. However, more experiments should be performed to state this.

The absence of hydrogen evolution from the aqueous oxidation of powder thermally treated at 300 °C indicates the formation of a thicker and more homogeneous oxide layer. The absence of hydrogen formation was verified by a low surface area, indicating that no colloidal silica had formed on the silicon particle surface.

Higher hydroxide content seemed to have a large effect on the onset time and the amount of hydrogen measured in the aqueous oxidation. It is therefore important to control this accurately if comparable results are wanted. Higher hydroxide content gave both earlier onset time and higher hydrogen flow in the aqueous oxidation experiments.

The correlation between hydrogen evolved, surface area and oxygen content measured seem to be good, making the method for measuring the hydrogen evolution

satisfying. However, reproduction of results of powder exposed to humid air seem to be difficult. This is believed to be both because of variation in the humidity exposure, even though the atmosphere conditions was the same, and problems with controlling the hydroxide concentrations in the slurry. The variation in hydroxide content, despite of the same pH measured, is believed to be the main reason for the variations from the expected trends. To be able to conclude anything it is therefore necessary to control the hydroxide content in each experiment. A better control of the sampling of the powder would also minimise the possible errors in the results.

SEM analysis could not differ between the silicon surface of reacted powders exposed to humid air with the same hydrogen evolution time. However, a clear difference could be observed for reacted thermally treated powder compared to reacted powder aged in humid air.

Raman Spectroscopy seemed to be a very useful method to study the silicon surface and the structure change occurring during oxidation. An obvious difference in the crystalline silicon peak could be seen between the silicon wafer, the humid aged powders and the aqueous oxidised sample.

A defect free green body can be obtained by reducing the hydrogen formation in the water based slip casting process. This can be obtained by ageing the powder in humid atmosphere before processing. Higher humidity and longer ageing time seems to affect the development of the oxide layer formed on the surface more than low humidity and short ageing time. To minimise the hydrogen formation, it is crucial to be able to control the hydroxide concentration in the aqueous oxidation accurately.

Chapter 7

Further work

The main focus regarding further work will be to analyse the silicon particles with Transmission Electron Microscopy (TEM) in order to see if the development of the oxide layer formed can be observed. The TEM analysis can supplement what is found in the Raman analysis.

Secondly more hydrogen measurements emphasising on the hydroxide concentration should be performed in order to state the effect of high pH both on onset time for hydrogen evolution and amount of hydrogen formed. Controlling the hydroxide content may also give clearer trends with respect to the exposure to humid air and the different humidities.

Bibliography

[1] Richerson, D. W. *Modern Ceramic Engineering, Properties, Processing and Use in Design;* Taylor and Francis Group, third ed., 2006.

[2] Ceramic products. Luoyang Beiyuan Special, C. C. **2011**.

[3] Dillinger, R.; Heinrich, J.; Huber, J. *Material Science and Engineering* **1988**, pages 373–378.

[4] Niwano, M.; Kageyama, J.; Kurita, K.; Kinashi, K.; Takahashi, I.; Miyamoto, N. *Journal of Applied Physics* **1994**, *76*(4).

[5] Nymark, A. M. Project work; Oxidation of silicon powder in humid atmosphere, **2011**.

[6] Cerfonlini, G.; Meda, L. *Physical chemistry of, in and on Silicon;* Springer-Verlag, 1989.

[7] Rong, H. M. *Silicon for the direct process to methylchlorosilanes* PhD thesis, NTNU, **1992**.

[8] Papirer, E., Ed. *Adsorption On Silica Surfaces*, Vol. 90 of *Surfactan science series;* Marcel Dekker, Inc, 2000.

[9] Hackley, V.; Paik, U.; Kim, B.-H.; Malghan, S. G. *J. Am. Ceram. Soc* **1997**, *80*(7).

[10] Iler, R. K. *The chemistry of silica;* Wiley-Interscience, 1979.

[11] Legrand, A. P., Ed. *The Surface Properties Of Silica;* John Wiley and Sons Ltd, 1998.

[12] Rahman, M. N. *Ceramic processing and sintering;* Marcel Dekker, Inc, 1995.

[13] Jørgensen, H. T. S. Oxidation of silicon in aqueous media Master's thesis, NTNU, **2011**.

[14] Okada, R.; Iijima, S. *App. Phys. Lett.* **1991**, *58*(15).

[15] Mortia, M.; Ohmi, T.; Hasegawa, E.; Kawakami, M.; Ohwada, M. *Journal of Applied Physics* **1990**, *68*(3), 1272.

[16] Cerfolini, G. F.; Meda, L. *Journal of Non-Crystalline Solids* **1997**, *216*, 140–147.

[17] Thermal oxidation. SiliconFarEast. **2004**.

[18] Chen, H.; Hou, X.; Li, G.; Zhang, F.; Yu, M. *Journal of Applied Physics* **1996**, *79*(3282).

[19] Liu, L. Z.; Wu, X. L.; Zhang, Z. Y.; Li, T. H.; Chu, P. K. *App. Phys. Lett.* **2009**, *99*.

[20] Romann, J. Personal communication, **2012**.

[21] Nymark, A. M. Study of surface analysis methods used for the investigation of the oxide layer on the silicon surface Technical report, NTNU, **2011**.

[22] Watts, J. F.; Wolstenholme, J. *An Introduction to Surface Analysis by XPS and AES;* John Wiley and Sons Ltd, 2003.

[23] X-ray photoelectron spectroscopy (xps). Scudiero, L. **2011**.

[24] Thøgersen, A.; Diplas, S.; Mayandi, J.; Finstad, T.; Olsen, A.; Watts, J. F.; Mitome, M.; Bando, Y. *Journal of Applied Physics* **2008**, *103*.

[25] Einarsrud, M. A. Personal communication, **2011**.

[26] Raman spectroscopy basics. Instruments, P. **2012**.

[27] Smith, E.; Dent, G. *Moder Raman Spectroscopy, A Practical Approach;* John Wiley and Sons Ltd, 2005.

[28] Nilsen, R. Silicon for si3ni4 bonded sic materials. Technical report, NTNU, **2009**.

[29] Brunauer, S.; Emmett, P. H.; Teller, E. *Journal of the American Chemical Society* **1938**, *60*(2), 309–319.

[30] Støre, A. Personal communication, **2011**.

[31] Forwald, A. G. Sem undersøkelse av si-pulver Technical report, Elkem Solar, **2012**.

[32] Diplas, S. Xps analysis of si powder Technical report, **2012**.

[33] Diplas, S. Personal communication, **2012**.

[34] Kristiansen, T. Personal communication, **2012**.

[35] Operating instructions, seven easy ph meter s20. Mettler Toledo.

[36] Richards, J. M. *Journal of Physics D: Applied Physics* **1971**, *4*(4).

[37] Technical regulations, general meteorological standards and recommended practices Technical report, Secretariat of the World Meterological Organization - Geneva - Switzerland, **1988**.

Appendix A

Improvement of the aqueous oxidation apparatus

The aqueous oxidation apparatus used in the project thesis had several limitations and it was hard to reproduce some of the results. The original apparatus is displayed in Figure A.1. The results obtained using this apparatus showed some scattering and variations with respect to the hydrogen flow [ml/min] vs. oxidation time [min] curves. It was observed that the magnet stirrer did not manage to agitate all the powder, resulting in sedimentation of some of the powders to the bottom of the reaction bottle. This was believed to be because of the round bottom of the bottle. The problem was solved by replacing the round bottle with at bottle with a flat bottom, as shown in Figure A.2. It was also difficult to make the connection between the pH-electrode and the reaction bottle tight, hindering leakage of gas, which had to be checked accurately before each measurement. To make this connection better and more tight, a glas junction with one grinded end and the other end connected to a ring gasket of teflon where made. This is shown in red at the pH-electrode input, *(d)*, in Figure A.2

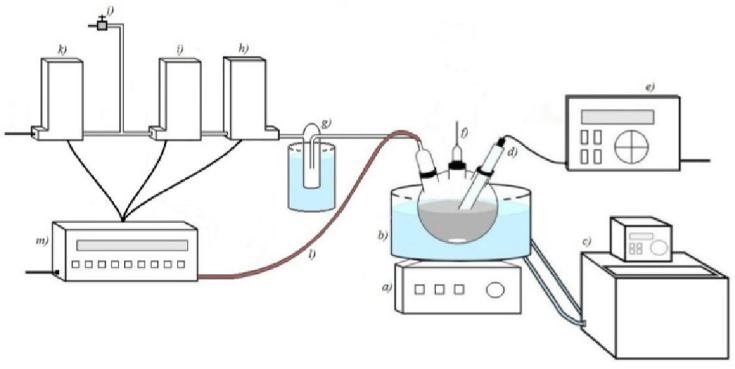

Figure A.1: Purpous-built apparatus used in the project thesis [5].

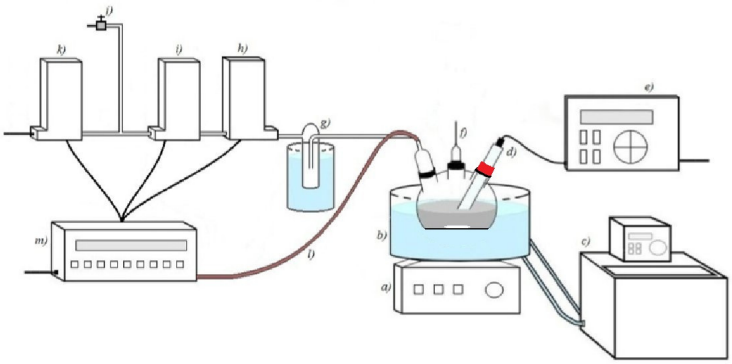

Figure A.2: Improved apparatus used in the master thesis. The reaction bottle is replaced with one that has a flat bottom and a new glas junction between the pH-electrode and reaction bottle is implemented, shown in red.

A.1 Calibration of the flow meters

To ensure that the performance of the flow meters was satisfying a calibration was performed. This was done by performing a "bubble-test" where a cylinder was filled with water and placed upside down in a bottle filled with water. Gas was led into the cylinder and the water height before and after the gas input was measured. The voltage, time and gas flow measured were implemented into a calibration-sheet. The result are shown in Figure A.1 for the coarse flow meter and in Figure A.2 for the fine flow meter. The values from the calibration was implemented to the Benchlink software and downloaded to the Agilink datalogger.

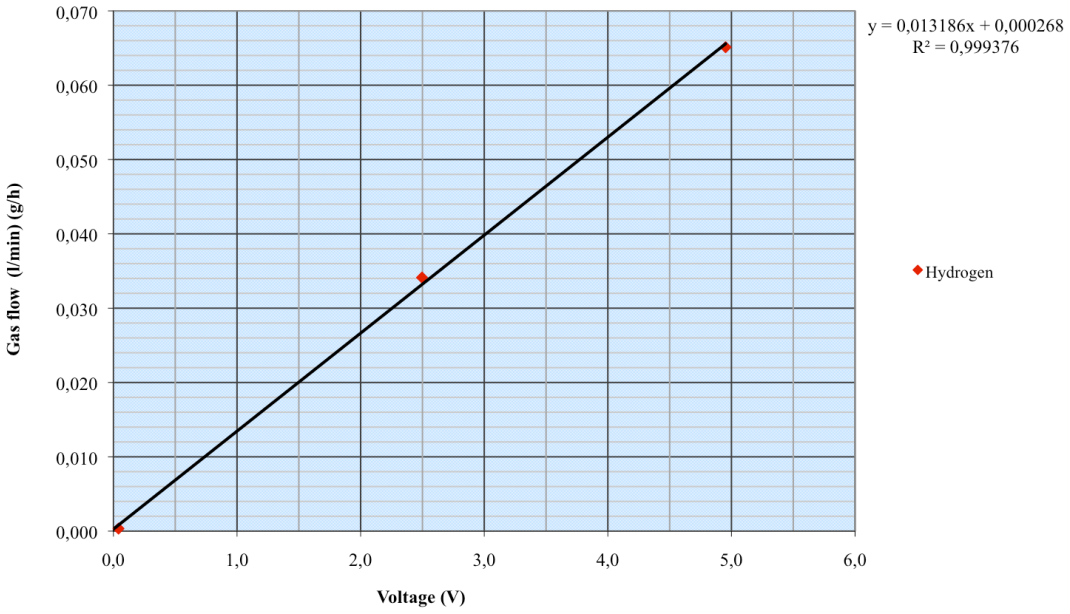

Figure A.1: Calibration curve for the coarse flow meter

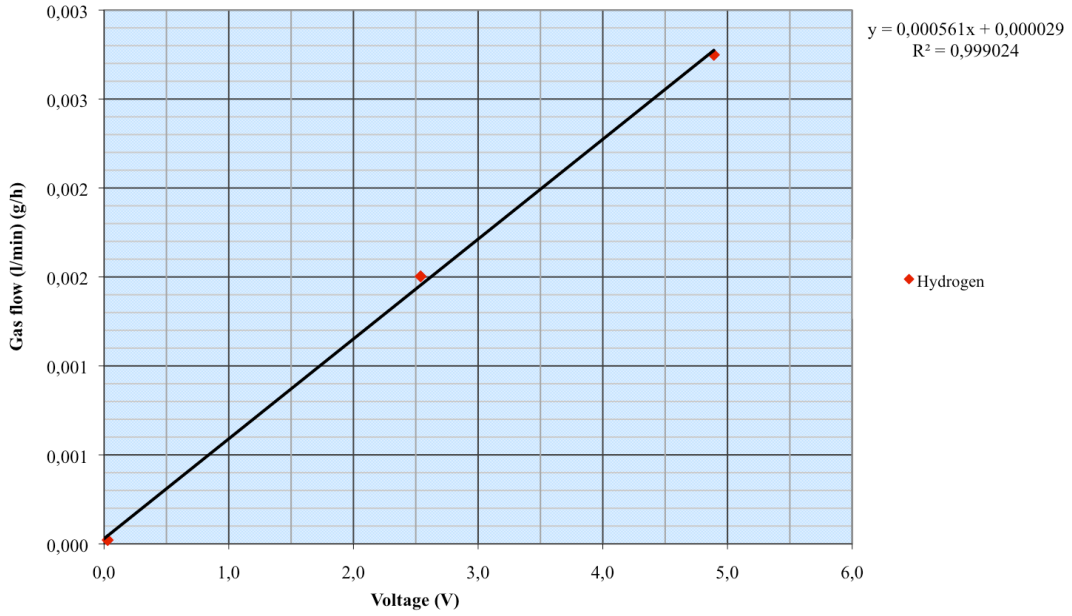

Figure A.2: Calibration curve for the fine flow meter

A.2 Cold mixture

During the experimental work problems with noise and scattering with respect to the hydrogen measurements were identified. It was clear that some of the gas measured probably was a result of evaporated nitrogen from the cold trap. The reason for this was that the cold trap was put into liquid nitrogen before the apparatus was flushed with nitrogen gas. This led to condensation of the nitrogen gas used to flush the apparatus, which filled the cold trap -column with condensed nitrogen. When the level of nitrogen in the cold trap and in the container for the liquid nitrogen was the same the nitrogen in the cold trap started to evaporate, thus affecting the gas flow measured. The liquid nitrogen was therefore replaced with a cold mixture. The cold mixture was made by mixing ice and NaCl(s) in a weight ratio 3:1. The temperature in the cold trap reached -20 °C, thus ammonia gas was not condensed and removed from the measured gas flow. This lead to further problems and noise in the result (because ammonia was not condensed in the cold-trap since the temperature only reached 20 °C). It was then decided to retry the use of liquid nitrogen, but put the cold trap in the liquid nitrogen first *after* the apparatus had been flushed with nitrogen gas. The resulting gas flow was much lower than earlier measured, thus the fine flow meter was used instead of the coarse flow meter. However, noise and scattering in the flow measurements disappeared resulting in acceptable flow curves.

A.3 Calibration of the pH-electrode

Before each experiment the pH-electrode was calibrated.

The calibration was performed as described in the manual for the pH-electrode [35]. The same pH-electrode model was used for all the measurements. The process is reprinted below.

Step 1 Place the electrode in a calibration buffer, pH 7.01, and press *Cal*

Step 2 The SevenEasy pH meter automatically endpoints when calibrating. To manually endpoint, press *Read*

Step 3 Use distilled water to rinse the electrode

Step 4 Place the electrode in the next calibration buffer, pH 10.01, and press *Cal*

Step 5 Use distilled water to rinse the electrode

After calibration the meter displays and freezes the relevant buffer value, and shows the electrode offset.

Appendix B

Vapour pressure and humidity

The silicon powder is transported around Norway and Europe after milling until it is further processed. The humidity in Norway and for example in Rome will be different, this affects the powder differently depending on where the powder is stored before processing.

In Rome the average relative humidity in the summer is 67% and the average temperature (using the average maximum and minimum summer temperature) is 23 °C. The saturated vapour pressure at 23 °C can be found using Goff-Gratch equation [36], given in Equation B.1. By using the calculated saturation vapour pressure at 23 °C and 67% relative humidity, Equation B.3 [37] can be used to find the actual vapour pressure at 23 °C.

$$e_s = e_{st} 10^Z \tag{B.1}$$

where e_s is the saturation vapour pressure at temperature T, e_{st} is the saturation vapour pressure at the boiling point of water T_1 equal to 1013.246 mb, and Z is given in Equation B.2

$$\begin{aligned} Z = -7.90298 \times (\frac{T_1}{T} - 1) + 5.02808 \times log_{10}(\frac{T_1}{T}) \\ -1.3816 \times 10^{-7}[10^{11.344(\frac{T}{T_1}-1)}] \\ +8.1328 \times 10^{-3}[10^{-3.49149(\frac{T_1}{T})} - 1] \end{aligned} \tag{B.2}$$

$$R.H\% = \frac{\text{The actual vapour pressure at temperature T } \times 100\%}{\text{The saturated vapour pressure at temperature T}} \tag{B.3}$$

This gives an average vapour pressure of 0.0183 atm. in Rome in the summer compared to the average vapour pressure in Norway in the summer months, which is 0.0118 atm. Storage of powder at 22°C gives a vapour pressure of 0.0260 atm. and storage at 10°C gives a vapour pressure of 0.0121 atm. This is summarised in Table B.1.

Table B.1: Overview of temperature and saturation vapour pressure at that temperature.

Storage conditions	*Temperature [°C]*	*Vapour pressure [atm.]*	*Comments*
Experimental storing	10°C	0.0121	Theoretical values used for the experiments
	22°C	0.0260	Theoretical values used for experiments
Actual conditions	6.7 °C	0.0118	Average values during the summer months at the coast of Norway
	23	0.0183	Average values during the summer months in Rome

Appendix C

BET surface area plot

In this 2 the BET surface area plot for three selected samples of the silicon powders is shown. First the BET surface area plot for unreacted, as-received, powder is shown, Figure C.1. In Figure C.2 result from sample B-D5.2-10C is shown and in Figure C.3 result from sample B-TO-300C is shown.

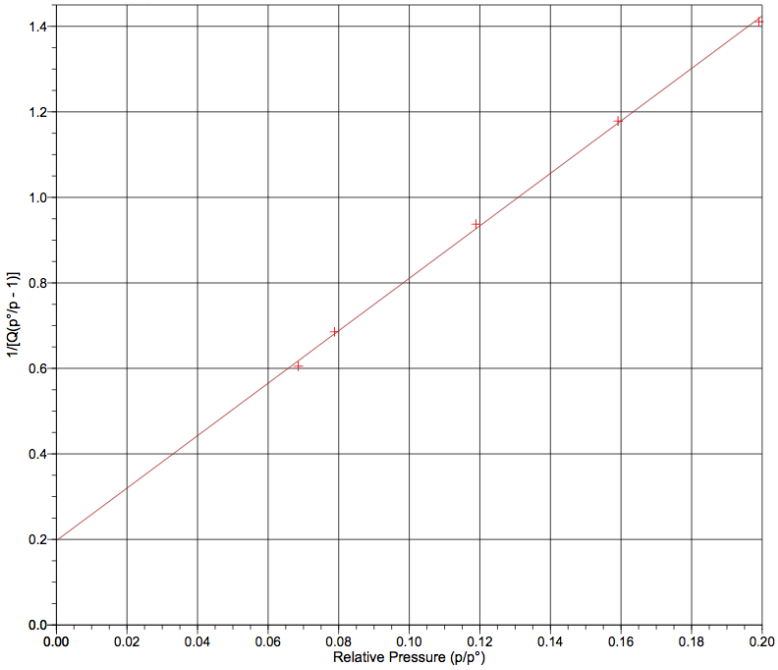

Figure C.1: BET surface area plot for the silicon powder, as received. Degas temperature 150°C.

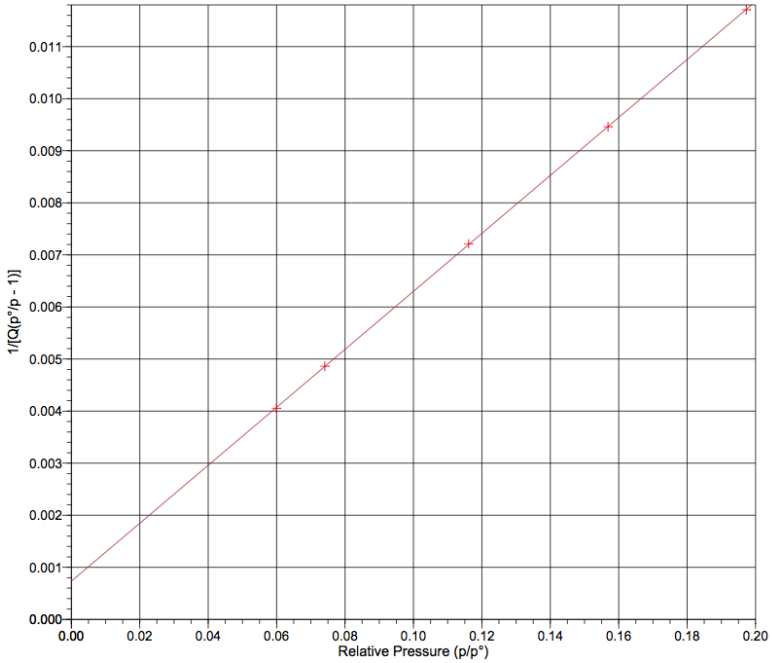

Figure C.2: BET surface area plot for sample B-D5.2-10C from Batch B. Degas temperature 250°C.

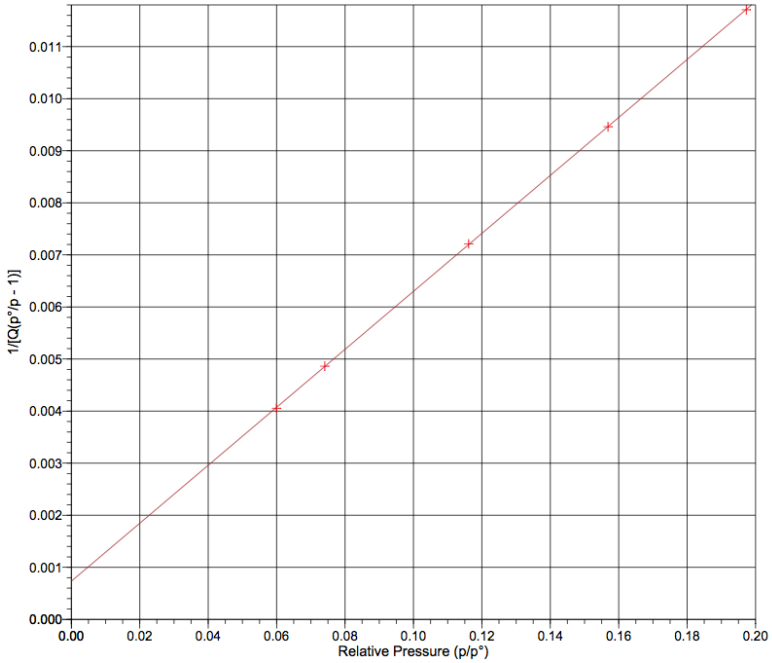

Figure C.3: BET surface area plot for sample B-TO-300C from Batch B. Degas temperature 250°C.

Appendix D

Hydrogen flow measurements

In this 2 the hydrogen flow curves as a function of oxidation time for silicon powder will be displayed. Two selected flow curves will be presented for powder Batch A, while all hydrogen flow curves will be presented for Batch B. Sample B-D7.1-22C and B-TO-300C did not form any hydrogen in the aqueous oxidations reaction and will therefore not be displayed.

D.1 Batch A

In this 2 two examples of the hydrogen flow curves obtained from the hydrogen measurement before the experimental routine was changed will be give. Figure D.3 shows the raw data from the hydrogen measurements for powder sample A-D10.2-10C (a) and A-D21.1-22C (b). The hydrogen evolution is shown as the black line and the pH is shown either as the red line or as red dots.

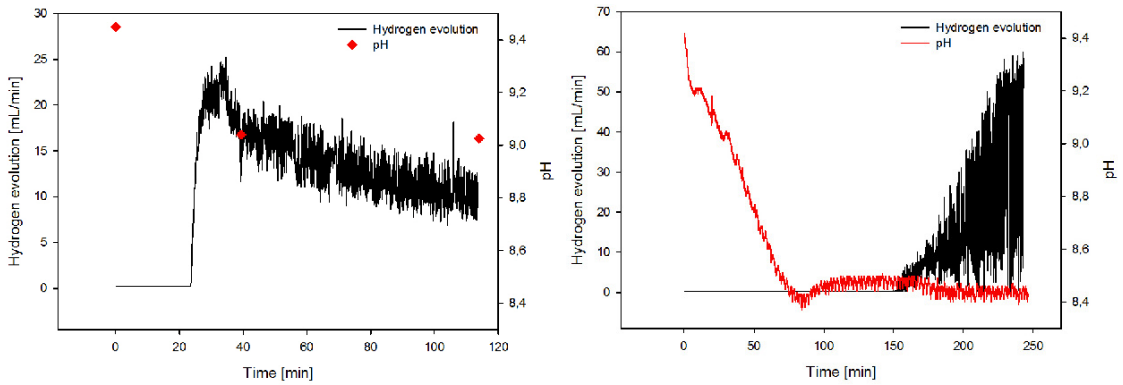

(a) (b)

Figure D.3: Silicon powders exposed to humid air for different periods of time. a) Sample A-D10.2-10C, 10 days in 10 °C b) Sample A-D21.1-22C, 21 days in 22 °C.

D.2 Batch B

Hydrogen flow curves for silicon powder, from Batch B, exposed to humid air at 10 °C are divided in two. Figure D.1 show the hydrogen flow curves obtained when pH-electrode I was used and Figure D.2 show the hydrogen flow curves obtained when pH-electrode II was used. The hydrogen evolution is shown as the black line and the pH is shown as red dots.

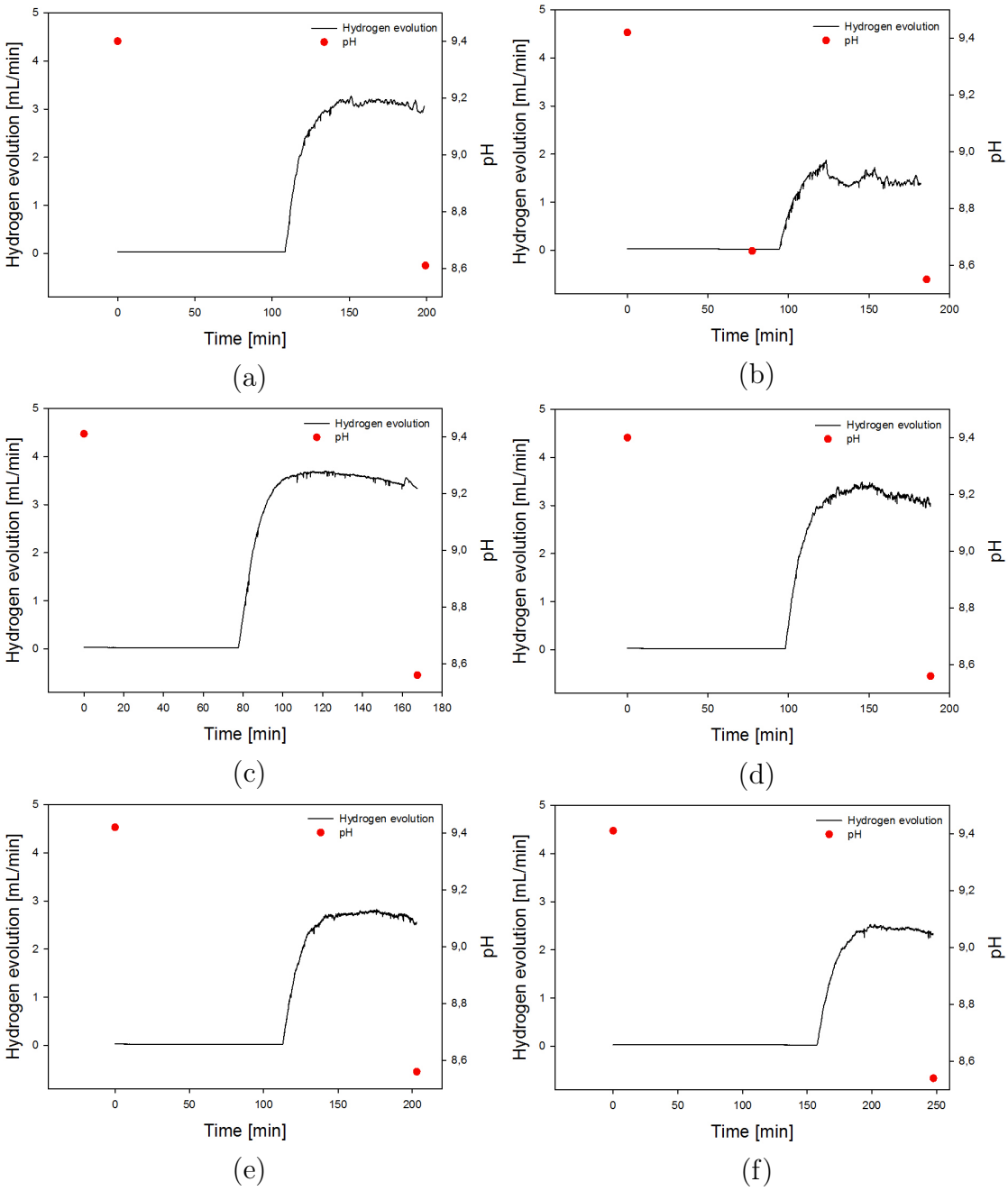

Figure D.1: Silicon powders exposed to humid air at 10 °C for different periods of time. a) Sample B-D1.1-10C, one days in 10 °C b) Sample B-D3.1-10C, 3 days in 10 °C c) Sample B-D3.2-10C, 3 days in 10 °C d) Sample B-D5.1-10C, 5 days in 10 °C e) Sample B-D7.1-10C, 7 days in 10 °C and f) Sample B-D14.1-10C, 14 days in 10 °C.

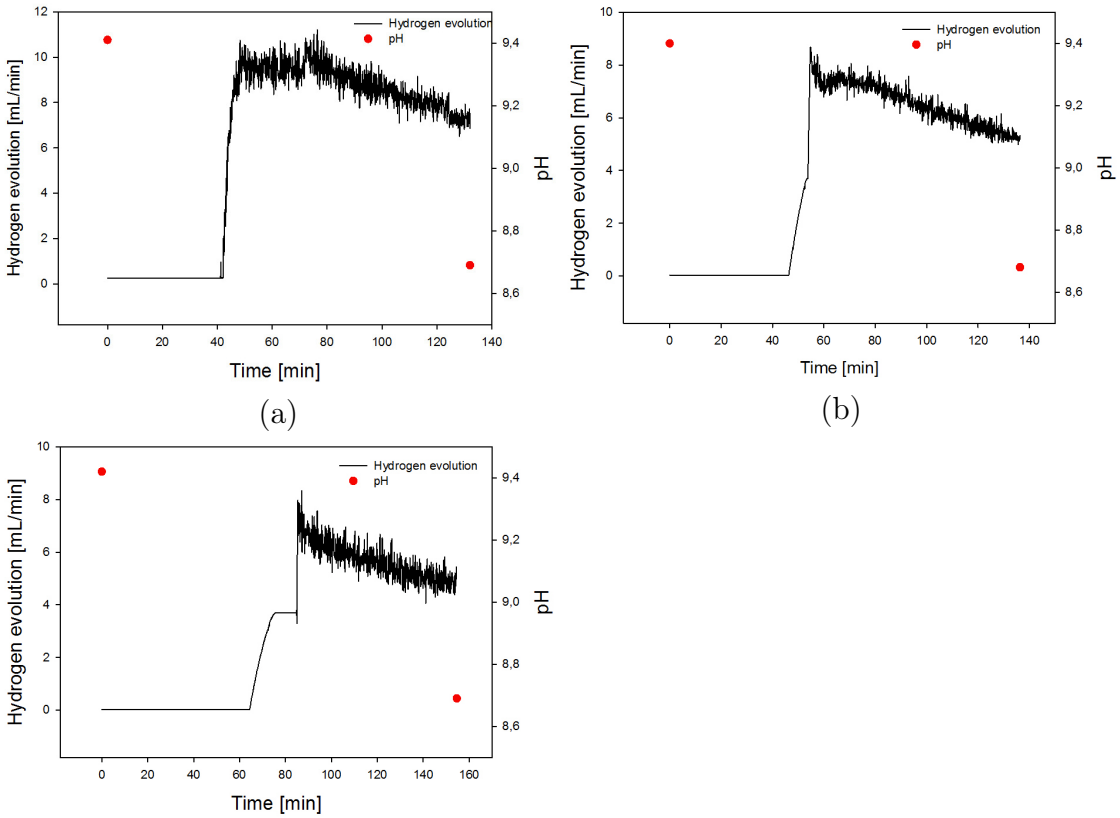

Figure D.2: Silicon powders exposed to humid air at 10 °C for different periods of time. a) Sample B-D5.2-10C, five days exposure b) Sample B-D14.2-10C, 14 days exposure c) Sample B-D28.1-10C, 28 days exposure.

Hydrogen flow curves for silicon powder, form Batch B, exposed to humid air at 22 °C are divided in two. Figure D.4 show the hydrogen flow curves obtained when pH-electrode I was used and Figure D.6 show the hydrogen flow curves obtained when pH-electrode II was used. The hydrogen evolution is shown as the black line and the pH is shown as the red dots.

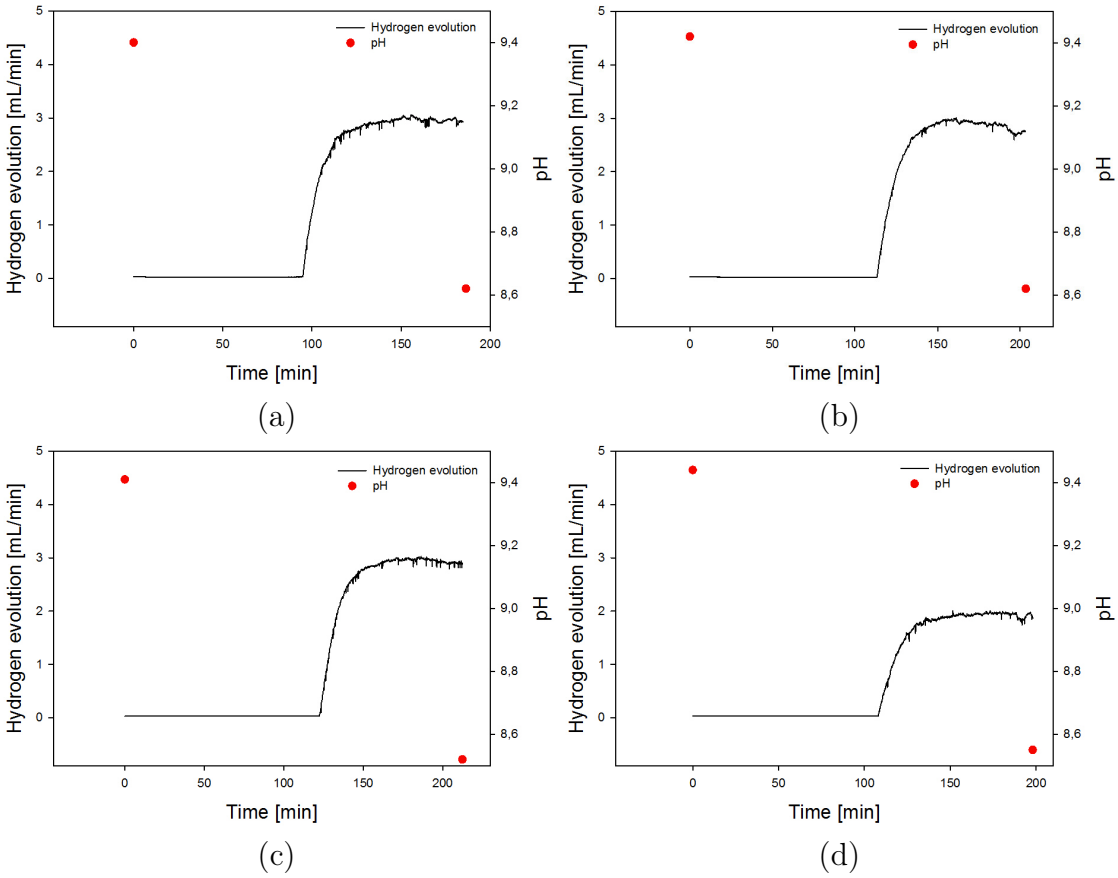

Figure D.4: Silicon powders exposed to humid air at 22 °C for different periods of time. a) Sample B-D1.1-22C, one days in 22 °C b) Sample B-D3.1-22C, 3 days in 22 °C c) Sample B-D5.1-22C, 5 days in 22 °C d) Sample B-D14.1-22C, 5 days in 22 °C.

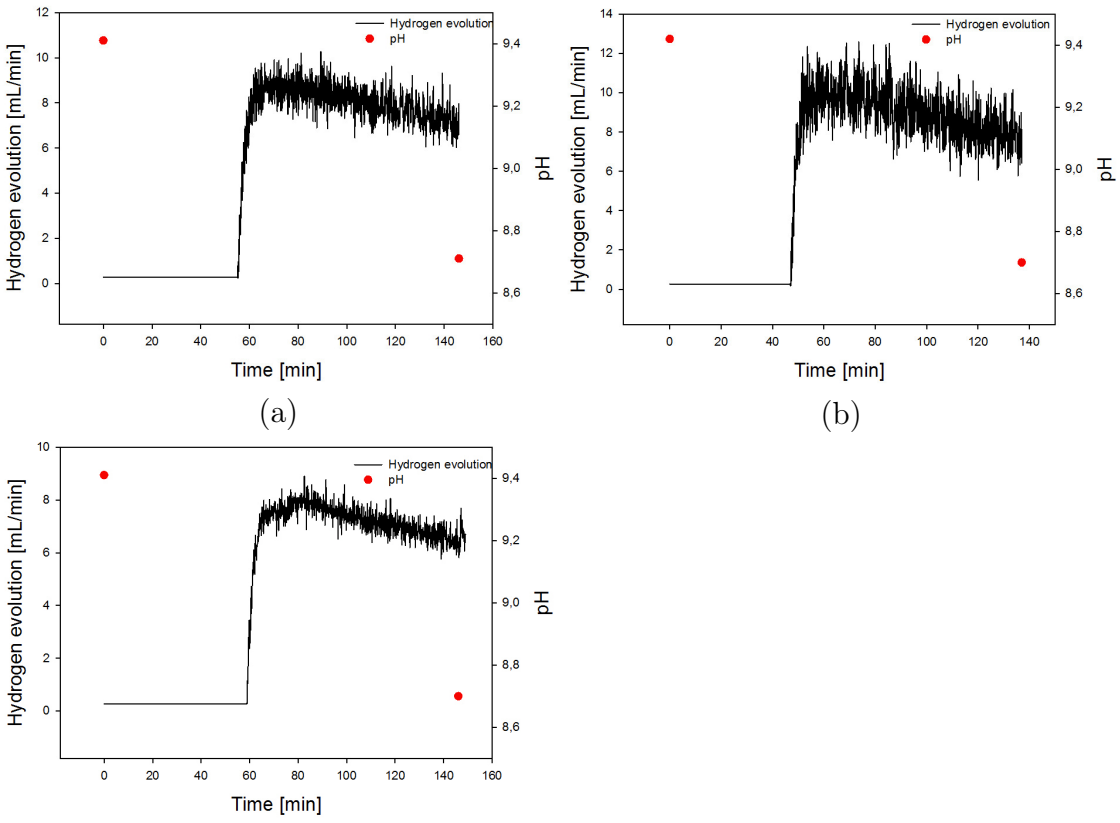

Figure D.6: Silicon powders exposed to humid air at 22 °C for different periods of time. a) Sample B-D5.2-22C, five days in 22 °C b) Sample B-D14.2-22C, 14 days in 22 °C c) Sample B-D28.1-22C, 28 days in 22 °C

Appendix E

SEM analysis of reacted silicon powders

In this 2 the SEM images of sample A-D0.3 and A-D2.2-22C not presented earlier will be displayed.

Figure E.1 and Figure E.2 show samples sprinkled onto a stub. 100X and 500X magnification is used, respectively in the two pictures. Image of sample A-D0.3 is shown in Figure E.1b and Figure E.2b and sample A-D2.2-22C is shown in Figure E.1a and Figure E.2a.

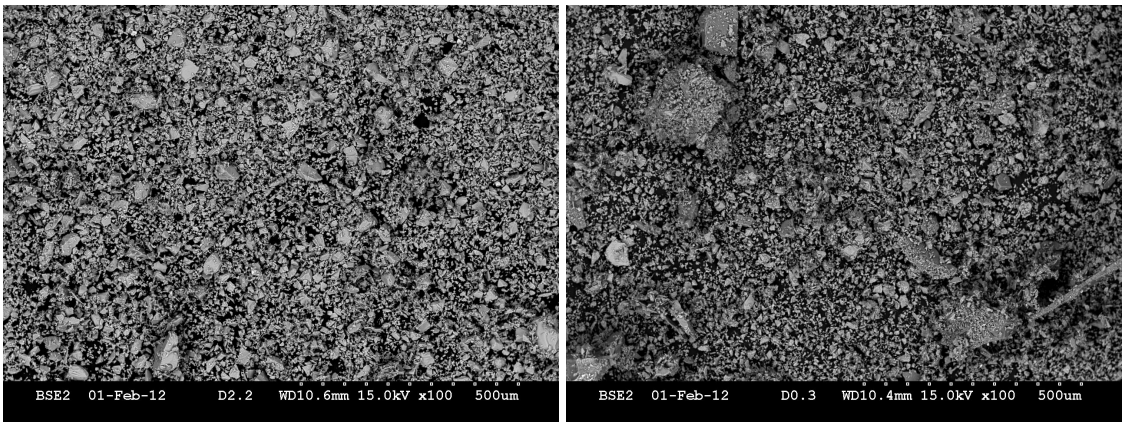

(a) (b)

Figure E.1: Pictures of both samples with magnification 100X. a) A-D2.2-22C b) A-D0.3

Pictures of the fine fraction from the ultra sound bath are shown in Figure E.3. Particles with dark colour indicates oxides or other species with low average atomic number. A clear difference between the samples can be observed.

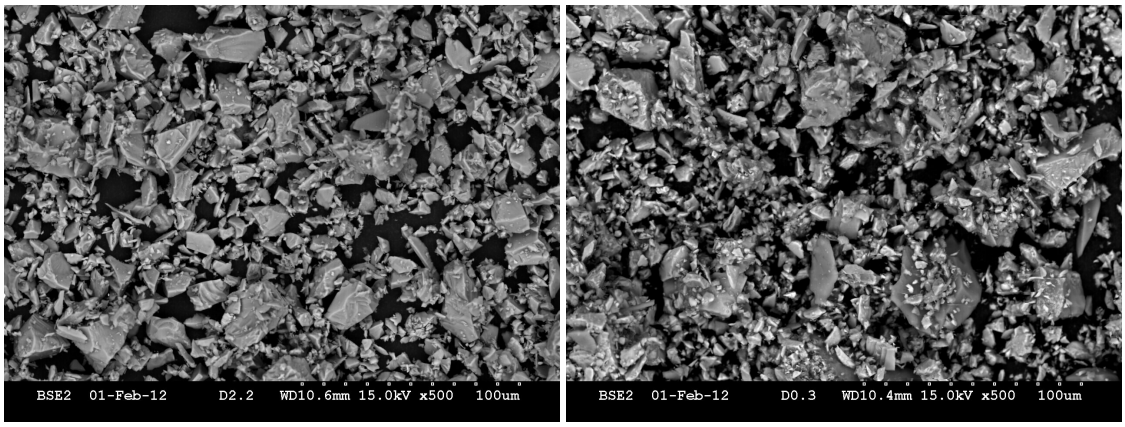

(a) (b)

Figure E.2: Pictures of both samples with magnification 500X. a) A-D2.2-22C b) A-D0.3

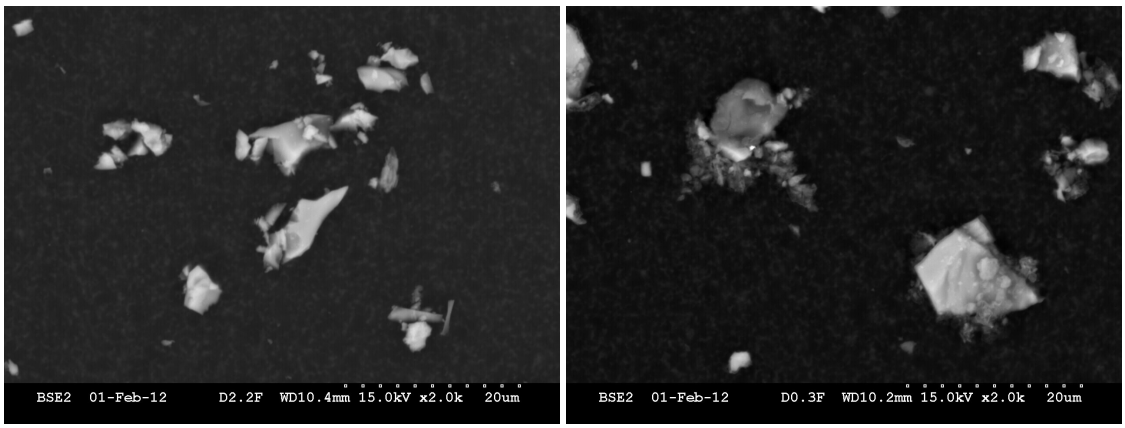

(a) (b)

Figure E.3: Pictures of fine fractions from both samples with 2.0 k magnification a) A-D2.2-22C b) A-D0.3.

Different areas of the fine fraction of sample A-D0.3 is given in Figure E.4. Different magnifications is used in the two images.

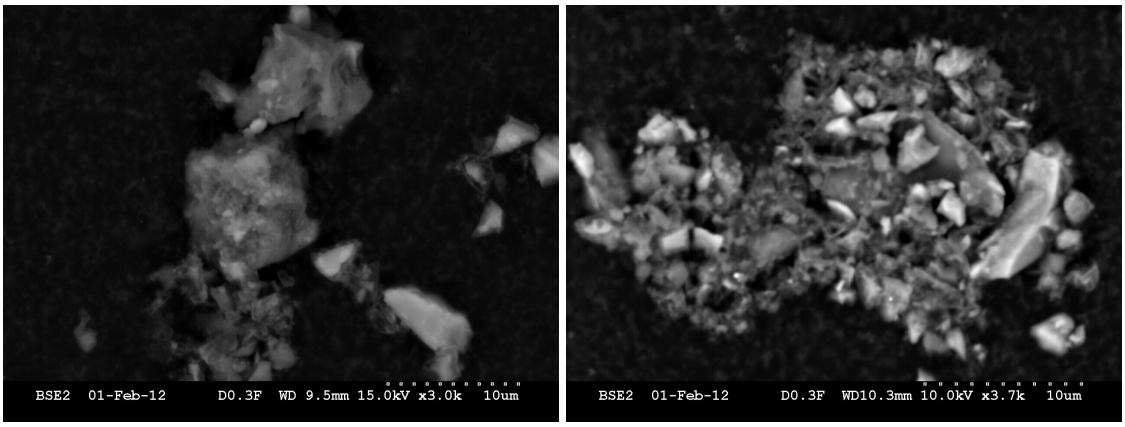

(a) (b)

Figure E.4: Pictures of fine fractions from sample A-D0.3 showing two different areas. Magnification 3.0k is used for the image in a) and 3.7k is used for the image in b).